# Altered signaling, but no cell fragility in mice lacking all type II keratin genes

Dissertation

zur

Erlangung des Doktorgrades (Dr. rer. nat.)

der

Mathematisch-Naturwissenschaftlichen Fakultät

der

Rheinischen Friedrich-Wilhelms-Universität Bonn

vorgelegt von

Preethi Vijayaraj

aus

Ootacamund, Indien

- Bonn, September 2007 –

Angefertigt mit Genehmigung der Mathematisch-Naturwissenschaftlichen Fakultät
der Rheinischen Friedrich-Wilhelms-Universität Bonn



Erscheinungsjahr: 2008
Tag der Promotion: 28.03.2008

Gutachters

1. Prof. Dr. Thomas Magin
2. Prof. Dr. Michael Hoch

Die vorliegende Arbeit wurde in der Zeit von June 2003 bis September 2007 am Institut für Physiologische Chemie der Universität Bonn, Nussallee 11 unter Leitung von Prof. Dr. Thomas Magin durchgeführt.

*In fond memory of my mom*

# ACKNOWLEDGEMENTS

Many people have contributed to this dissertation in innumerable ways, and I am grateful to all of them. Firstly, I would like extend my sincere gratitude to my supervisor, Prof. Thomas Magin for having entrusted such an ambitious project on me. I am very appreciative of his generosity with his time, advice, encouragement, and references, to name a few of his contributions. Without his support, this project would not have been possible.

Mrs. Ursula Reuter offered excellent technical support that was very instrumental in analyzing the mutant mice from this project in-depth. Her invaluable assistance accelerated the completion of this thesis to a very great extent. I am extremely grateful to her for all her help.

Our collaborators, Prof. Dieter Hartmann, University of Bonn and Dr. David Simmons, University of Calgary have offered novel data by analyzing the mutants. They have been instrumental in adding a new dimension to keratin function. I deeply appreciate their time, invaluable discussions and support.

Dr. Michael Hesse, Ms. Cornelia Kroeger, Dr. Joachim Degen and Ms. Christina Landwehr brought unique perspectives to my research, enriching it greatly. I thank them for their numerous stimulating discussions, time and encouragement.

I am especially grateful to Mrs. Rodica Maniu who successfully generated chimeric mice for this project, for her support and patience.

This project was funded by the DFG (Deutsche Forschungsgemeinschaft), and I am deeply grateful to them for the same.

I owe my sincere gratitude to Prof. P. Vijayan and Dr. H.C. Jha for their motivation and invaluable guidance in helping me pursue my career goals.

I sincerely thank all my colleagues for offering a very conducive environment in the lab, making it a home away from home. I thank them for their discussions, advice, critical comments and time. I deeply appreciate the help of Andrea, Veena, Vani, Shiv, Saran, Hari and Steffi for giving critical comments on this thesis. I would once again like to specially thank my sister Veena and brother-in-law Shiv for having taken time off their busy schedules and offering me help to fix pictures for this thesis. My life in Germany would not have been so memorable if not for my wide circle of friends here, and of particular mention, I would specially like to thank Saran, Andrea, Deepak, Shincy and Vinod.

I would like to extend my deepest gratitude to my family, especially my parents. They have always provided unwavering love and encouragement and believed in me. I deeply regret that my mother is no longer there to cherish my achievements. She would have been very proud to see this thesis taking this form.

FIGURES

LIST OF TABLES



ABBREVIATIONS

| | | | |
|---|---|---|---|
| μg | Microgram | JNK | Jun N-terminal kinase |
| μl | Microlitre | K | Keratin protein |
| °C | Grad Celsius | kDa | Kilodalton |
| Ag | Agouti | KO | Knockout |
| APS | Ammonium persulphate | Krt | Keratin gene |
| ATF1 | Activating transcription factor 1 | L | Litre |
| bp | Base pair | *LoxP* | Locus of X-over P1 |
| BSA | Bovine serum albumin | LIF | Leukaemia inhibitory factor |
| $CO_2$ | Carbon dioxide | MAPK | Mitogen activated protein kinase |
| Cre | Cyclization recombination | Mb | Megabase |
| CREB | cAMP response element-binding | MEK | Mitogen-activated protein kinase |
| DAPI | 4,6-Diamidino-2-phenylindole | Mg | Milligram |
| DMSO | Dimethyl sulphoxide | Min | Minutes |

| | | | |
|---|---|---|---|
| DNA | Deoxy ribonucleic acid | miRNA | microRNA |
| dNTP | Deoxynucleoside-triphosphate | mm | Millimeter |
| dpc | Days post coitum | mRNA | Messenger RNA |
| E | Embryonic day | mTOR | Mammalian target of rapamycin |
| *E. coli* | Escherichia coli | Neo | Neomycin |
| E.g. | Example | nm | Nanometer |
| EDTA | Ethylene diamine tetra acetic acid | PAGE | Polyacrylamide gel electrophoresis |
| EPC | Ectoplacental cone | PBS | Phosphate buffered saline |
| ES | Embryonic stem | PCR | Polymerase chain reaction |
| FCS | Foetal calf serum | pmol | Picomole |
| FISH | Fluorescent *in-situ* hybridization | RT | Room temperature |
| Fig. | Figure | RT-PCR | Reverse transcription – polymerase chain reaction |
| Gcm1 | Glial cells missing homologue 1 | SDS | Sodium dodecyl sulfate |
| HAT | Hypoxanthine, aminopterin and thymidine | PAGE | Polyacrylamide gel electrophoresis |
| HBSS | Hank's balanced salt | Puro | Puromycin |
| HGF | Hepatocyte growth factor | Sec | Seconds |
| HPRT | Hypoxanthine-guanine phosphoribosyltransferase | SynA | Syncytin A |
| hr(s) | Hour(s) | SynT | Syncytiotrophoblast |
| IB | Immunoblot | TBS | Tris buffered saline |
| ICM | Inner cell mass | TGC | Trophoblast giant cells |
| IF | Immunfluoresence | TNF | Tumor necrosis factor |
| IF | Intermediate filament | Ty | Tyrosinase |
| IHC | Immuno histochemistry | WT | Wild type |

# 1. INTRODUCTION

*"Intermediate filaments that may function to integrate mechanically, the various structures of the cytoplasmic space, in a way, that is tailored to the differentiated state of the cell" – Elias Lazarides, 1980*. One of the greatest challenges in this field is to unravel the cell type restricted function and regulation of the intermediate filament (IF) protein family

## 1.1. Keratin genes

Keratins are proteins which build the intermediate filament cytoskeleton of all epithelia. They are composed of two classes – 28 type I acidic keratins (K9-K28; epithelial keratins and K31-K40; hair keratins) and 26 type II basic keratins (K1-K8, K71-K74; epithelial keratins and K81-K86; hair keratins) encoded by two large gene families comprising >50 genes in the mouse and human (Schweizer et al., 2006). Individual keratin genes are compact, spanning about 5-8 kb of DNA.

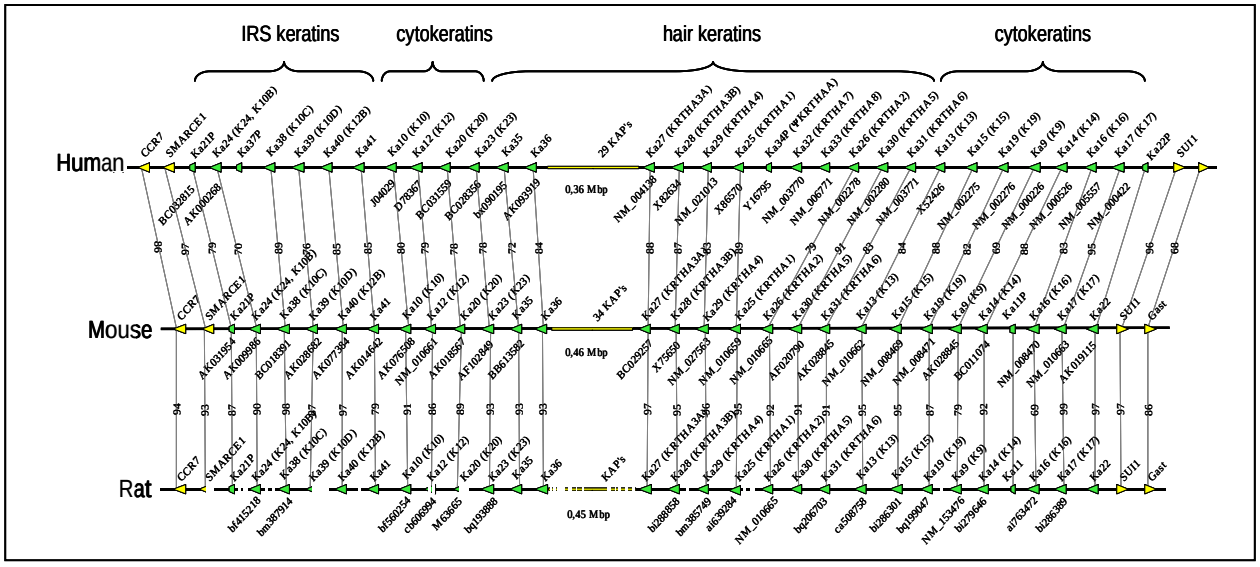


Fig.1.1. Type I keratin gene clusters of human (H), mouse (M) and rat (R). Sequence gaps in the rat keratin type I cluster are indicated by gaps and breaks in the corresponding sequence line. Keratin genes are marked by green triangles with the tip corresponding to the 3' end. Keratin genes are identified by the numbers used in the proposed nomenclature. For convenience, previously used numbers are added in parenthesis. Pseudogenes are marked by P. If available, cDNA accession numbers are provided. Accession numbers of EST sequences start with small letters. The genes flanking the type I cluster are depicted as yellow triangles. The approximate position of the multiple KAP genes interrupting the type I cluster is given. Conservation of synteny is indicated by the thin lines connecting corresponding human/mouse and mouse/rat genes, respectively. Numbers on these lines give the percent sequence identity at the protein level (modified from Hesse et al., 2004).

Unlike members of many other gene families, the type I and type II keratin gene families are arranged in contiguous clusters spanning 1.2 Mb on chromosome 11 and 0.68 Mb on chromosome 15, respectively, in the mouse (Fig. 1.1 & 1.2). No other known open reading frames, except the hair-

specific high sulfur keratins, are contained in the two keratin gene clusters. All keratins are expressed in various combinations of at least one type I and one type II keratin from the 2-cell stage mouse embryo onwards in a tissue-specific fashion (Lu et al., 2005). About half of the keratins are expressed in various, but highly specific combinations in simple and stratified epithelia. The other half are found in epithelial appendages including hair, nail, and others (Herrmann et al., 2003; Langbein et al., 1999; Langbein et al., 2001).

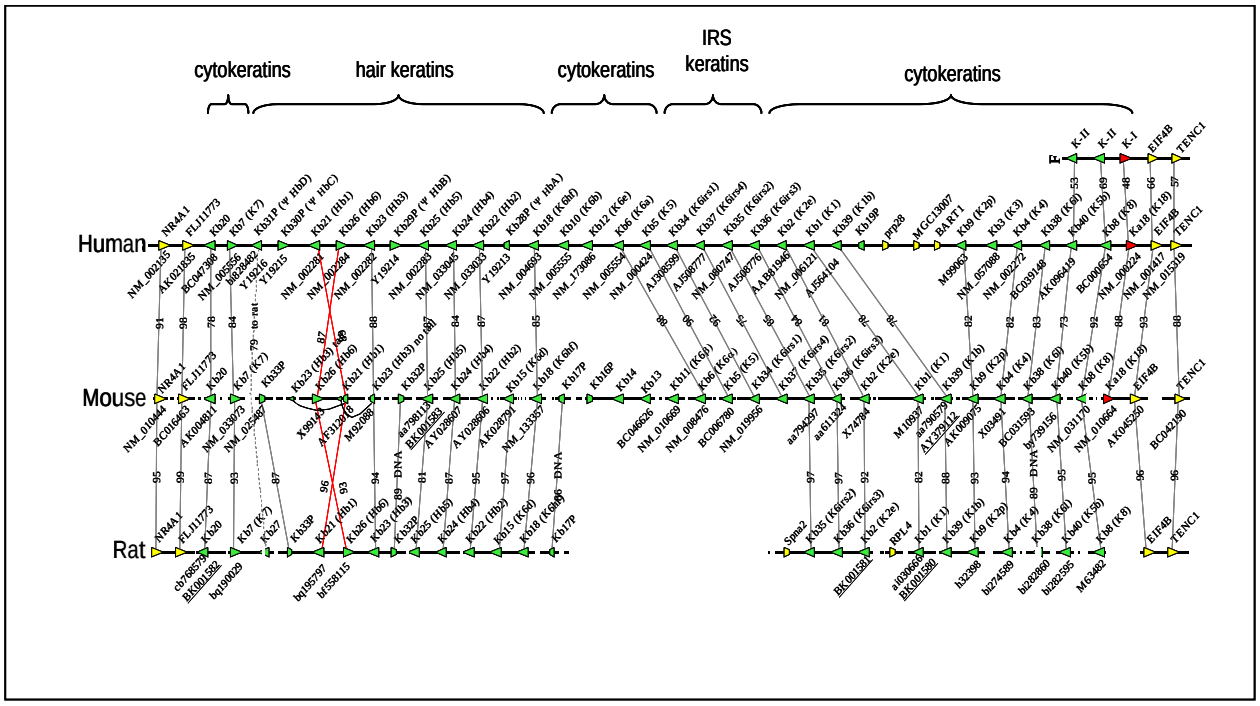


Fig.1.2. Type II keratin gene clusters of human (H), mouse (M) and rat (R). Sequence gaps in the mouse and rat clusters are indicated by gaps and breaks in the corresponding sequence lines. Keratin genes are marked by green triangles with the tip corresponding to the 3' end. Keratin genes are identified by the numbers used in the proposed nomenclature. For convenience, previously used numbers are added in parenthesis. Pseudogenes are marked by P. Flanking genes for the type II cluster are depicted as yellow triangles. When available, cDNA accession numbers are provided. Accession numbers of EST sequences start with small letters. The only type I keratin *Ka18 (Krt18)* gene at the end of the keratin II cluster is given in red. Conservation of synteny is indicated by the thin lines connecting corresponding human/mouse and mouse/rat genes respectively. A potential case of violation of synteny is depicted in red crossed lines. Numbers on these lines give the percent sequence identity on the protein level, except for the cases marked DNA (modified from Hesse et al., 2004).

## 1.2. Keratin structure and organization within the cell

All keratins share a tripartite domain structure, with the defining feature being a centrally located, 310-residue-long -helical domain containing long-range heptad repeats of hydrophobic/apolar residues (Fig. 1.3). This domain mediates coiled-coil dimer formation and represents the major driving force sustaining self-assembly (Fuchs et al., 1994; Herrmann and Aebi, 2004). The rod is flanked, at both ends, by non-helical sequences that differ in length, sequence, substructure, and properties. A "one gene/one protein" rule seems to prevail within the family, but for a few exceptions like lamin A/C, GFAP,

peripherin, and synemin which yield distinct protein products via alternative splicing (rev. Kim and Coulombe, 2007).

Owing to the presence of long-range heptad repeats (Fig.1.3), type I and type II keratin proteins readily form highly stable coiled-coil dimers (10 nm in length), in which the two participating monomers exhibit a parallel, in-register alignment. Dimers then associate along their lateral surfaces, with an anti-parallel orientation, to form apolar tetramers.

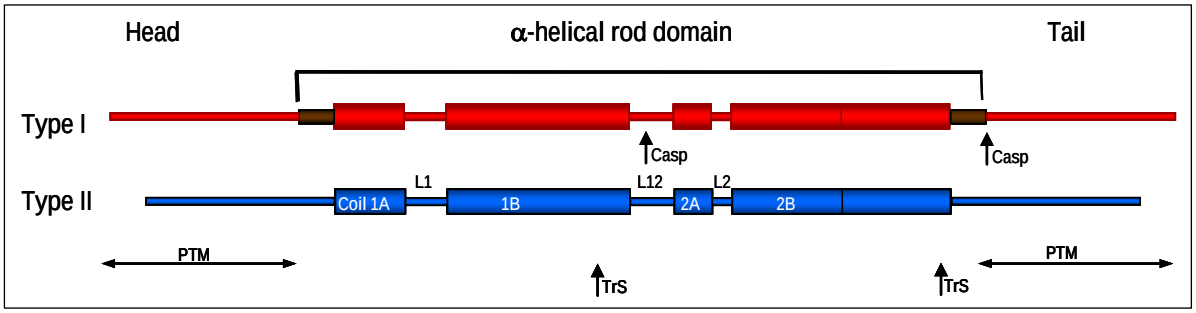


Fig.1.3. Schematic representation of the tripartite domain structure shared by type I and type II keratins. A central α-helical "rod" domain acts as the major determinant of self-assembly and is flanked by non-helical "head" and "tail" domains at the N and C termini, respectively. Within this 310-amino-acid-long rod domain, the heptad repeat-containing segments 1A, 1B, 2A, and 2B are interrupted at three conserved locations by linker sequences L1, L12, and L2. Rod domain boundaries consist of highly conserved 15- to 20-amino-acid regions (shown in brown) that are crucial for polymerization and are frequently mutated in human disease. The elements of biochemical regulation indicated include: the trigger sites (TrS) that mediate nucleation of keratin heterodimerization via coiled coil interactions; caspase-sensitive cleavage sites (Casp); and the major location of post-translational modifications (PTMs) (Modified from Magin TM).

All keratins share the same domain organization. Despite a limited degree of sequence identity, which ranges from 50-90 % in each subfamily, any type I and type II protein can co-assemble into filaments *in vitro* (Hatzfeld and Franke, 1985). The greatest extent of sequence variability resides in the head and tail domains of keratins which are rich in Ser-Thr residues in simple epithelial and rich in Gly-Gly-X in epidermal keratins. These domains are involved in specific protein interactions (Coulombe and Omary, 2002; Herrmann et al., 2003).

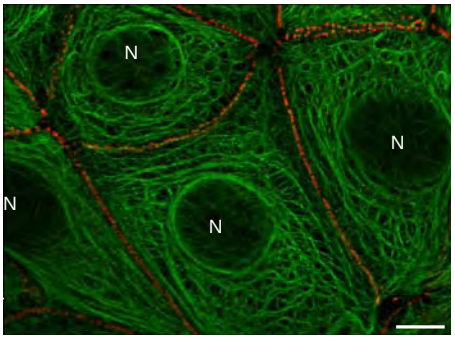


Fig.1.4. Organization of keratin filaments via indirect immunofluorescence, in MCF-7 cells. Keratin IFs (green) are organized in a network that spans the whole cytoplasm, and are attached to desmosomes (red) at points of cell–cell contacts. N, nucleus. Scale bar, 10 μm (Courtesy Dr. S. Loeffek and A.Wester).

Keratins are integrated with other key elements making up the cells' interior. They interact with the other major determinants of cellular architecture, including microtubules, F-actin, and various types of adhesive complexes spanning the outer cell membrane, including desmosomal (cell–cell) attachments and integrin-based linkages to the extracellular matrix (Fuchs and Cleveland, 1998; Green and Jones, 1996; Jefferson et al., 2004 Garrod, 2002 #619; Svitkina et al., 1996) (Fig.1.4). The desmosome is an electron-dense complex found in tissues subjected to mechanical stress, such as stratified squamous epithelia cells and the myocardium. This intercellular junction is composed of a core region, which mediates tight cell-cell adhesion, and a plaque region, which mediates attachment to the intermediate filament cytoskeleton. The core region contains the extracellular domains of the desmosomal cadherins, the desmocollins and desmogleins. The cytoplasmic plaque region includes the C-terminal tails of the desmosomal cadherins, which associate directly and indirectly with various cytoplasmic proteins. The armadillo family proteins in the desmosome include plakoglobin and plakophilins. These proteins mediate interactions between the desmosomal cadherin tails, desmoplakin, a plakin family protein that binds directly to intermediate filaments and keratins. These components of the desmosome allow tethering of the intermediate filaments to the plasma membrane, thereby acting as a scaffold to provide structural integrity to cells and tissues (Fig.1.5).

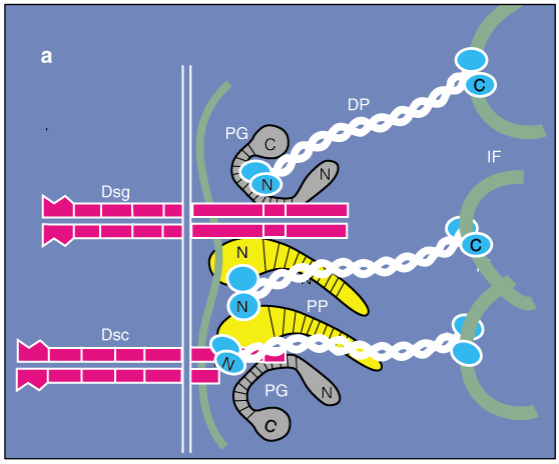


Fig.1.5. Structural organization of the desmosome. In the desmosome, desmogleins (Dsg) bind directly to plakoglobin (PG) and plakophilin (PP), which provide links to the N terminus (N) of desmoplakin (DP). DP also binds directly to the juxtamembrane domain of desmocollin-1a (Dsc). The DP C-terminal domain (C) interacts with intermediate filaments (IF). PP and DP co-cluster desmosomal components. PP binds IFs *in vitro* and associates with lateral keratin filaments in a DP N-terminal-dependent fashion *in vivo*. Modified from Hatsell and Cowin, 2001.

## 1.3. Keratin expression

All embryonic and adult internal epithelia express at least K8 and K18, which are complemented by keratins K7, K19, K20, K23, and others in many specialized epithelia. K8 and K18 are the first embryonic keratins, forming intermediate filaments from the 2-cell stage of mouse embryo (Fuchs and

Weber, 1994; Hashido et al., 1991; Herrmann et al., 2003; Lu et al., 2005). The basal layer of all stratified epithelia expresses K5, K14 and K15, which become replaced by other keratins, e.g., K1, K10, during terminal differentiation and by K6, K16 and K17 during wound healing and inflammation (Fuchs and Weber, 1994; Moll et al., 1982). Notably, there is a very significant variation in the amount of keratins per cell which might be of great importance for their function. Hepatocytes contain about 1%, whereas, epidermal keratinocytes contain up to 30 % keratin of their total protein content (Fuchs and Weber, 1994). The complex expression pattern has led to the hypothesis that keratin expression pairs have distinct functions. In support, keratins K5 and K14 form more stable protein complexes than K8 and K18 *in vitro* in the presence of increasing concentrations of urea (Franke et al., 1983).

### 1.3.1. Keratin expression during early embryogenesis

K8 and K18 are the first IF proteins expressed during embryogenesis in the mouse. In pre-implantation embryos, mRNAs coding for K7, K8, K18, and K19 are present. However, only K7 and K8 accumulate as proteins, which are deposited in aggregates and not as filaments since their expression begins earlier than their filament forming counterpart, K18 or K19 (Lu et al., 2005).

| Tissue | K7 | K8 | K18 | K19 |
|---|---|---|---|---|
| E3.5 | + | + | + | + |
| E6.5 | | | | |
| - trophoblast | + | + | + | + |
| - visceral endoderm | - | + | + | - |
| E9.5 | | | | |
| - yolk sac | - | + | + | - |
| - trophoblast | + | + | + | + |
| - amnion | - | + | + | + |
| - embryo primitive gut | + | + | + | + |
| - embryo surface Ectoderm | (+) | + | + | + |
| - embryo notochord | (+) | + | + | + |

Table.1.1. Expression of simple epithelial keratin proteins during early mouse development (modified from Lu et al., 2005)

In late morula and blastocyst stages, K7 and K8 form short filaments with K18 in the trophectoderm and the inner cell mass (Brulet et al., 1985; Jackson et al., 1980; Lu et al., 2005; Oshima, 1981; Paulin et al., 1980; Paulin, 1981). During later stages, K8 and K18, together with K7 and K19, are maintained in all simple epithelia of the embryo proper and in the single-layered surface ectoderm until

periderm formation, which starts at E12 in the mouse. Transcription of K8 and K18 becomes restricted to periderm cells, which are finally shed off during later developmental stages (Bickenbach et al., 1995). Thus K7, K8, K18, and K19 are regarded as the bona-fide embryonic and simple epithelial keratins (Bi et al., 2005). K5 protein expression starts in the forelimb surface ectoderm as early as E9.25, while the expression of its partner, K14, begins at E9.75. From E9.25 to E9.75, K5 forms atypical filaments with K18 in a subset of forelimb epithelial cells. Thus, it can be concluded that during preimplantation mouse development, keratins are preferentially expressed in the trophectodermal lineage. This extra-embryonic lineage forms the fetal–maternal interface within the placenta. Table 1.2 summarizes keratin expression during early mouse embryogenesis.

## 1.4. The molecular basis of development of primitive endoderm derived yolk sac and extra-embryo derived placenta

### 1.4.1. The mouse yolk sac – the only pre-hepatic site for hematopoiesis

Twenty four hours following formation of the blastocyst, two morphologically distinct populations from the inner cell mass (ICM) are established, one forming the epiblast which gives rise to the embryo, and the other to the primitive endoderm, which gives rise the extra-embryonic tissue, the yolk sac. However, the fate determination of the individual cells within the inner cell mass is highly debated. These inner cells are produced by two successive rounds of asymmetric division, first, during the 8- to 16-cell transition and then during the 16- to 32-cell transition. Cells that express K8 within the ICM were found to be derived almost exclusively from secondary inner cells (Chisholm and Houliston, 1987).

The primary function of the yolk sac epithelium is endocytic absorption of macromolecules from the uterine lumen and to maintain permeability barriers between the maternal (uterine) compartment and underlying fetal compartments (Jollie, 1990). The intracellular junction between these endoderm cells consists of the typical zonulae occludentes, gap junctions, and desmosomes (King, 1982). An additional function of the yolk sac is its role as a haematopoietic stem cell niche.

The yolk sac serves as the first site of hematopoiesis and vasculogenesis for supporting the developing embryo. It contains spontaneously developed blood islands, formed by clusters of hematopoietic cells surrounded by a layer of vascular endothelial cells at around E7.5. Primitive hematopoiesis is initiated by producing primitive, nucleated erythroblasts from unique erythroid progenitors, termed the EryP-CFC. These progenitors expand transiently in numbers within the yolk sac and are ultimately extinguished by E9.0 (McGrath and Palis, 2005). Hematopoiesis moves on to other sites later on within the embryo proper as development proceeds (Baron, 2003). After E10.5, the intra-

embryonic mesoderm, at sites called the aorta-gonad-mesonephros (AGM), generates the first definitive hematopoietic stem cells (HSC) that eventually colonise the fetal liver (Dzierzak, 2003). The third source of HSC's lies in the labyrinth region (discussed in section 1.4.2) at mid-gestation. These cells eventually mobilize into the fetal liver (Gekas et al., 2005; Ottersbach and Dzierzak, 2005).

### 1.4.2. The mouse placenta

The placenta begins to form at a time when the metabolic requirement of the growing mouse embryo approaches the capacity of the yolk sac. It is formed from the fusion of two tissues: the allantois, which is derived from extra-embryonic mesoderm and eventually develops into the umbilical cord, and the extra-embryonic chorion, which is derived from the polar trophectoderm overlying the inner cell mass of the blastula. The placenta mediates implantation and establishes the interface for nutrient and gas exchange between the maternal and fetal circulation. Moreover, it initiates maternal recognition of pregnancy, alters the local immune environment and maternal cardiovascular and metabolic functions through the production of paracrine and endocrine hormones (Cross et al., 2002a). Abnormalities in any one of these functions can be associated with mild outcomes like intrauterine growth restriction to severe outcomes manifesting in implantation failure and embryonic, fetal or perinatal death. Studies of many mouse mutants with disrupted placental development indicate that signaling interactions between the placental trophoblast and embryonic cells have a key role in placental morphogenesis and embryonic development (Cross et al., 2002a).

#### 1.4.2.1. General anatomy and development of the mouse placenta

The fetal placenta is composed of an outer epithelial layer derived from the trophectoderm and an inner vascular and stromal layer derived from the allantois (extra-embryonic mesoderm) (Cross et al., 2002b). The trophoblast layer of the placenta arises from the first cell type to differentiate in the mammalian embryo — the outer trophectoderm layer of the blastocyst (Fig.1.6). By E3.5 of development, two distinct cell lineages are formed: the outer, specialized trophectodermal epithelium, which pumps fluid internally to form the blastocoelic cavity, and the inner cell mass (ICM). Around the time of implantation at E4.5, different trophoblast cell types begin to form. The trophectoderm cells overlying the ICM continues to proliferate and gives rise to the diploid extra-embryonic ectoderm and the ectoplacental cone of the early postimplantation conceptus (Copp, 1979) (Fig.1.6). The trophectoderm cells that are not adjacent to the ICM stop dividing but continue to endoreduplicate their DNA to form trophoblast giant cells. In the postimplantation embryo, more giant cells form from the outer regions of the ectoplacental cone and surround the entire conceptus. As development proceeds, the extra-

embryonic ectoderm expands to form the chorionic epithelium, which is lined by a thin layer of mesothelial cells. The allantois arises from the mesoderm at the posterior end of the embryo and makes contact with the chorion at around E8.5. This event is termed chorioallantoic fusion, although no actual cell fusion takes place. After hours of allantoic attachment, folds appear in the chorion that marks the sites where feto-placental blood vessels grow in from the allantois to generate the fetal components of the placental vascular network.

The trophoblast, with its associated fetal blood vessels, undergoes extensive villous branching to create a densely packed structure called the labyrinth. Coincident with the onset of morphogenetic branching, chorionic trophoblast cells begin to differentiate into two layers of syncytiotrophoblast cells that are in direct apposition to the endothelial cells of the fetal-derived blood vessels. An additional mononuclear cell type of unknown origin and function remains outside the syncytiotrophoblast layer (Rossant and Cross, 2001). The trophoblast layer continues to specialize throughout gestation and, in general, fulfils two functions in every mammalian species. First, it generates the extensive surface area for nutrient exchange and provides the barrier between the maternal and fetal circulation. Second, trophoblast cells interact closely with the uterus and produce hormones that target maternal physiological systems and promote maternal blood flow to the implantation site. The trophoblast giant cells and spongiotrophoblast cells produce many specialized products like hormones [e.g. placental lactogens (Soares et al., 1996)], angiogenic factors [e.g. proliferin (Groskopf et al., 1997) and vascular endothelial growth factor (Achen et al., 1997; Vuorela et al., 1997)] and tissue re-modelling factors [e.g., matrix metalloproteinases (Teesalu et al., 1999) and urokinase type plasminogen activator (Teesalu et al., 1998)]. Hence, the mouse placenta behaves as a highly specialized unit that is supported by other cells involved in both its structure and function in fetal–maternal exchange.

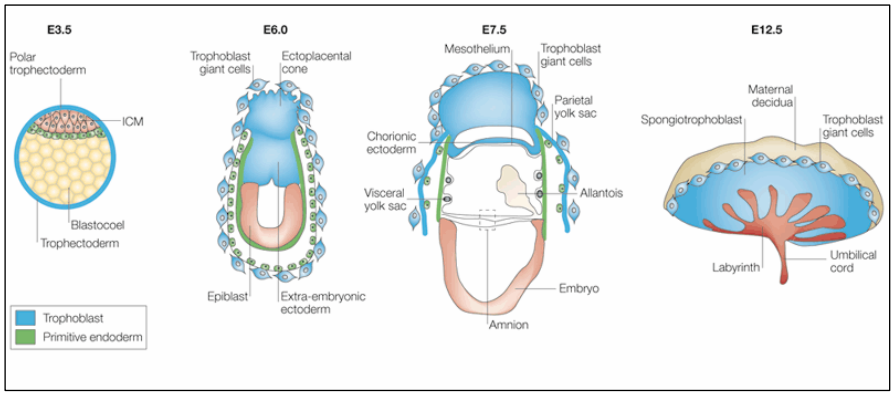


Fig.1.6. Placental development in the mouse. Early development of the mouse embryo from embryonic day (E) 3.5–12.5, showing the origins of the extra-embryonic lineages and the components of the placenta. ICM, inner cell mass (Adapted from Rossant and Cross, 2001).

### 1.4.2.2. Structures for transport functions in the mouse placenta

Survival and growth of the fetus are critically dependent on the placenta. It forms the interface between the maternal and fetal circulation, facilitating metabolic and gas exchange as well as fetal waste disposal. In addition, the placenta produces hormones that alter maternal physiology during pregnancy and forms a barrier against the maternal immune system (Cross et al., 2003). In humans and rodents, the fully developed placenta is composed of three major layers: the outer maternal layer, which includes decidual cells of the uterus as well as the maternal vasculature that brings blood to/from the implantation site; a middle "junctional" region, which attaches the fetal placenta to the uterus and contains fetoplacental (trophoblast) cells that invade the uterine wall and maternal vessels; and an inner layer, composed of highly branched villi that are designed for efficient nutrient exchange (Rossant and Cross, 2001). The villi are bathed by maternal blood and are composed of outer epithelial layers that are derived from the trophoblast cell lineage and an inner core of stromal cells and blood vessels. At E9.0, immediately after chorioallantoic fusion occurs, primary villi begin to develop, evenly spaced across the chorionic surface (Cross et al., 2003), and blood vessels soon fill in the villous folds (Rossant and Cross, 2001) (Fig.1.7). This vascular invasion of the chorion requires active participation of chorion trophoblast and allantoic mesoderm. The branchpoints are actively selected by clusters of chorion trophoblast cells which branch extensively into villi.

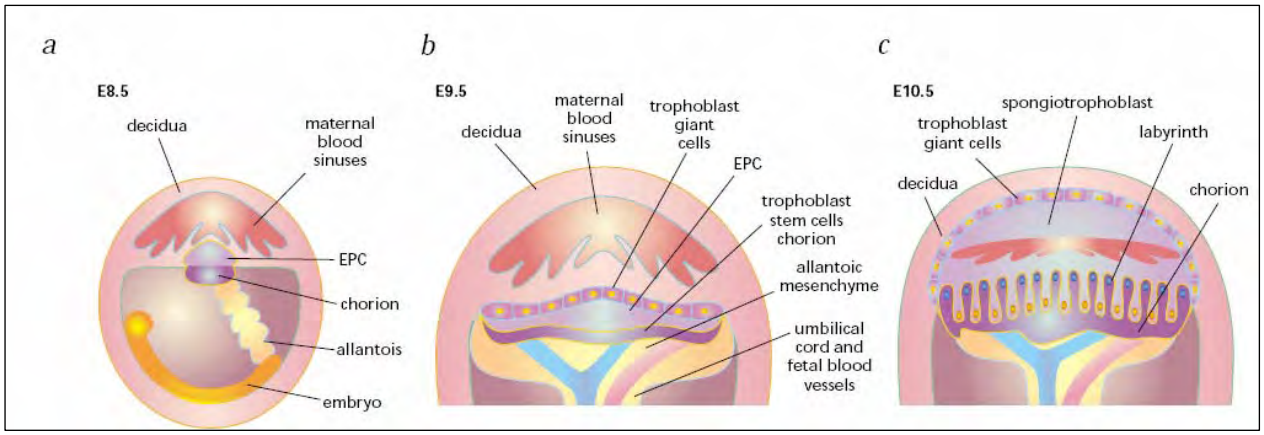


Fig.1.7. Development of transport structures during mid-gestation mouse development. (a) Formation of placenta by fusion of the extra-embryonic mesoderm derived allantois and the extra-embryonic chorion. (b) The fetal vessels from allantoic mesoderm penetrate the chorion and invade the labyrinth. Syncytiotrophoblast (indicated in purple) forms around the developing fetal vessels. Maternal blood sinuses also enter the labyrinth and supply blood to the fetal vessels across the syncytiotrophoblast barrier. (c) Trophoblast cells fuse, forming syncytiotrophoblasts, and the three layers (allantoic mesoderm, interstitial syncytiotrophoblasts and chorion) come together to form the haemotrichorial labyrinth. Integration of fetal and maternal blood vessels within the labyrinth is critically dependent on the differentiation of the trophoblast stem cells to syncytiotrophoblasts (Modified from Rinkenberger and Werb, 2000).

Nutrients are transferred across the placental barrier via several mechanisms, including passive diffusion, facilitated diffusion, and active transport (Doughty et al., 1996). A significant amount of solute

flux across the mouse placenta is achieved by passive diffusion (Sibley et al., 2004). Therefore, in addition to the overall surface area and permeability (Doughty et al., 1996), diffusional distance is a major factor influencing overall diffusional capacity of the placenta. In mice, a trilaminar layer of trophoblast cells separates the fetal capillary from the maternal sinusoids: a bilayer of syncytiotrophoblast surrounds the fetal blood vessel endothelium and a layer of mononuclear cells lines the maternal blood sinuses (Adamson et al., 2002) (Fig.1.8). Consequently the nutrients, gases, and waste must diffuse or be transported across four layers to get from one blood compartment to the next.

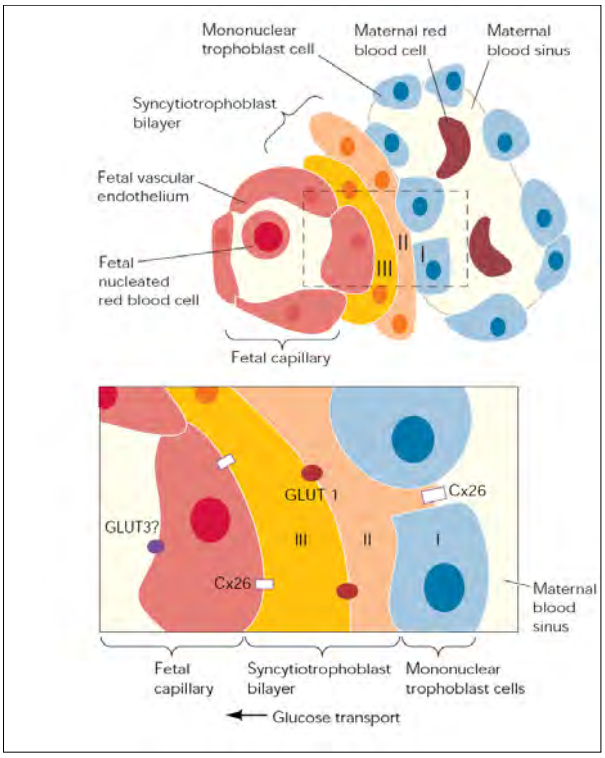


Fig.1.8. Interaction between trilaminar trophoblast layer and blood spaces within the labyrinth. The trilaminar trophoblast layer consists of a bilayer of syncytiotrophoblast cells (layers II and III) that surround the fetal blood vessel endothelium and a mononuclear layer of trophoblast cells (layer I) that lines maternal blood sinusoids. Nutrients such as glucose must be transported through four cell layers to get from the maternal blood space into fetal blood vessels. Cx26 and GLUT1 have been shown to aid in the transport of glucose (Adapted from Watson and Cross, 2005).

A common feature among most of the mouse mutants that die at mid-gestation is the reduced ability to transport nutrients, which results in fetal growth restriction or, under more serious circumstances, embryonic death. Most of these mutants have defects in the establishment or maturation of the placental villi, which in mice comprise the labyrinth layer. The labyrinth layer begins to develop at E9.0 and becomes larger and more extensively branched until birth (E18.5–19.5) (Adamson et al., 2002). Maternal and fetal blood flows in a countercurrent manner within the labyrinth to maximize nutrient transport (Adamson et al., 2002). If the labyrinth is not appropriately vascularized with suitable patterning, branching, and dilation, placental perfusion is impaired. This results in poor oxygen and

nutrient diffusion (Pardi et al., 2002), eventually leading to embryonic lethality. When morphogenesis of the labyrinth is diminished, one of the most obvious differences is that the layer remains cell dense and there are fewer maternal and fetal blood spaces. There is strong evidence that the trophoblast cells, which are of epithelial origin, regulate fetal vascularization of the placenta. This comes from the observation that the receptors and/or signaling proteins of key signaling systems like Fgfr2, Met, Sos1, Mek1, Gab1 and Fzd2, are either exclusively expressed in the trophoblast compartment and/or their function is only required in the trophoblast compartment (rev. in Rossant and Cross, 2001). Therefore, in the vast majority of labyrinth mutants, the differences are likely to be secondary effects, and only few mutants exist with primary vascular defects. Some of these mutants with a primary vascular defect includes vascular cell adhesion molecule, VCAM-1 (Kwee et al., 1995), connexin- 45 (Kruger et al., 2000) and notch signaling genes (Fischer et al., 2004; Krebs et al., 2000).

Given that keratins are expressed in all embryonic epithelial cells, one might expect phenotypes with altered embryonic and extra-embryonic development.

## 1.5. Analysis of keratin function

In a quest to analyse keratin function, a number approaches have been undertaken in the past. These include identification of keratin associated proteins, assessing properties of *in vitro* cultured cells transfected with mutant keratins and *in vivo* approaches (Coulombe and Omary, 2002; Herrmann et al., 2003). The two former routes have led to limited success, since cell culture models presently available, in combination with a limited number of function-assessing assays, have not yielded appropriate conditions to study keratin function. On the other hand, mouse genetics has been most rewarding and has identified a vital role of keratins in certain epithelia. The analysis of these model systems carried out so far suggests that keratins have a major impact on cell architecture, cell size and proliferation depending on cell context but do not act as major regulators of epithelial differentiation.

### 1.5.1. Knockout approaches

Gene knockouts of 13 keratins analyzed so far has demonstrated phenotypes ranging from major defects causing embryonic lethality or skin fragility to subtle and late onset liver alterations (Coulombe and Omary, 2002; Herrmann et al., 2003). Deletions of K5 and of K14, both of which are expressed in basal epidermis, cause very extensive tissue fragility and perinatal death (Herrmann et al., 2003). However, the deletion of K10, which is expressed in suprabasal epidermis and represents about 30% of total epidermal protein, caused no structural defect. This is due to a compensatory effect from

K14 which otherwise is normally restricted to basal cells. This suggested that at least some K10-specific functions are replaceable by K14. In older mice, however, the absence of K10 led to an increased basal cell proliferation and cell turnover in epidermis, probably caused by accelerated keratinocyte turnover via activated p38 MAPK (Reichelt et al., 2004). Furthermore, the authors also identified that keratinocyte proliferation was regulated by interaction of K10 with 14-3-3σ. Whether this results from K10-specific functions or from the lower amount of K14 versus K10, has not been resolved yet (Reichelt et al., 2001). The above experiments have established that the primary keratin function is to provide resilience against mechanical strain in basal epidermis and in the tongue epithelium, most likely, because these epithelial compartments are exposed to severe mechanical stress. This coincides with data from mutation analysis of patients suffering from point mutations in the corresponding keratin genes (Irvine and McLean, 1999).

The function of keratins during embryonic development and in simple epithelia is less clear than in epidermis. All embryonic epithelia express at least the type I protein K18 and the type II protein K8, which are complemented by keratins K7, K19, K20, and K23 during the course of epithelial specialization (Hutton et al., 1998). Upon formation of the embryonic epidermis around E15, K8 and K18 are sequentially replaced by K5 and K14, typical of the proliferative compartment of stratified epithelia. The functional significance of this expression change is not clear at present. It has recently been shown, that in embryonic K5 knockout mice, K8 is able to compensate for K5 until E14.5, the time at which K8 expression ceases in the single-layered surface ectoderm (Lu et al., 2006). This suggests that an “embryonic” type keratin might be able to replace an epidermal one, if driven by an appropriate promoter. Mice deficient for K8 die from liver placental failure at E12.5 in the C57BL/6 strain of mice and display colonic hyperplasia in adult FVB/N mice (Baribault et al., 1994). The latter strain suffers from diarrhea, possibly resulting from the mislocalization of ion transporters in colonic epithelial cells (Toivola et al., 2004). Mice with a targeted deletion of either K18 or K19 develop normally, because these two keratins are co-expressed in embryonic epithelia. Hence they compensate for each other and form filaments with K8, although there is only a limited extent of sequence identity between K18 and K19 (Magin et al., 1998).

### 1.5.2. Keratin null mutants with mid-gestation phenotypes

Mice deficient for K8 die from placental failure at E12.5 in the C57BL/6 strain of mice. In order to clarify whether embryonic development requires keratins, the combined deletion of K18/K19 or of K8/K19 was carried out. As K18 and K19 represent the only type I keratins during early embryonic development, no filaments should form. In fact, all double-deficient mice died at E9.5 – E10 from

trophoblast fragility or from defects in the labyrinth layer formation, respectively (Hesse et al., 2000; Tamai et al., 2000). The K18/K19 double deficient embryos were accompanied by the deposition of K7/K8 aggregates in trophoblast cells, reminiscent of the deletion of the chaperone hsp40 which resulted in a similar keratin aggregate phenotype (Hunter et al., 1999). At this time of development, the embryo proper appeared normal in the absence of keratin filaments. This pathology was interpreted as a result of mechanical fragility by our lab, similar to keratinocyte fragility in EBS. Given the potential toxicity of K7/K8 aggregates in the K18/19 double-deficient embryos (Hesse et al., 2000), the precise function of keratins in development is still unclear and requires deletion of all 4 genes.

| Gene | | Comments | References |
|---|---|---|---|
| Type II | K4 | Compensation by K6 | Ness et al., 1998 |
| | K5 | K14 aggregates - gain of toxic function | Bousquet et al., 2001 |
| | K6a | Total compensation by K6b | Wojcik et al., 2000; Wojcik et al., 2001; Wong et al., 2000 |
| | K8 | Phenotype stain dependent, compensation by K7 | Baribault et al., 1994; Baribault et al., 1993 |
| Type I | K10 | Compensation by K14 | Reichelt et al., 2001 |
| | K14 | Compensation by K15 | Lloyd et al., 1995 |
| | K17 | Compensation by K16 | Wong et al., 2005 |
| | K18 | K8 aggregates - gain of toxic function | Magin et al., 1998 |
| | K19 | Compensation by K18 or K20 | Hesse et al., 2000; Tamai et al., 2000 |
| | K18K19 (double) | Aggregates of K8 and K7, gain of toxic function | Hesse et al., 2000 |
| Type I and Type II | K19 K8 (double) | Compensation by K7 and K18 | Tamai et al., 2000 |

Table.1.2. **Compilation of keratin null mutations**. A compilation of *in vivo* approaches that have been undertaken in order to characterize keratin function.

Another interpretation for the trophoblast fragility and embryonic death was provided by Oshima and colleagues. They argued that the absence of keratin filaments rendered trophoblast giant cells more susceptible to maternal TNF which would trigger an apoptotic response. This was based on the finding that K8 and K18 can moderate apoptosis by sequestering TNFRI and TRADD (Oshima, 2002). It appears that the protective role of K8 and K18 in apoptosis is independent of them being soluble, aggregated or assembled into a cytoskeleton. Data to support the notion that K8 and K18 regulate apoptosis via sequestration of the c-Flip protein (caspase 8 homologue FLICE-inhibitory protein) has also been reported (Gilbert et al., 2004). However, this hypothesis is controversial since Ku et al., have assessed c-Flip expression in livers of K8 and K18 null mice and in transgenic mice that express K18

Arg89Cys or K18 Gly61Cys mutants (Ku and Omary, 2006). They were unable to detect alterations in c-Flip levels in murine K8 null hepatocytes using two independent antibodies. Possibly, following death receptor stimulation, K8 may sequester the pro-apoptotic JNK thereby preventing JNK from phosphorylating pro-apoptotic nuclear transcription factor targets (He et al., 2002).

Taken together, the data regarding specific keratin function *in vivo* are conflicting and cannot be resolved by targeting individual genes or pairs of them, due to redundancy. Therefore, knockouts of individual keratin genes suffered from a problem seen in many, if not all knockouts of other gene family members, namely compensatory upregulation/stabilization of other gene family members (Table 1.1). Also, the precise expression pattern of keratins is unclear, especially with regard to epithelial stem cells. An approach to circumvent these problems is genetic ablation of all keratin genes and their sequential replacement with individual genes.

## 1.6. Large scale genome deletion approach

In order to achieve genetic ablation of all keratin genes, a large scale genome deletion approach was undertaken in this thesis, which involved gene targeting in mouse ES cells and the Cre-*loxP* system. It has previously been demonstrated that up to 10 Mb of the genome can be deleted without deleterious consequences (Zheng et al., 2000). The approach is based on two consecutive homologous recombination events, one at each end of the keratin cluster target locus in *cis* using two different targeting constructs followed by a Cre-mediated deletion of the keratin cluster. This approach is dealt with in detail in the chapter 2 “Aim and strategy”.

This thesis, however, has focused on the deletion of the keratin type II cluster along with a single type I keratin, K18, by taking the following into consideration.

- The keratin type II cluster contains at one end, the region coding for the type I keratin K18 (Hesse et al., 2001). K8 and K18 are the first keratins to be expressed during embryonic development in mice (Fuchs and Weber, 1994). Hence, by deleting the type II cluster alone, one would abolish formation of keratin filaments as well as avoid aggregates of the early type I keratins thereby circumventing dominant negative effects of the aggregates, if any.
- It has been reported that type II keratins precede type I keratins during early embryonic development (Lu et al., 2005). These results will identify the developmental stage and processes that rely on keratins and clarify whether protein aggregates or soluble keratins, if any, display important functions.

# 2. AIM AND STRATEGY

## 2.1. Aim

Generation of large scale genomic deletions, followed by replacement of individual genes has been instrumental in understanding development of model organisms, e.g. *Drosophila melanogaster*. Using the keratin multigene family as a paradigm, the major aim of this project was to elucidate whether individual family members have exclusive functions in epithelia of the mouse. Keratins have comparable functions in different tissues. The general function of keratin IF network is to endow epithelial cells with the mechanical resilience that they require to sustain incident mechanical stress and to aid in tissue repair following wounding (e.g. K6 and K17 in wound healing (Fuchs and Weber, 1994; Moll et al., 1982). Apart from these structural functions, regulatory functions for keratin pairs have also been reported (e.g. protective role of K8 during TNF (Oshima, 2002) and Fas mediated apoptosis (Ku et al., 2003), role of K8/K18 in c-Flip/ERK1/2 anti-apoptotic pathway (Gilbert et al., 2004) and K18 in metastasis (Fujii et al., 1988). This raises the question of functional significance of the multiplicity of keratin sequences. Is it that keratin genes have simply duplicated and diverged over evolution, but functionally the gene products are redundant? Or, did different keratin genes evolve to suit the particular functional needs of the tissues in which they are expressed? To begin to explore the answer to this fundamental issue of keratin biology, an approach to delete all type II keratins using the Cre/loxP based strategy was adopted. Deleting all the type II keratins which are expressed earlier than the type I keratins(Lu et al., 2005), would lead to keratin null situation since many reports confirm that the type I keratins are rapidly degraded in the absence of its filament forming type II counterpart (Caulin et al., 1997; Oshima, 2002).

## 2.2. Strategy based on the Cre/*loxP* system

The approach is based on two consecutive homologous recombination events, one at each end of the keratin cluster target locus in *cis* using two different targeting constructs followed by a Cre mediated deletion of the keratin cluster. However, for the restoration of the *hprt* function, the use of *hprt*-deficient ES cells such as AB2.2 (Ramirez-Solis et al., 1995) or HM-1 (Magin et al., 1992) is required. Nevertheless, this is a method of choice given the number of ready-to-use targeting vectors for the *hprt* selection system available from the Mutagenic Insertion and Chromosome Engineering Resource (Adams et al., 2004) (MICER; http://www.sanger.ac.uk/micer), rather than the use of retroviral vectors to

target the second *loxP* site (Lindsay et al., 2001; Su et al., 2000; Yan et al., 2004), and the panel of rearranged chromosomes that has been engineered (Adams et al., 2004; Zheng et al., 1999b).

### 2.2.1. Targeting constructs

The first of the two constructs consists a neomycin resistance gene for gene targeting, a *loxP* site, a 5'-half-*hprt* (hypoxanthine phosphoribosyl transferase) minigene (non-functional *hprt* fragment) for chromosome engineering and about 4-10 kb genomic DNA homologous to one end of the keratin cluster (Fig. 2.1A). Similarly, the second constructs contains a puromycin resistance gene, a *loxP* site, a 3'-half *hprt* minigene (non-functional *hprt* fragment) and about 4-10 kb genomic DNA homologous to the other end of the keratin cluster (Fig. 2.1B) (Ramirez-Solis et al., 1995). The constructs used for this purpose were isolated directly from genomic libraries of pre-made targeting vectors (Adams et al., 2004). The overall strategy is outlined in Fig.2.2.

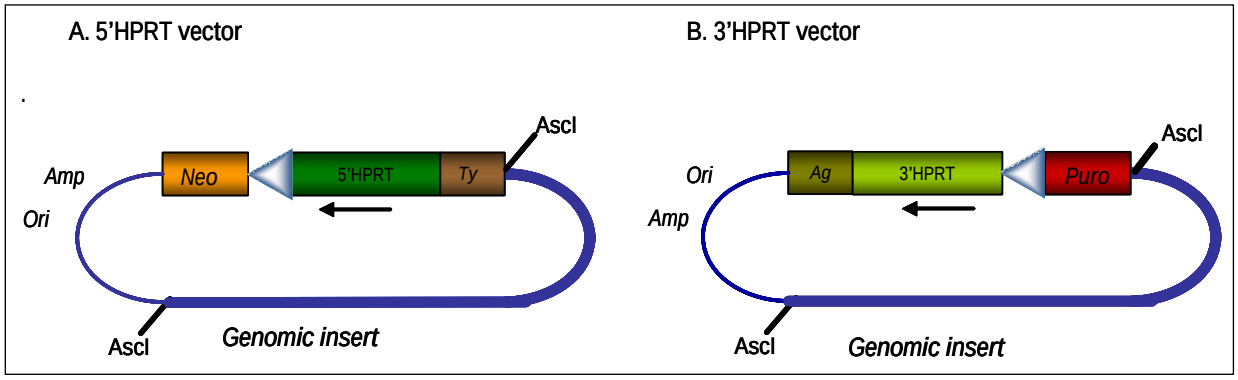


Fig.2.1. Targeting constructs for the Cre/*loxP* mediated deletion of the keratin type II cluster. A. 5' *hprt* vector. B. 3' *hprt* vector. The genomic sequence homologous to the ends of the targeted locus are flanked by rare *AscI* sites to aid in changing of the orientation of the *loxP* site by one sub-cloning step if required.

### 2.2.2. Homologous recombination

All targeting vectors have been prepared from isogenic chromosomal DNA (AB2.2 ES cell line). After the first step of targeting into AB2.2 mouse ES cell line using one of the targeting vectors mentioned above, antibiotic resistant clones that are positive for the homologous recombination event would be used for the second targeting step. Double targeted clones would be isolated and confirmed for homologous recombination events (Ramirez-Solis et al., 1995).

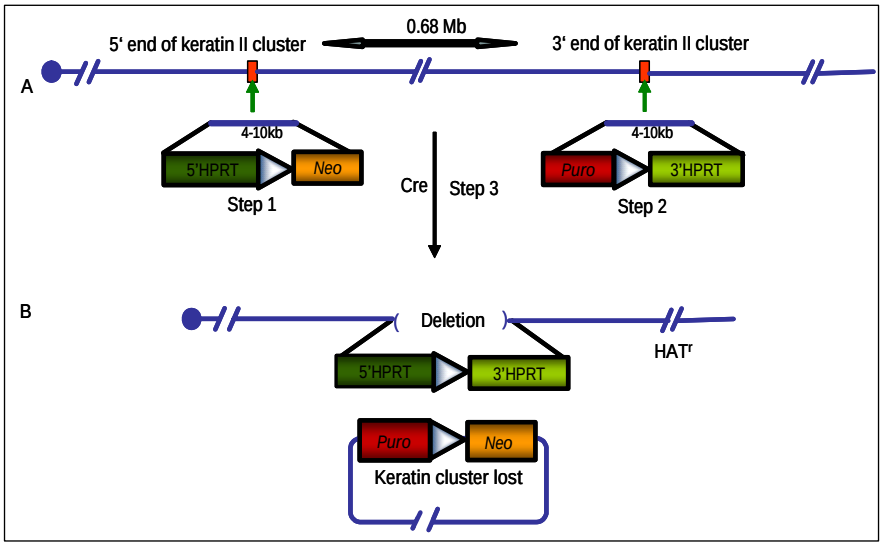


Fig.2.2. The Cre/*loxP* based chromosome engineering strategy in *cis*. A. Targeting of the 5' and 3' *hprt* vectors to either end of keratin type II cluster in two steps in mouse embryonic stem cells. Both the *loxP* sites are targeted in same orientation. B. Cre mediated recombination between two *loxP* sites of double targeted clones in *cis* (on the same chromosome) leading to a deletion of the keratin cluster thereby rendering the clones neomycin and puromycin sensitive due to the loss of the *Neo*- and *Puro*-carrying reciprocal product but HAT resistant.

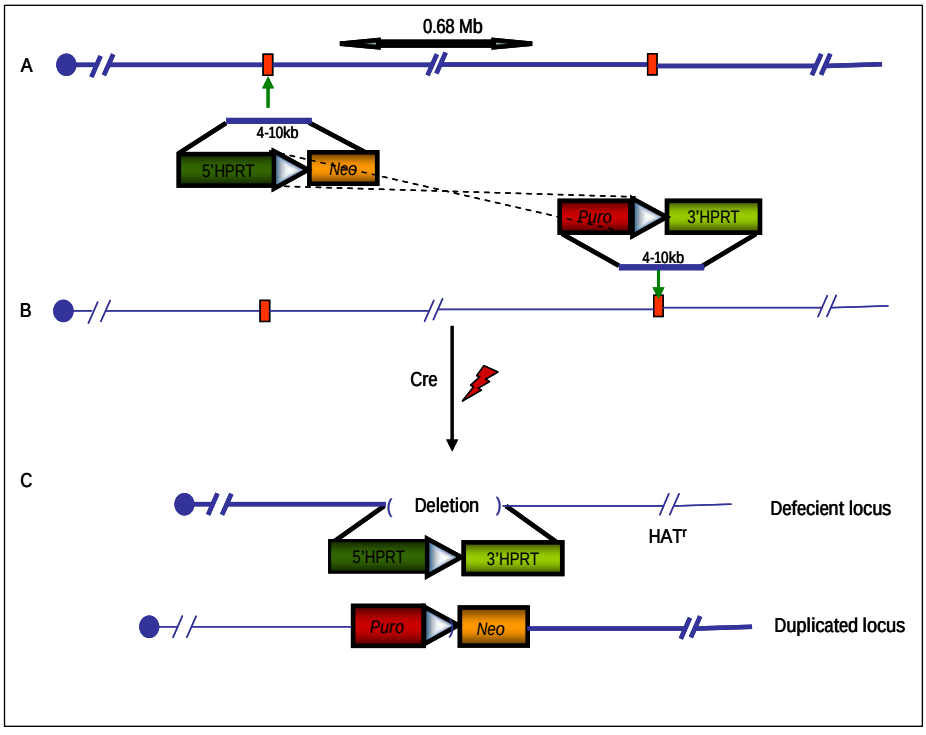


Fig.2.3. The Cre/*loxP* based chromosome engineering strategy in trans. A. Targeting of the 5' *hprt* vector to one end of keratin type II cluster B. Targeting of the 3' *hprt* vector to the other end of the cluster on the homologous allele (*trans*). C. Cre mediated recombination between two *loxP* in *trans* (on two different chromosome homologues) leading to a deletion that is neomycin and puromycin sensitive as well as duplication that is neomycin and puromycin resistant.

At least 50% of the recombination events would have occurred on the same chromosome (*cis*) (Fig. 2.2). A *cis* recombination event between two *loxP* sites in the same orientation, in the presence of Cre recombinase, will lead to the deletion of the *loxP* flanked keratin cluster sequence in a circular molecule (Fig.2.2), whereas a trans recombination event will lead to deletions and duplication events (Fig.2.3).

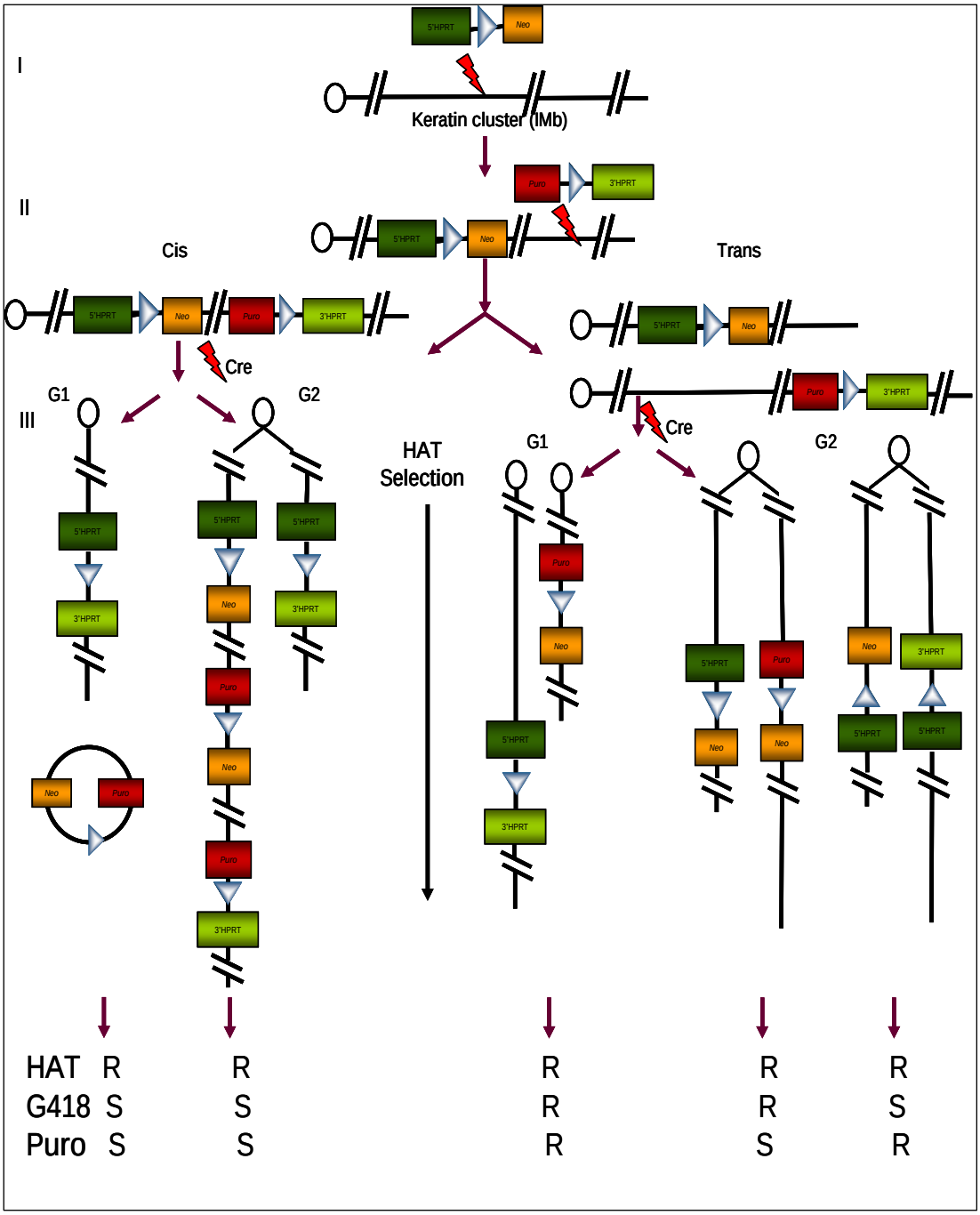


Fig.2.4. Engineering a deletion and/or a duplication in embryonic stem cells (modified from Yu Y *et al.*, 2001) I. Targeting of the 5' vector to the 5' end of the keratin cluster. II. Targeting of the 5' vector to the 5' end of the target locus. Both cis and trans recombination events are shown. III. Recombination products after Cre recombination in G1 and G2 phases of the cell cycle. In G2, four *loxP* sites are located on duplicated chromatids, and recombination events will result in various products. Drug selection will help with identifying the desired rearrangements.

Complex recombination products can arise when recombination takes place between sister chromatids and between the non-sister chromatids in the G2 phase of cell cycle (Fig.2.4). Recombination between the *loxP* sites in *cis* unites the two non-functional 5'- and 3'- *hprt* fragments and reconstitutes a functional *hprt* minigene. This provides a positive selection for this event when the ES cells are cultured in medium that contains hypoxanthine, aminopterin and thymidine (HAT). Recombination between the *loxP* sites in *trans* leads to a mixture of those with the desired chromosomal deletion and with the undesired chromosomal duplication (Fig.2.3), which have been produced due to recombination events in the G1 and G2 phases of the cell cycle(Yu and Bradley, 2001).

Since the distance of the two integration sites would be large, double labeled FISH using empty 5' and 3' *hprt* vectors as probes would be used to identify double targeted clones in *cis.*

### 2.2.3. Generation and analysis of mice lacking keratin type II cluster

Chimeras generated by injecting the double targeted ES cells in *cis* into mouse blastocysts would yield progeny devoid of the keratin type II cluster in one allele by interbreeding the chimeras with wild type C57Bl6. The presence of coat color markers in targeting vectors, allows an easy discrimination of mice carrying the recombined chromosome (Zheng et al., 1999a). Inbreeding of these heterozygotes will yield progeny null for the keratin type II cluster. The resulting mutants can be analyzed for tissue fragility defects by histology, immunocytochemistry and electron microscopy. Given the mechanical and non-mechanical functions of keratins, particular focus of the analysis on the mice will be on the integrity of cells, proliferation, apoptosis, translational control and alteration in p38 signaling.

# 3. MATERIALS AND METHODS

## 3.1. Materials

### 3.1.1. Chemicals used

Unless otherwise stated, chemicals were purchased from Serva (Heidelberg, Germany), Sigma (Deisenhofen, Germany), Roche (Basel, Switzerland), Fermentas (St.Leon-Rot, Germany), Merck (Darmstadt, Germany), Fluka (Deisenhofen, Germany), Invitrogen Life Technologies (Karlsruhe, Germany), or Applichem (Darmstadt, Germany).
All cell culture solutions, buffers, DNase I, antibiotics & normal goat serum were from Sigma (Deisenhofen, Germany), Invitrogen/Life technologies (Karlsruhe, Germany) & GibcoBRL (Karlsruhe).

In vitro High Prime DNA labeling kit was from purchased from Roche (Basel, Switzerland).

[$\alpha$-$^{32}$P]-dCTP was obtained from Amersham Biosciences (Buckinghamshire, UK).

Restriction enzymes, protein and DNA markers dNTPs and NTP's were from Fermentas (St.Leon-Rot, Germany).

PCR reaction mix (Buffers, Taq polymerase enzyme, $MgCl_2$), RT-PCR kit were purchased from Invitrogen/Life technologies (Karlsruhe, Germany).

### 3.1.2. Ready-to-use solutions / reagents

Acetic Acid
Acrylamide solution (37.5:1) Acrylamide/Bisacrylamide for protein-SDS-gel
Chloroform
Colcemid 10 $\mu$g/ml (Roche, 295892), for Karyotyping of ES cells and for FISH
DAB substrate (Biogenex, DC138R006)
Dimethylsulfoxide (DMSO)
ES-PBS- (Dulbecco's Phosphate buffered saline) for ES cell culture
Ethanol
Ethidiumbromide, 10mg/ml
Formaldehyde, 37 %
Isopropanol

Mayer's Hemalum Solution (Merck, 9249)

M2 Medium (Sigma) for resuspending ES cells for blastocyst injection

Methanol

ProLong® Gold antifade reagent (Molecular Probes, P36930)

Roti-Phenol TE equilibrated for purification of nucleic acids

TEMED for protein-SDS gel

Tissue-Tek OCT

TRIzol for isolation of RNA

Xylene

Taq-Polymerase (Invitrogen, 10342-020)

Tween-20

Triton-X100

DPX Mountant for histology (Fluka, 44581)

### 3.1.3. Kits

Biotin/Streptavidin system (BioGenex, HK340-9K)

High Prime DNA labeling system (Roche, 11585584001)

QIAEX II Gel Extraction Kit (Qiagen, 20021)

Qiagen Plasmid Maxi kit (Qiagen, 12163)

Qiagen Plasmid MIDI Kit (Qiagen, 12143)

Superscript II Reverse Transcriptase (Invitrogen, 18064-014)

### 3.1.4. Solutions for eukaryotic cell culture and blastocyst injections

| Name | Final Concentration | Constituents and their amounts |
|---|---|---|
| ES WT | | Was prepared by combining the following; |
| Medium / | | 500 ml Glasgow-MEM |
| Feeder | 15% | 84 ml FCS, ES-culture pre-tested |
| Medium | 1mM | 5.6 ml Na-pyruvate, 100 mM |
| | 2mM | 5.6 ml Glutamax™-1, 200 mM |
| | 1x | 5.6 ml Non-essential aminoacids, 100x |
| | 1:50000 | 0.54 ml home made LIF |

| | | |
|---|---|---|
| | 0.007% | 0.91 ml Monothioglycerol<br>Medium was stored at 4°C and used within a week. |
| Gelatine stock | 1% | Was prepared by adding 5 g Gelatine (G2500 swine skin Type I) to cell culture grade water and autoclaved twice. 0.1% working dilution was prepared in cell culture grade water. The stock and working stock solutions were stored at 4° C. |
| ES trypsin | <br>1 mM<br>0.025% | 400 ml Cell culture grade PBS<br>100 ml ES-EDTA-Solution (1.85 g/l in cell culture grade water)<br>5 ml Trypsin, 2.5%<br>Solution was stored at -20° C and once thawed, it was stored at 4° C. |
| ES freezing medium | <br>20%<br>20% | 18.75 ml ES-WT Medium<br>1.25 ml ES culture tested FCS<br>5 ml Dimethylsulphoxide (DMSO) |
| 10x HEPES buffered saline (HBS buffer) | <br>20 mM<br>2.5 M | 180 ml cell culture grade PBS<br>16 g Sodium chloride<br>0.74 g Potassium chloride<br>0.252 g Disodium hydrogen phosphate<br>10 g HEPES, 1 M<br>240 µl Glucose, 100x<br>pH was adjusted to 7.2 and the volume was adjusted to 200 ml. The solution was filtered through 0.1 µm pore filter and stored at -20° C. To prepare 1x HBS, 10x HBS was diluted 10 times with sterile water which brings the pH to 7.05. |
| Mitomycin C Stock | 2 mg/ml | Mitomycin C stock of 2 mg/ml was prepared just before use, and feeder inactivation was performed at a concentration of 2 µg/ml. |
| G418 Stock | 100 mg/ml | Stock was prepared by dissolving 1000 mg of G418 sulfate (Biochrom AG, A291-25) in 10ml cell culture grade water, filter sterilized, and stored at -20° C. Final concentration used was 350 µg/ml. |
| Puromycin Stock | 3 mg/ml | Stock was prepared by dissolving 3 mg of puromycin dihydrochloride (Calbiochem, 540411) in 1 ml cell culture grade water, filter sterilized, and stored at -20° C. Final concentration used was 3 µg/ml. |

| | | |
|---|---|---|
| HAT | 1x | HAT Media Supplement (50x) Hybri-Max™. 1 vial was reconstituted with 10 ml sterile cell culture medium. Final working concentration: 100 µM hypoxanthine, 0.4 µM aminopterin, 16 µM thymidine. |
| Pregnant Mares Serum Gonadotropin (PMSG) Stock | 500 U/ml | Intergonan for animals (Intervet, Germany). Stock was prepared by dissolving 1 aliquot of 1000 I.E (lyophilized powder) in 2 ml 0.9 % sodium chloride solution, aliquoted and stored at -80°C. Final concentration used to induce superovulation in mice was 50 U/ml. |
| Human Chorionic Gonadotropin (HCG) stock | 500 U/ml | Predalon for animals (Organon, Germany). Stock was prepared by dissolving 1 aliquot of 5000 I.E (lyophilized powder) in 10 ml 0.9% sodium chloride solution, aliquoted and stored at -80°C. Final concentration used to induce superovulation in mice was 50U/ml. |

### 3.1.5. Solutions for DNA Analysis

| Name | Final Concentration | Constituents and their amounts |
|---|---|---|
| Sodium acetate | 3 M | 40.82 g Sodium acetate in 100ml water. pH was adjusted to 5.2 with acetic acid and stored at room temperature. |
| DNA loading buffer | 30% | Ficoll Type 400 |
| | 100 mM | 3.72 g EDTA |
| | 0.25% | 125 mg Bromphenolblue |
| | 0.25% | 125 mg Xylenecyanol |
| | 0.25% | Orange G |
| | 2% | 20% SDS |
| Lysis buffer | 100 mM | 10 ml of 1 M Tris-HCl |
| | 5 mM | 1 ml of 0.5 M EDTA |
| | 0.2% | 1 ml SDS-solution, 20 % |
| | 200 mM | 4 ml 5 M NaCl |
| | | The above ingredients were added to 84ml of DNase/RNase free water and stored as 10ml aliquots at -20°C. |
| 10 x TBE | 0.89 M | 54 g Tris-base |
| | 0.89 M | 27.5 g Boric acid |

| | | |
|---|---|---|
| | 8 mM | 20 ml from 0.5 M pH 8 EDTA<br>The solution was autoclaved and stored at room temperature. |
| 20x SSC transfer buffer | 1.5 M<br>0.5 M | 175.3 g NaCl<br>88.2 g Sodium citrate<br>pH was adjusted to 7.0 with a few drops of 10N NaOH solution. The volume was adjusted to 1L and sterilized by autoclaving. |
| DNA denaturation solution | 0.4 M | 16 g NaOH in 1 L of water. Stored at room temperature. |
| Hybridization buffer | 50%<br>5x<br>5x<br>1%<br>0.1 mg/ml<br>10% | 250 ml Formamid ultrapure<br>125 ml 20x SSC<br>5ml 100x Denhardt's solution (Eppendorf, 0032007.155)<br>25 ml 20% SDS<br>5ml DNA, MB-grade; from fish sperm 10 mg/ml<br>50 g Dextransulfate<br>The contents were mixed and the volume was adjusted to 500 ml with sterile water, aliquoted and stored at -20°C. |
| Proteinase K solution | 20 mg/ml | 1 g Proteinase K (Applichem, A38300025) was added to 50 ml DNAase/RNAse free water, aliquoted and stored at -80°C. |
| RNase Solution | 20 mg/ml | 500 mg RNase was dissolved in 25 ml DD water and heated for 15 min at 95°C. Aliquoted and stored at -80°C. |
| TBE (10 x) | 900 mM<br>900 mM<br>25 mM | 109 g Tris-base<br>55.6 g Boric acid<br>0.93 g EDTA<br>Dissolved in 1L water and pH adjusted to 8.3. |
| TE buffer | 10 mM<br>1 mM | 121 mg Tris<br>37.2 mg EDTA<br>Dissolved in 100 ml DD water, pH adjusted to 8.0 and sterilized by autoclaving. Stored at RT. |
| 10x Nick translation (NT) buffer | 0.5 M<br>50 mM<br>0.5mg/l | 250 µl 2M Tris-HCl, pH 8.0<br>50 µl 1M Magnesium Chloride<br>0.5mg BSA<br>Adjusted volume to 1ml and stored at –20°C. |
| DNAse | 1 mg/ml | 3 mg DNAse I |

| | | |
|---|---|---|
| solution | 50%<br>50% | 0.5 ml 0.3 M NaCl<br>0.5 ml glycerol<br>Stored at -20°C. |
| dNTP's for nick translation | 0.5 mM<br>0.5 mM<br>0.5 mM<br>0.1 mM | 25 µl 2 mM dATP<br>25 µl 2 mM dCTP<br>25 µl 2 mM dGTP<br>5 µl 2 mM dTTP<br>Volume was adjusted to 100 µl with DNAase free water and stored at -20°C. |
| β-Mercaptoeth--anol | 0.1 M | 69 µl of 14.4 M β-mercaptoethanol in 10 ml of DD water. Stored at 4°C. |
| Pepsin stock solution | 10% | 1 g of pepsin dissolved in 10 ml of DD water. Stored at –20°C.<br>Pepsin working dilution: 50 µl pepsin stock solution was added to 70 ml of DD water containing 700 µl of 1 M HCl. |
| 10x PBS | 137 mM<br>2.7 mM<br>10 mM<br>2 mM | 40 g NaCl<br>1 g KCl<br>89 g $Na_2HPO_4.2H_2O$<br>12 g $KH_2PO_4$<br>Salts were dissolved in 4.5 L water, pH was adjusted to 7.4 with HCl, and volume was adjusted to 5 L with water and autoclaved. Stored at RT. |
| Magnesium chloride | 1 M | 101.65 g $MgCl_2$ in 500 ml water. |
| PBS-Magnesium Chloride | 0.25 M | 5 ml 1 M Magnesium chloride<br>95 ml 1x PBS<br>Prepared fresh. |
| Denaturation mix for FISH | 2x | 100 µl 20x SSC<br>200 µl DNase/RNase free water<br>700 µl de-ionised formamide<br>pH was adjusted to 7.0 and prepared fresh. |
| Washing solution for FISH | 4x<br>0.2% | 140 ml 20x SSC<br>1.4 ml Tween 20<br>560 ml Distilled water |

| | | |
|---|---|---|
| Blocking solution for FISH | 3% | 0.09 g BSA<br>3 ml 4x SSC/Tween 20 solution |
| Detection solution for FISH | | Blocking solution : Washing solution : : 1:2 |

### 3.1.6. Solutions for Bacterial Cultures

| Name | Final Concentration | Constituents and their amounts |
|---|---|---|
| Ampicillin solution | 5% | 50 g ampicillin in 50 ml of water. Sterile filtered. End concentration used was 100 mg/ml. |
| LB Agar | 2% | 1 L LB Medium<br>32 g LB Agar in 1 L water<br>Sterilized by autoclaving. Antibiotics were added at 55°C and plates were poured. |
| LB Medium | | 25 g LB medium was dissolved in 1 L water and sterilized by autoclaving. |

### 3.1.7. Solutions for Protein Biochemistry

| Name | Final Concentration | Constituents and their amounts |
|---|---|---|
| 5x Laemmli sample buffer | 50 mM | Sodium phosphate pH 6.8 |
| | 5% | SDS |
| | 40 mM | DTT |
| | 5 mM | EDTA |
| | 5 mM | EGTA |
| | 20% | Glycerol |
| | 0.01% | Bromophenol blue |
| | | Solution was stored at -20°C and freeze/thawed not more than 5 times. |
| APS | 10% | 1g Ammonium persulphate in 10ml water.<br>Stored at 4°C for not longer than 1 month. |
| Stacking gel | 0.5 M | 15.1 g Tris-base |

| | | |
|---|---|---|
| buffer (Upper Tris) | 0.4% | 1 g SDS<br>Volume made up to 250 ml after adjusting pH to 6.8, sterile filtered and stored at 4°C. |
| Separating gel buffer (Lower Tris) | 1.5 M<br>0.4% | 181.7 g Tris<br>4 g SDS<br>Volume made up to 1 L after adjusting to pH 8.8, sterile filtered and stored at 4°C. |
| SDS-running buffer (1x Laemmli buffer) | 23 mM<br>190 mM<br>0.1% | 2.78 g Tris Base<br>14.26 g Glycine<br>5 ml 20% SDS stock<br>The contents were mixed in 1 L water and pH was adjusted to 8.8. Stored at room temperature. |
| Coomassie staining solution | 0.4%<br>5 %<br>40% | 1.0 g Coomassie Brilliant Blue G-250<br>25 ml Acetic Acid<br>200 ml Methanol<br>Volume was adjusted to 500 ml with distilled water, filtered through a Whatmann filter paper and stored at room temperature. Solution was used more than once. |
| Coomassie destaining solution | 10%<br>30% | 50 ml Acetic Acid<br>150 ml Methanol<br>Solution made up to 500 ml with water. |
| Ponceau S staining solution | 0.5%<br>1% | 0.5 g Ponceau S<br>1 ml Acetic acid<br>Contents were dissolved in 100 ml distilled water and filtered; Solution was stored in dark at room temperature. |
| Transfer buffer (1x Towbin buffer) | 25 mM<br>192 mM<br>0.1%<br>10% | 3.028 g Tris<br>14.41 g Glycine<br>1 g SDS<br>100 ml Methanol<br>The contents were dissolved in 1 L water, and pH was adjusted to 8.3. Solution was stored at room temperature. |
| 10x Tris buffered saline (TBS) | 0.1 M<br>1.5 M | 12.1 g Tris<br>87.6 g NaCl<br>Contents were dissolved in 750 ml water, pH was adjusted to 7.5 |

| | | |
|---|---|---|
| | | and the volume was made up to 1 L. Solution was sterilized by autoclaving and stored at room temperature. |
| Western washing buffer | 1x<br>0.1% | 100 ml 10x TBS<br>1 ml Tween 20<br>Volume was made up to 1 L with water. |
| Blocking solution | 5%<br>1x<br>0.5% | 5 g Skimmed milk (Sucofin)<br>100 ml 10x TBS<br>1 ml Tween 20<br>Always prepared fresh. |
| Alternative blocking solution | 5%<br>1x<br>0.5% | 5 g BSA fraction V<br>100 ml 10x TBS<br>1 ml Tween 20<br>Always prepared fresh. |
| Protease inhibitor | 1x | Complete Protease Inhibitor Cocktail Tablets. 7 x stock solution was prepared by dissolving one tablet in 1.5 ml water, aliquoted and stored up to 6 months at -20°C. |
| Phosphatase inhibitor | 1x | Phosphatase Inhibitor Cocktail Tablets. 10 x stock solutions was prepared by dissolving one tablet in 1 ml water, aliquoted and stored up to 6 months at -20°C. |

### 3.1.8. Solutions for Histochemistry

| Name | Final Concentration | Constituents and their amounts |
|---|---|---|
| 20 % PFA | 20% | 100 g paraformaldehyde<br>1.9 ml 10 N NaOH<br>DEPC water to 500 ml<br>Solution was heated to 56$^{o}$C until solution was almost clear, filtered through a Whatmann filter paper and stored as 10 ml or 50 ml aliquots at -20°C. The solution was diluted to 4% in 1x PBS before use. |
| Eosin | 1% | 1 g in 100 ml of distilled water. Filtered and used for a maximum of 3 weeks. |
| Citrate buffer | 0.1 M<br>0.1 M | 10.5 g Citric acid in 500 ml water (Solution A)<br>14.71 g Sodium citrate in 500 ml water (Solution B) |

| | | |
|---|---|---|
| | | Before use, 9 ml of solution A and 41 ml of solution B was added to 450 ml distilled water. pH was adjusted to 6.0. |
| EDTA buffer | I mM | 0.37 g EDTA<br>1 L water<br>Solution was adjusted to pH 8.0, autoclaved and stored at RT. |
| Hydrogen peroxide | 1% (or 3%) | 3.3 ml or (10 ml) of 30% Hydrogen peroxide<br>100ml water.<br>Prepared fresh. |
| Washing solution (TBS-T) | 1x<br>0.1% | 100 ml 10x TBS<br>1ml Tween 20<br>Volume was made up to 1L with water. |
| Blocking solution | 5% | 50 µl normal goat serum<br>950 µl TBS-T<br>Prepared fresh. |

### 3.1.9. Plasmids

| Name [size in base pairs] | Description | Reference |
|---|---|---|
| 3' *hprt* vector [10654 bp] | Targeting vector and FISH probe | Adams DJ et al., 2004 |
| 5' *hprt* vector [9912 bp] | Targeting vector and FISH probe | Adams DJ et al., 2004 |
| MHPN117k13 [15915 bp] | 5' *hprt* vector + insert homologous to 5' end of keratin type II cluster | Adams DJ et al., 2004 |
| cMHPN117k13 [14413 bp] | Gapped insert of MHPN117k13 to aid in insertional targeting using *NheI* and *BstBI* followed by adding linkers to regain a *NotI* restriction site. | This work |
| MHPP332c09 [17586 bp] | 3' *hprt* vector + insert homologous to 3' end of keratin type II cluster. | Adams DJ et al., 2004 |
| fMHPP332c09 [17586 bp] | Insert flipped from MHPP332c09 in order to change orientation of *loxP* site. | This work |
| cfMHPP322c09 [16182 bp] | Gapped insert of MHPN117k13 to aid in insertional targeting using *SacI*. | This work |
| Cre Pac [6000 bp] | Expression of Cre in double targeted ES clones in *cis*. | Taniguchi M et al., 1998 |

### 3.1.10. Primers

| | | |
|---|---|---|
| Sense | 5’ GAT AAC CGT ATT ACC GCC TTT G 3’ | Product size : 2562 bp |
| Antisense | 5’ CGC CCT CTT GTC TAT ATC AAC C 3’ | |
| Primers used to identify homologous recombinants of 5’ end of keratin type II cluster targeting by PCR. | | |
| Sense | 5’ CCC AAG GTT AGC CAA TAA TAA CC 3’ | Product size : 397 bp |
| Antisense | 5’ AGC ACT TAT CTG ACC AAA TCC AG 3’ | |
| Primers to prepare probes for Southern confirmation of 5’ end of keratin type II cluster targeted clones (*BsrG1* fragment). | | |
| Sense BN 1007 | 5’ AGG GAA GAA AGC GAA AGG AG 3’ | Product size : 2708 bp |
| Antisense BN 1008 | 5’ GCA GTT CCA GAC CTG ATG GT 3’ | |
| Primers used to identify homologous recombinants of 3’ end of keratin type II cluster targeting by PCR. | | |
| Sense BN 1017 | 5’ GCC GAT GTC GTG TGA TAT TG 3’ | Product size : 487 bp |
| Antisense BN 1018 | 5’ TGC AGC TGG AGA CAC GTA AC 3’ | |
| Primers to prepare probes for Southern confirmation of 3’ end of keratin type II cluster targeted clones (*EcoRI* fragment). | | |
| Sense BN 1023 | 5’ GTG GGA CTC TGT AGG GAC CA 3’ | Product size: 826 bp |
| Antisense BN 1024 | 5’ TGA ACC CAG GAG GTT GAG AC 3’ | |
| *Hprt* primers to identify Cre mediated deletion in ES cells as well as in mice. | | |
| Sense BN 5 | 5’ TGG GAC AGG AAG AGA GGT GAT C-3’ | Product size: 1.8 Kb |
| Antisense BN 159 | 5’ ACC AAA ACC AAA TCC ACT GCC G 3’ | |
| Primers to identify WT KtyII cluster allele – recognizes K5. | | |
| Sense BN 1047 | 5' CAT TCT GCA CGC TTC AAA AG 3' | Product size: 616 bp |
| Antisense BN 1048 | 5' GAT TCA GCC CCA GTC CAT TA 3' | |
| Primers to prepare 5’ *hprt* probes to identify targeted and recombined loci. | | |
| Sense BN 1049 | 5' AGG GCA AAG GAT GTG TTA CG 3' | Product size: 656 bp |
| Antisense BN 1050 | 5' CCT GAC CAA GGA AAG CAA AG 3' | |
| Primers to prepare 3’ *hprt* probes to identify targeted and recombined loci. | | |
| Sense BN 1154 | 5’ ATC AAG GAT GCT CAT GC 3’ | Product size: 184 bp |
| Antisense BN 1155 | 5’ TTC CGT CTC CAG ACA AC 3’ | |
| Primers to identify mouse keratin 7 expression (RT-PCR). | | |

| | | |
|---|---|---|
| Sense BN 1156 | 5' TGC AGA ACA TGA GCA TTC 3' | Product size: 158 bp |
| Antisense BN 1157 | 5' GGT GCG GCT GAA AGT GTT 3' | |
| Primers to identify mouse keratin 8 expression (RT-PCR). | | |
| Sense BN 1158 | 5' GAC GCT GAG ACC ACA CT 3' | Product size: 137 bp |
| Antisense BN 1159 | 5' TCC ATC TGT GCC TTG TAT 3' | |
| Primers to identify mouse keratin 18 expression (RT-PCR). | | |
| Sense BN 1160 | 5' TAA GCA AGA CCG AAG TCA 3' | Product size: 152 bp |
| Antisense BN 1161 | 5' CAC GCT CTG GAT CTG TGA 3' | |
| Primers to identify mouse keratin 19 expression (RT-PCR). | | |
| Sense BN 1164 | 5' ACC CAG AAG ACT GTG GGA TGG 3' | Product size: 300 bp |
| Antisense BN 1165 | 5' GAG ACA ACC TGG TCC TCA G 3' | |
| Primers to identify mouse GAPDH expression (RT-PCR). | | |

### 3.1.11. Bacterial Strain

| Description | Characteristics and Application | Reference |
|---|---|---|
| E. coli XL1-blue MRF | Genotype: recA1 endA1 gyrA96 thi-1 hsdR17 supE44 relA1 lac [F´ proAB lacIqZΔM15 Tn10 (Tetr)] ; Amplification of plasmid | Bullok et al., 1987 (Bullock and Wright, 1987) |

### 3.1.12. Mouse lines

| Genotype | Short description | Source |
|---|---|---|
| C57BL/6 | Wild type mice with black color for breeding and back crossing; females used as blastocyst donors for BCI. | Charles River, Germany |
| NMRI | Wild type mice, albino; females were used as surrogate mothers and vasectomized males were used to create false pregnancies in the surrogate mothers. | Charles River, Germany |

All mice were kept under the rule of the animal license: 50.203.2-BN 24, 20/04.

### 3.1.13. Eukaryotic cell line

| Description | Characteristics and Application | Reference |
|---|---|---|
| AB 2.2 | 129S7/SvEvBrd-HPRT$^{b-m2}$ - *Hprt* inactivated ES cells used for targeting *loxP* sites at either end of the keratin typeII cluster followed by generation of mice. | (Ramirez-Solis et al., 1995) – A gift from Prof. Allan Bradley |
| Cos-7 | Green African Monkey kidney cell line used to produce LIF. | ATCC - CRL-1651 |

### 3.1.14. Antibodies

#### 3.1.14.1. Primary antibodies

| Name | Antigen | Source | Subclass | Dilution/Application | Source |
|---|---|---|---|---|---|
| B A 0 3 0 0 | Biotinylated anti-avidin D | Goat | | 1/200 [FISH] | Vector Labs |
| 1333062 | Anti-DIG | Mouse | Monoclonal IgG1 | 1/500 [FISH] | Boehringer |
| OVTL 12-30 | K7 | Mouse | Monoclonal IgG1 | Undiluted [IF] | Progen |
| Troma 3 | K19 | Rat | Monoclonal | 1/20 [IF] | Baribault, Kemler |
| Ks 18.04 | K18 | Mouse | Monoclonal IgG1 | 1/10-20 [IF] | Progen |
| Ks 8.07 | K8 | Mouse | Monoclonal IgG1 | 1/100 [IF] | Progen |
| Asp175 | Cleaved caspase-3 | Rabbit | Polyclonal | 1/500 [IF]<br>1/200 [IHC] | Cell signaling |
| RR002 | Anti-phospho-Histone H3 (Ser10) | Mouse | Monoclonal IgG | 1/1000 [IF]<br>1/1000 [IHC] | Upstate |
| # 9212 | p38 | Rabbit | Polyclonal | 1/50 [IHC]<br>1/1000 [IB] | Cell Signaling |
| # 9211 | P-p38 | Rabbit | Monoclonal | 1/50 [IHC]<br>1/1000 [IB] | Cell Signaling |

### 3.1.14.2. Secondary / conjugated antibodies

| Name | Anti-species | Species | Sub-class | Dilution | Application | Source |
|---|---|---|---|---|---|---|
| Cy2-Streptavidin | | | | 1/100 | FISH | Dianova |
| Alexa 594 | Mouse | Goat | IgG H+L | 1/400 | Immunofluoresence | Molecular probes |
| Alexa 488 | Mouse | Goat | IgG H+L | 1/400 | Immunofluoresence | Molecular probes |
| Alexa 488 | Rat | Goat | IgG H+L | 1/400 | Immunofluoresence | Molecular probes |
| Alexafluor 488 Phalloidin | | | | 1/40 | Immunofluoresence | Molecular Probes |
| HRP | Mouse | Goat | | 1/30,000 | Immuno blotting | Molecular probes |
| HRP | Rabbit | Goat | | 1/30,000 | Immuno blotting | Molecular probes |

### 3.1.15. General Lab Materials

All sterile cell culture plastic-ware were purchased from Falcon, Sarstedt, Nunc and Becton Dickinson
Pipette Tips and tubes were purchased from Sarstedt
Fuji Medical X-Ray film (Fuji)
High density photopaper (Mitsubishi)
Hybond-N- blotting membrane 30cm x 3m (Amersham, RPN303B)
Microscope slides 76 x 26 mm (Engelbrecht)
Protran Nitrocellulose Hybridization Transfer Membrane, 0.2 µm, 30 cm x 3 m Roll (Schleicher & Schuell)
Sterile filters 0.45 µm, 0.2 µm, 0.1 µm (Schleicher & Schuell)
SuperFrost® Plus microscope slides (Menzel #041300)
Universal agarose
Whatman 3mm-Paper GB 002 (Schleicher & Schuell #426693)

Whatmann filter paper (Schleicher & Schuell)

Microspin G50 columns (Amersham, 27533001)

### 3.1.16. Equipment and Materials used

| Instrument / Software | Model / Version | Company |
|---|---|---|
| Agarose gel electrophoresis system | B2; B1A | Angewandte Genetechnologie |
| AIDA software | Aida 2.11 | Raytest |
| Blotting Chamber | Fast blot B49 | Biometra |
| Centrifuges | 5417R, 5810R, 5417C | Eppendorf |
| $CO_2$ incubator | CB150; CB210 | Binder |
| Cryostat | CM3050S | Leica |
| Film Developer | Curix 60 | Agfa |
| Fluoresence Microscope | AxioPhot II | Zeiss |
| Incubators for bacterial cultures | Function line | Heraeus Instruments |
| Inverted tissue culture microscope | Telaval 31 | Zeiss |
| Laminar flow system-type | Herasafe | Heraeus Instruments |
| Microtome | RM2155 | Leica |
| Microwave Vacuum Histoprocessor | RHS-1 | Milestone |
| Paraffin embedding machine | Tissue-Tek TEC | Samura |
| PCR-Thermocycler | TGradient | Biometra |
| pH-Meter | 761 Calimatic | Knick |
| Phosphorimager | ES 1000 | Raytest |
| Polytron | Ultra-turrax T25 | Janke & Kunkel |
| Scintillation counter | Beckmann LS-6500 | Beckmann |
| Stereoscopic zoom microscope | SMZ1500 | Nikon |
| Tissue drying oven | TD066 | Medite |
| UV-spectrophotometer | Genesys 10UV | Thermoelectron corporation |
| Vacuum Infiltration Processor | Tissue-Tek VIP 5E-F2 | Samura |
| Water purifier Milli-Q Plus | Nanopure | Barnstead |
| Electroporator | Gene Pulser II | Biorad |

## 3.2. Methods

### 3.2.1. Routine culture, generation and characterization of genetically altered mouse embryonic (ES) cells

AB2.2 ES cell line derived from Hprt-deficient 129s7/SvEBrd-Hprt b-m2 mice was used for all targeting experiments and generation of mice (Bradley et al., 1998). This line was a gift from Dr. Alan Bradley. These cells are grown on immortalized feeder cells, called snlp feeders (also a gift from Dr. Alan Bradley) which express G418 and puromycin resistance genes.

For routine culture, AB2.2 ES cells were passaged twice a week, splitting them between 1:6 and 1:12, depending on conditions. Medium was changed every other day as long as the culture was thin. At later stages, medium was changed every day.

#### 3.2.1.1. Thawing and plating cells

Cell culture flasks were gelatinized by using enough 0.1% gelatine to completely cover the surface for at least 10 min. The gelatine was aspirated off before plating cells. Appropriate amount of feeder cells (as per section 3.2.1.2) were plated together with ES cells or plated 3-4 h before. Feeder coated dishes could be used for up to 7-10 days. The integrity of the monolayer was checked before using them to plate ES cells.

AB2.2 ES cells were thawed quickly in a 37°C bath and transferred into 10 ml pre-warmed ES cells medium. The cells were pelleted by centrifuging at 100 x g for 5 min. The medium was aspirated and replaced with 5 ml of fresh medium and re-plated on a feeder coated 25 $cm^2$ flask. The cells were incubated at 37°C with 5% $CO_2$. Fresh medium was added to the cells on the following day.

To subculture, medium was aspirated and cells were washed with 1 ml pre-warmed trypsin per 25 $cm^2$ flask (2ml per 75 $cm^2$). Trypsin was removed and replaced with fresh trypsin and incubated at 37°C incubator until cells dislodged by gentle agitation. 4 ml ES cell medium per 1 ml of trypsin was added and pipetted up and down against flask wall about 10 times to obtain a single cell suspension. The cells were pelleted by centrifugation for 5 min at 100 x g at RT. The supernatant was aspirated and the pellet was re-suspended in medium. The cells were re-plated at desired density and in 10 ml medium for a 25 $cm^2$ flask and in 30 ml for a 75 $cm^2$ flask.

### 3.2.1.2. Inactivation of snlp feeder cells

Mitomycin C treatment was used to inactivate feeder cells. 10 µg/ml mitomycin C was added to a confluent culture of feeder cells that were cultured in ES medium minus LIF and incubated at 37°C in 5% $CO_2$ for 3 h. The cells were washed 5x with pre-warmed PBS, collected by trypsinization and pelleted by centrifugation for 3 min at 100 x g at RT. The cells were resuspended in ES cell medium, counted, adjusted to an appropriate seeding density, e.g. $10^6$cells/ml and frozen following the same regimen as described for ES cell freezing in section 3.2.1.5. For use in ES cell growth, feeders were plated on gelatine-coated dishes 1-2 h before plating ES cells at a density of 50,000 cells/$cm^2$.

### 3.2.1.3. Electroporation of ES cells

All targeting experiments were carried out using a BioRad gene pulser and cuvettes of 0.4 cm electrode gap at a setting of 800 V, 3 microfarads using 200 µg of linearized column purified and phenol-chloroform extracted plasmid. About 40 million ES cells were trypsinised and the cell number was determined using a counting chamber. Cells were resuspended in 0.8 ml of 1x HBS buffer and added to 200 µg linearized DNA, dissolved in 100 µl sterile TE in an Eppendorf tube and mixed by pipetting up and down using a 1 ml cell culture pipette. This was transferred into an electroporation cuvette. One pulse was applied and allowed to stand for 10 min. at RT. Cells were added to appropriate amount of medium and plated on feeder coated plates at about 2 x $10^6$ cells per 10 cm dish in 10 ml of medium. Positive selection was started after 24 h. One plate did not receive any selection and served as a control to check cell recovery. Thereafter, medium was changed every day for about 8–10 days until visible antibiotic resistant colonies appeared. Colonies were isolated as described in ES cell colony isolation protocol (section 3.2.1.4), using 1/2 for PCR and leaving the remaining cells in a well of a 24 well plate with approximately 1 ml of medium. PCR and Southern positive clones for the homologous recombination event were expanded and frozen down as per section 3.2.1.5.

### 3.2.1.4. Isolation of ES cell DNA for PCR-based genotyping

About 100-400 colonies were tested for each targeting experiment. The colonies were picked along with approximately 150 µl of medium using a Gilson pipette tip. The colony was transferred to a well of a 24 well plate and dispersed by pipetting up and down 3-4 times. Half the cells were left in the plate and the other half was transferred into an Eppendorf tube for PCR analysis. 1 ml of selective medium with feeder was added to the wells and allowed to grow until 80% confluent. For PCR analysis

for homologous recombined clones, the cells were pelleted by centrifugation in Eppendorf tube for 2 min at full speed. The supernatant was aspirated off and 50 µl of 1x PCR buffer containing approximately 0.5% of Triton X-100 for cell lysis and 200 µg/ml proteinase K was added. The tubes were then vortex briefly and incubated for 1h at 65°C at slow motion on a rotating wheel. The cell lysates were heated for 10 min at 95°C to inactivate proteinase K and then spun briefly. 5 µl of cell lysate was used for a 25 µl PCR reaction.

### 3.2.1.5. Freezing of ES cells

Cells from a confluent dish were trypsinized as mentioned in section 3.2.1.1, were counted and resuspended gently in x ml of ES cell medium such that one aliquot of frozen cells contain about 2-4 x $10^6$ cells. x ml of 2 x freezing medium was added drop wise and mixed gently and transferred instantly to a Nalgene freezing container and frozen at -80°C overnight . Thereafter, cells were transferred to liquid nitrogen cell storage container.

### 3.2.1.6. Karyotyping of ES cells

Before any clone was used for further targeting or for blastocyst injections, the number of chromosomes was determined by karyotype analysis. A confluent 25 $cm^2$ flask of ES cells was arrested in metaphase by incubating the cells for 1h at 37°C with 5% $CO_2$ in 1 ml fresh medium containing 10 µl Colcemid solution. Medium was removed and washed twice with PBS. 1ml of trypsin solution was added and incubated for 4 min at 37°C. Activity of trypsin was arrested by adding 5 ml ES cell medium, and the cells were pelleted by centrifuging the cells at 100 x g for 10 min. Medium was removed and 1 ml of 0.56% KCl was added drop wise to the cell pellet. The cells were gently resuspend by flicking the falcon tube and then another 4 ml of 0.56% KCl was added drop wise and mixed by flicking. The tube was incubated at 37°C for 8-10 min and once again the cells were pelleted by spin down gently at 60 x g for 5 min at RT. Supernatant was discarded, pellet was loosened by flicking the tube and 2-3 ml of chilled fixative solution (methanol/acetic acid 3:1, freshly prepared) was added drop wise to the cells. The tube was incubate 5 min at room temperature and once again pelleted by spinning down gently for 5 min at 60 x g. Supernatant was discarded. The fixation procedure was repeated once or twice and finally the pellet was resuspended in 0.5-1 ml fixation solution. The solution was then dropped on clean glass slides, previously dipped in ice cold 45% acetic acid and allowed to spread for about 30 sec to a minute. As the methanol disappeared from the surface and the cells became visible to the naked eye, the cells were briefly exposed to steam from a 70°C water bath for 1-3 sec, and then the slide was

quickly dried on a hot plate maintained at 70°C. The slides were then incubate for 1 min in Giemsa staining solution (Giemsa stain, modified, 0.4%, Sigma), washed twice with distilled water, air-dried. The slides were mounted with DPX mounting medium. The number of chromosomes in metaphase spreads of the nuclei were counted and checked for the required 40 chromosome number.

#### 3.2.1.7. Preparation of double targeted AB2.2 cells for blastocyst injections

Cells were thawed 4 days before injection and passaged once. Medium was changed about 4h before cells were taken for injection. Cells were trypsinized by first aspirating the medium, washing one time with 2 ml of trypsin and then by adding 3 ml of trypsin and incubating for 5-10 min at 37°C to receive single cell suspension. 5 ml of medium was added and pipetted up and down gently. Cells were pelleted by centrifugation for 5 min at 100 x g at RT, aspirating the medium and resuspending cells in 1 ml of M2 medium. All blastocyst injections and generation of chimeras were performed by Mrs. Rodica Maniu.

### 3.2.2. Transformation

XL1 blue competent cells were used to amplify the plasmid either in a sub-cloning step or prior to transfection. The cell wall of this bacterial strain was permeabilized to accept the plasmid DNA by chilling them in the presence of divalent cations such as $Ca^{2+}$. Cells were incubated on ice with the DNA and then briefly heat shocked by incubating them at 42°C for 90 sec followed by immediate incubation on ice for 90 sec. During this time, the DNA enters the cell. The cells were allowed to recover by the addition of 400 µl of pre-warmed LB medium and incubating them at 37°C for 1h. The cells were then spread on antibiotic resistant plates and the cultures were placed at 37°C o/n. The following day, colonies were picked and processed for amplification of the plasmid after confirmation of the plasmid using restriction digestion.

### 3.2.3. Plasmid Prep

Amplification of plasmid was carried out either prior to a sub-cloning step or prior to transfection by using Qiagen MAXI kit and prepared according to the manufacturers' protocol.

### 3.2.4. Polymerase Chain Reaction

#### 3.2.4.1. PCR to identify homologous recombinants from 5' of keratin type II cluster targeting

PCR conditions (5 µl DNA prep and 20 µl PCR master mix)

2.5 µl 10x PCR buffer
0.75 µl $MgCl_2$ (50mM)
1.0 µl 5mM dNTP's
1.0 µl typeII fwd1a sense primer
1.0 µl typeII15'rev1 anti-sense primer
0.2 µl (IU) Taq polymerase
13.55 µl water

PCR programme

| Step | Temperature | Time | Cycles |
|---|---|---|---|
| 1 | 95°C | 2 min | 1 |
| 2 | 95°C | 30 sec | 35 |
| 3 | 60°C | 30 sec | |
| 4 | 72°C | 2 min 30 sec | |
| 5 | 72°C | 5 min | 1 |
| 6 | 4°C | ∞ | 1 |

Product size: 2562 bp

#### 3.2.4.2. PCR to identify homologous recombinants from 3' of keratin type II cluster targeting

PCR conditions (5 µl DNA prep and 20 µl PCR master mix)

2.5 µl 10x PCR buffer
0.75 µl $MgCl_2$ (50mM)
1.0 µl 5mM dNTP's
1.0 µl BN1007 sense primer
1.0 µl BN1008 anti-sense primer
0.2 µl (IU)Taq polymerase
13.55 µl water

PCR programme

| Step | Temperature | Time | Cycles |
|---|---|---|---|
| 1 | 95°C | 2 min | 1 |
| 2 | 95°C | 30 sec | 35 |
| 3 | 60°C | 30 sec | |
| 4 | 72°C | 2 min 45 sec | |
| 5 | 72°C | 5 min | 1 |
| 6 | 4°C | ∞ | 1 |

Product size: 2708 bp

3.2.4.3. PCR to identify WT allele in ES cells as well as in mice (Identifies K5 locus)

PCR conditions (1 µl DNA prep and 24 µl PCR master mix)

2.5 µl 10x PCR buffer
0.75 µl MgCl2 (50mM)
1.0 µl 5mM dNTP's
1.0 µl BN6 sense primer
1.0 µl BN189 anti-sense primer
0.2 µl (IU) Taq polymerase
17.55 µl water

PCR programme

| Step | Temperature | Time | Cycles |
|---|---|---|---|
| 1 | 95°C | 5 min | 1 |
| 2 | 95°C | 30 sec | |
| 3 | 66°C | 30 sec | 35 |
| 4 | 72°C | 2min | |
| 5 | 72°C | 10 min | 1 |
| 6 | 4°C | ∞ | 1 |

Product size: 1.8 Kb

3.2.4.4. PCR to identify deleted cluster in ES cells as well as in mice (Identifies the HPRT gene after Cre-mediated recombination)

PCR conditions (1 µl DNA prep and 24 µl PCR master mix)

2.5 µl 10x PCR buffer
0.75 µl MgCl2 (50mM)
1.0 µl 5mM dNTP's
1.0 µl BN1007 sense primer
1.0 µl BN1008 anti-sense primer
0.2 µl (IU) Taq polymerase
17.55 µl water

PCR programme

| Step | Temperature | Time | Cycles |
|---|---|---|---|
| 1 | 95°C | 2 min | 1 |
| 2 | 95°C | 30 sec | |
| 3 | 60°C | 30 sec | 35 |
| 4 | 72°C | 50 sec | |
| 5 | 72°C | 5 min | 1 |
| 6 | 4°C | ∞ | 1 |

Product size: 826 bp

### 3.2.4.5. RT-PCR of simple epithelial keratins and GAPDH from mouse embryo

PCR conditions (1 μl cDNA prep and 24 μl PCR master mix)

2.5 μl 10x PCR buffer
0.75 μl $MgCl_2$ (50mM)
1.0 μl 5mM dNTP's
1.0 μl BN sense primer (listed in 3.1.10)
1.0 μl BN anti-sense primer (listed in 3.1.10)
0.2 μl (IU)Taq polymerase
17.55 μl water

PCR programme

| Step | Temperature | Time | Cycles |
|---|---|---|---|
| 1 | 95°C | 2 min | 1 |
| 2 | 95°C | 30 sec | |
| 3 | 60°C | 30 sec | 20/25/35 |
| 4 | 72°C | 30 sec | |
| 5 | 72°C | 5 min | 1 |
| 6 | 4°C | ∞ | 1 |

Product size: listed in section 3.1.10.

## 3.2.5. Processing of nucleic acids

### 3.2.5.1. Analysis of targeting constructs

Restriction analysis served for the identification of targeting constructs that were received from Sanger Institute, for flipping of insert in order to change the orientation of the loxP site, for generating gaps in insert to aid in insertional targeting and for linearization of the plasmid prior to targeting. Following restriction analysis, the plasmid was analysed by performing agarose gel electrophoresis and visualizing the DNA fragments using ethidium bromide.

### 3.2.5.2. Southern Analysis

In order to identify correctly targeted ES clones, Southern analysis was carried out. Here, about 10 μg pre-digested genomic DNA (prepared as detailed in section 3.2.1.4) from PCR positive ES clones was separated on a 0.7% TBE-agarose gel for 450 volt hours. The DNA was then denatured using 0.4N NaOH and then the nucleic acids were transferred onto a positively charged nylon membrane using capillary transfer. The membrane was then dried and baked for 2h at 80°C. A DNA fragment encoding the gap region in the targeting construct was labelled with [$\alpha$-$^{32}$P]dCTP using High Prime

labelling kit (Roche) and was used as a probe. The nylon membranes were pre-hybridized at 42°C for 3 hours in pre-hybridization solution and the membrane was then hybridized in the same solution containing the $\alpha$-$^{32}$P labelled probe at 42°C for 20 – 24 hours. The membrane was then washed three times at 68°C for 20 min each in 0.1x SSC containing 0.1% SDS and subjected to autoradiography. In case of confirming Cre mediated deletion of the keratin type II cluster in ES clones, a DNA fragment spanning the 5' and 3' regions of the human HPRT gene from the targeting construct were used as probes and labelled and processed similarly as above.

### 3.2.5.3. Fluorescent *in-situ* hybridization

Double targeted ES clones in *trans* will give rise to a deletion and duplication product on Cre expression, while in *cis* will yield only a deletion product (Fig.2.2 and 2.3). In order to identify if the double targeted ES clones were in *cis* or *trans*, fluorescent *in-situ* habitation was employed.

Metaphase chromosome spreads from ES cells were prepared similar to karyotyping of ES cells outlined in section 3.2.1.6, and stopped where the slides were dried at 70°C. The region with good metaphase chromosomes were marked using a diamond pen and the slides were fixed at 65°C, overnight.

Empty 3' HPRT and 5' HPRT vectors were biotin and DIG labeled respectively by nick translation as follows. Working dilution of DNAse I was determined beforehand as follows. 1 µl of DNAse I (1 mg/ml) stock solution was diluted to 1ml with ice-cold water immediately before use. A series of digestions with 2 µg of probe DNA was carried out using 10 µl of 10x buffer, 10 µl of b-mercaptoethanol, and 1 µl, 2 µl, 5 µl and 10 µl of the DNAse I dilution respectively in a 100 µl reaction volume. The reaction was incubated for 2h at 15°C. Thereafter, aliquots of 5-10 µl were loaded on a 1% agarose gel and size of the digested DNA was determined using a 1Kb ladder. The volume of DNAse that results in probe fragments of 100-500nt in length was chosen for the nick translation reaction.

*Labeling of probes by nick translation*

*Labeling 3' HPRT probe*

| | |
|---|---|
| X µl DNA containing 2µg DNA | 10 µl 10x NT buffer |
| 10 µl 0.1M β-Mercaptoethanol | 10 µl dNTP's |
| 2 µl Biotin dUTP | X µl DNAse (diluted 1:100 fresh) |
| 2 µl DNA polymerase | Volume made up to 100 µl with sigma wate |

*Labeling 5' HPRT probe*

| | |
|---|---|
| X μl DNA containing 2μg DNA | 10 μl 10x NT buffer |
| 10 μl 0.1M β-Mercaptoethanol | 10 μl dNTP's |
| 2 μl Digoxigenin dUTP | X μl DNAse (diluted 1:100 fresh) |
| 2 μl DNA polymerase | Volume made up to 100 μl with sigma water |

The reaction was incubated for 2h at 15°C and the size of the fragments was determined by running a small aliquot on a 1% agarose gel. The reaction was stopped by adding 3 μl of 0.5M EDTA and 0.5 μl of 20% SDS. The labeled probe was purified using G50 Sepahadex columns (Amersham Biosciences, UK). The probe was precipitated by combining 200ng of biotin labeled DNA, 200ng of digoxigenin labeled DNA (~15 μl if yield was good), 1 μl Salmon sperm DNA (10 mg/ml), 1/10$^{th}$ volume 3M sodium acetate and 2.5 volumes of 100% chilled ethanol (-20°C) and incubating at -80°C for 30 min. The probe was pelleted by centrifugation at 14,000 rpm for 30 min at 4°C and washing once using 70% ethanol. The pellet was air dried and to it 6μl of de-ionized formamide was added and mixed in a shaking block for 1h at 37°C followed by an addition of 6μl hybridization solution and additional 15 minute incubation at 37°C without shaking.

In the meantime, the slides were pretreated with 0.005% pepsin/0.01 M HCl , post fixed by incubating the slides in PBS-Magnesium chloride containing 3% of 37% formaldehyde for 5 min at room temperature and finally dehydrated in ethanol series (70%, 90%, 100%) and air dried. Once the slides were dry, 100 μl of pre-warmed (75°C) denaturation mix was placed on the area of the slide marked with good metaphase chromosomes, a 24 x 50 mm coverslip was placed over the slide and incubated for 1 minute 45 sec at 75°C on a heated PCR block. The slides were dipped in ice-cold 2x SSC followed by a dehydration in ice-cold ethanol series (70%, 90%, and 100%) and air-dried.

The probes were then denatured by heating at 75°C for 5 min and quickly cooling on ice. They were placed on the marked area of the slides, an 18 x 18mm coverslip was placed over it and sealed using rubber cement and hybridized for 20-24h in a humidified chamber. The signals were amplified and detected using anti-avidin and cy2-labelled streptavidin antibodies for the biotin labeled probe and anti-DIG and Alexa-594 antibodies for the DIG labeled probe.

A red and a green signal (or a yellow overlap) on a single chromosome confirmed *cis* targeted clones. Such clones were used to generate mice with the floxed allele as well as the deleted keratin cluster allele.

### 3.2.5.4. Genotyping of ES cells or mice from tail tip DNA

Metallic ear marks were used for labeling mice. After ear marking, 0.5 - 0.8 cm mouse tail biopsies or ES cells (1 x 25 $cm^2$ flask) were subjected to lysis using 200 µl of lysis buffer containing 0.5 µg/µl proteinase K and 0.5µg/µl RNase and incubated overnight at 55°C. After incubation, lysates were centrifuged at RT for 5 min at 20,000 x g. Supernatant was transferred to a new tube and 160 µl isopropanol was added and mixed well. DNA was fished out by using the yellow Gilson tip and washed by dipping in 500 µl 70% ethanol for 5 sec. After washing, the tip with DNA was placed into a new tube containing 200 µl TE buffer. The tubes were incubated for 10 min at 65°C to evaporate residual ethanol. The tubes with DNA were closed and further incubated at 55°C for 1 - 2h to facilitate complete DNA dissolution. 1 µl of this DNA was used for genotyping using appropriate primers listed in section 3.1.10.

### 3.2.6. Dissection and processing of mouse embryos

All mice were housed in a facility maintaining 12:12h light:dark cycle. For the generation of homozygous mutants of the keratin type II cluster, 6-18 week old heterozygous females were placed along with 8-48 week old males late in the evening. The presence of a vaginal plug the following morning indicated that mating had taken place. The day on which the vaginal plug was observed was designated day 0.5 of gestation (E0.5). The pregnant females were sacrificed at various stages of gestation by cervical dislocation and the uteri were dissected out. Individual implantation sites were embedded in Tissue Tek OCT in a cryo mould, immediately frozen in pre-cooled isopentane and stored at -80$^o$C for immunohistochemical studies. For histological analysis, the implantation sites were incubated in 4% paraformaldehyde overnight with constant rotation. The implantation sites were washed 3 times 5 min in ice cold PBS and then incubated with constant rotation in 15% sucrose o/n 4$^o$C followed by 30% sucrose ON at 4$^o$C or until the tissue sunk to the bottom of the container. The tissues were then processed for paraffin embedding. For protein biochemistry and RNA isolation, the uterine muscle was carefully ripped off from the implantation sites. The decidua was then carefully ripped apart to retrieve the embryo and the yolk sac. A part of the yolk sac was retained for genotyping, and the embryo and the yolk sac were processed for protein isolation or total RNA isolation.

### 3.2.7. Total RNA isolation

Embryos along with their yolk sac (approx 10 mg) were collected as described above and immediately homogenized in 1 ml TRIzol reagent using a Polytron. The homogenized samples were

incubated for 5 min at 15 to 30°C to permit the complete dissociation of nucleoprotein complexes. 0.2ml of chloroform was added per 1 ml of TRIZOL reagent. Tubes were shaken vigorously by hand for 15 sec and incubated at 15 to 30°C for 2 to 3 minutes. The samples were centrifuged at no more than 12,000 x g for 15 min at 2 to 8°C. Following centrifugation, the aqueous phase was transferred to a fresh tube. 0.5 ml of isopropanol was added (per 1 ml of TRIZOL reagent used for the initial homogenization). Samples were incubated at 15 to 30°C for 10 min and centrifuged at no more than 12,000 x g for 10 min at 2 to 80°C. After the supernatant was removed, the RNA pellet was washed once with 1 ml 75% ethanol pre-equilibrated at 4°C. The samples were mixed by vortexing and centrifuged at no more than 7,500 x g for 5 min at 2 to 8°C. The supernatant was discarded and the RNA pellet was briefly air-dried for 5-10 min. RNA was dissolved in RNase-free water and incubated for 10 min at 55 to 60°C. RNA concentration was determined by UV spectrophotometer and the RNA quality was checked on a 0.8% agarose gel. Total RNA samples were stored at -80°C.

### 3.2.8. RT-PCR for keratin mRNA expression in embryos

For the reverse transcription reaction, 2 μg total RNA isolated from embryos was incubated with 20 pmol of oligonucleotide primers at 70°C for 10 min. After a short cooling on ice, 1x first strand buffer, 10mM dithiothreitol, 1 mM dNTP's, 20 U of RNAsin (1U) were added to a total volume of 19 μl with RNase free water, mixed and incubated at 42°C for 2 min. 200 U of Superscript II reverse transcriptase was added to the reaction mix, mixed by pipetting up and down and incubated at 42°C for 50 min. The reaction was stopped by incubating the reaction at 72°C for 15 min. The reaction mix was taken directly for the PCR reaction. PCR was performed in a 25 μl reaction mixture containing 1 μl of template cDNA, as detailed in section 3.2.4.5 for 20, 25 and 35 cycles.

### 3.2.9. Histotechniques

#### 3.2.9.1. Cryosectioning and Immunofluoresence

##### 3.2.9.1.1. Cryosectioning

Cryosectioning steps were carried out using a Leica CM3050 S Cryostat (Leica Microsystems, Bannockburn, IL). Implantation sites dissected from the mice were oriented in OCT in an appropriate sized cryo mould (Samura Finetek, Europe, NL) and dropped into pre-cooled isopentane (in dry ice), and then stored at -80°C until further processing. When the tissue was ready for cryosectioning, the

block was equilibrated at -21°C (in the cryostat chamber) for 1 to 2hs. OCT. compound was applied to the chuck and spread using the heat extractor. While about the freeze, the cryo block was placed on the chuck and pressed firmly. Excess OCT was trimmed and 12 μm thick sections were prepared. The sections were collected on SuperFrost® plus microscope slides and allowed to dry for 3-4h. The slides were then processed for immunohistochemistry or stored at -80°C until further use.

#### 3.2.9.1.2. Immunofluoresence staining of tissues

Frozen sections (12 μm thick) were fixed for 10 min in –20°C acetone, and dried for 30 min before further processing. All antibodies were diluted in PBS containing 1% BSA. The primary antibody was applied with optimal dilution (listed in section 3.1.14.1) and incubated for 1h at room temperature. After washing 3 times in PBS for 5 min, appropriate secondary antibody at optimal dilution (listed in section 3.1.14.2.) was applied and incubated for 45 min. The nuclei were counterstained using 1:800 diluted 4,6- Diamidino-2-phenylindole (DAPI) along with the secondary antibody. After washing 3 times in PBS for 5 min, slides were mounted with Prolong Gold (Invitrogen, Germany). Image analysis and processing were performed using the AxionVision 2.05 (Carl Zeiss) and Adobe Photoshop 6.0 software.

#### 3.2.9.2. Paraffin sectioning and haematoxylin & eosin staining

Implantation sites were fixed and processed as detailed in section 3.2.6. Once the tissues were embedded in paraffin blocks, they were cut into 5 μm thick sections using a microtome. The sections were the floated on a warm water bath (40°C) in order to remove wrinkles. They were then picked up on a glass microscopic slide and processed for H & E staining. The sections were de-waxed by immersing the slides in 3 changes of xylene for 5 min each followed by rehydration in a 100%, 96%, 70% alcohol series for 3 min each. The slides were then immersed in water before they were stained with H & E. For staining, the slides were immersed in filtered Hematoxylin for 1 minute and washed with warm water until the water was clear. The slides were then immersed in eosin for 30 sec and rinsed well with distilled water until the water was clear. The slides were then dehydrated in alcohol series – 2 times 70% alcohol, 2 times 96% alcohol and 2 times 100% alcohol, 5 minutes each time. Finally the slides were cleared with two changes of xylene and coverslips were mounted on to the glass slides using DPX mounting medium.

#### 3.2.9.3. Immunohistochemistry (IHC)

The paraffin sections were de-parafinized by incubating 3x for 10 min in xylene. The sections were then re-hydrated by incubating 2 times, for 2 min each in alcohol series (100%, 95%, and 70%). The sections were then subjected to antigen retrieval by subjecting them to microwave treatment for a gradual increase up to 100°C, 10 min, followed by maintaining the temperature at 100°C for 10 min either in citrate buffer or EDTA buffer. The sections were allowed to cool at bench top for 30 min followed by three washes for 5 min each in distilled water. Endogenous peroxidase was quenched by incubating the slides for 10 min in either 1% or 3% hydrogen peroxide depending on the specification of the antibody. After three washes with distilled water for 5 min each, the sections were blocked with 5% normal goat serum for 1 h at RT. Primary antibody dilution was prepared in 5% normal goat serum diluted in TBS-T ON at 4°C. The sections were washed 3x 5 min, followed by linking and detection using Biotin/Streptavidin system (BioGenex) according to the manufacturers' protocol.

### 3.2.10. Protein biochemistry

#### 3.2.10.1. Preparation of protein lysates

Protein lysates from total embryo or yolk sac at E9.5 were prepared by dropping them directly into boiling 5x sample Laemmli buffer containing 1x protease inhibitor and 1x phosphatase inhibitor in a volume of 50 µl. The samples were boiled for 15 min and centrifuged at 20,000 g for 2 min. The supernatant was transferred into a fresh 1.5 ml Eppendorf tube and were shock frozen using methanol and dry ice. The samples were stored at -20°C.

#### 3.2.10.2 SDS-PAGE

Protein lysates were separated on a SDS-polyacrylamide gel prepared according to the compositions mentioned in table 3.1.

*Table.3.1 Reagents for SDS-PAGE separating gel*

Total volume: 10 ml

| Ingredients | Percentage of Gel | | | | |
|---|---|---|---|---|---|
| | 8% | 9% | 10% | 12% | 15% |
| 30% Acrylamide | 2.7 ml | 3 ml | 3.3 ml | 4 ml | 4.5 ml |
| Lower Tris | 2.5 ml | 2.5 ml | 2.5 ml | 2.5 ml | 2.5 ml |
| Distilled water | 4.8 ml | 4.5 ml | 4.2 ml | 3.5 ml | 3 ml |
| Temed | 10 µl | 10 µl | 10 µl | 10 µl | 10 µl |
| 10 % APS | 100 µl | 100 µl | 100 µl | 100 µl | 100 µl |

*Table.3.2. Reagents for 5% SDS-PAGE stacking gel*

| Ingredients | Volume for 4.5 ml |
|---|---|
| 30% Acrylamide | 440 µl |
| Upper Tris | 1000 µl |
| Distilled Water | 2.6 ml |
| Temed | 6 µl |
| 10% APS | 40 µl |

The protein samples were denatured at 98°C for 5 min, centrifuged briefly and allowed to cool to room temperature. Depending on the molecular weight of the protein analysed, the samples were loaded onto SDS-PAGE of 8% or 10% or 125% gels, in an apparatus containing running buffer in both chambers. A constant voltage of 40 V was applied per gel until the loading dye (bromophenol blue) entered the separating gel. Then the voltage was increased to 80 V until the dye reached the bottom of the gel. The proteins were then blotted onto nitrocellulose membranes.

### 3.2.10.3. Western Blotting

PVDF membrane was activated in methanol for 1 min and then equilibrated for 10 min in 1x Towbin buffer. The SDS-polyacrylamide gel was dismantled from the electrophoresis equipment and the stacking gel was excised. The separating gel was equilibrated in 1x Towbin buffer for 10 min and set up for semi-dry blotting as per manufacturers' directions. Protein transfer was achieved at a constant current of 1.0 mA/cm$^2$ of membrane. After blotting, the membrane was stained with Coomaasie G250

stain and destained with destaining solution. The marker was re-marked using a pencil and the membrane was scanned for future reference.

For Western blotting, the membrane was washed with TBST buffer. Non specific binding sites were blocked by incubating the membrane with either 5% skimmed milk powder or 5% BSA in TBS containing 0.1% tween-20 (TBS-T) for 1h. After blocking, the membrane was incubated with primary antibody diluted in blocking solution for 1 hour at RT or o/n at 4°C and washed thrice with TBS-T for 5 min each at RT, to remove any unbound antibodies. The membrane was then incubated with corresponding secondary antibody, diluted in blocking solution for 1 hour at RT and washed thrice with TBS-T for 5 min each at RT. A final wash was carried out with 1x TBS, pH 7.5. Bound antibodies were visualised with ECL system (Amersham Pharmacia) according to the manufacturers' protocol or with indigenous ECL system.

# 4. RESULTS

Generation and analysis of keratin type II null mice. An approach to overcome functional redundancy of keratin genes by a global deletion of type II keratins.

## 4.1. Insertional targeting in ES cells

### 4.1.1. Targeting constructs

For the purpose of a large scale genomic deletion up to about 0.7 Mb, the scheme developed by Bradley and colleagues has been used. This is based on two consecutive homologous recombination events, one at each end of the target locus (Zheng et al., 1999). The targeting vectors used in this project have been isolated directly from genomic libraries of pre-made targeting vectors (Adams et al., 2004). The libraries were generated from genomic DNA prepared from the livers of male 129S5 mice and they are indexed and displayed in the Ensembl website (www.ensembl.org). These libraries were constructed with phage vectors with automatic plasmid excision capabilities. In the phage vector, a plasmid backbone (bacterial origin of replication and ampicillin resistance gene) and two tandemly arrayed *loxP* sites that flank all the elements except the phage arms, were included. Any phage clone from the library can be excised into a plasmid by Cre-induced *loxP* site recombination in a Cre-expressing bacterial strain. The *loxP* site that is retained is used in the consecutive chromosome engineering steps. The genomic insert is flanked by rare *AscI* sites which can be used to change the orientation of the insert relative to the vector sequence in one sub-cloning step, if required (Zheng et al., 1999). These indexed vectors constitute a public resource (Mutagenic Insertion and Chromosome Engineering Resource; MICER) for high-throughput targeted manipulation of the mouse genome (Adams et al., 2004).

The construction and details of the 5' *hprt* and 3' *hprt* have been discussed in section 2.2.1. The 5' *hprt* (MHPN) vectors sequenced at both ends are displayed as either black or red arrow bars depending on the orientation of the *loxP* site and indexed on the Ensembl webpage. Similarly, the 3' *hprt* (MHPP) vectors, sequenced at both ends, are colored either blue or green depending on the orientation of the *loxP* site and are indexed on the Ensembl webpage (Fig.4.1a). The unique feature of these libraries is that, any clone that is isolated from the library is essentially ready to be used in targeting experiments. An added advantage in using clones from these libraries is that, they are indicated along with the expected orientation of the *loxP* site on targeting. Hence, selection of targeting

constructs, initially with identical orientation of *loxP* sites, eliminates the possibilities of undesirable inversion events in the initial stages of targeting (Adams et al., 2004).

These insertion vectors integrate into the target locus, generating an allele characterized by an insertion of the entire vector sequence, flanked by a duplication of the region of homology (Hasty et al., 1994) (Fig.4.1b). This feature makes this type of vector highly mutagenic.

The MICER vectors carry the agouti (*A*) (Kucera et al., 1996) or tyrosinase (*Tyr*) (Yokoyama et al., 1990) coat-color markers. These are useful in tracking targeted alleles during breeding, in many cases eliminating the need for molecular genotyping. Both minigene cassettes are susceptible to position effects; different loci exhibit different degrees of pigmentation. The agouti minigene mediates a visible pigmentation change in all loci examined to date, but the tyrosinase minigene is silent in some loci (Klysik et al., 2004; Nishijima et al., 2003; Walz et al., 2003; Zheng et al., 2002).

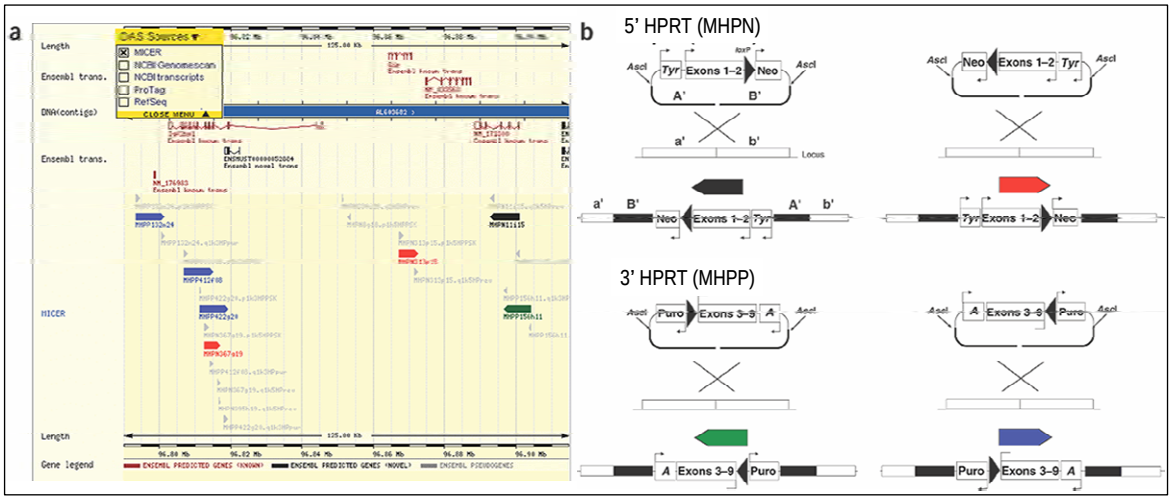


Fig.4.1. Indexed targeting vectors displayed on Ensembl, under the DAS source MICER (a) End-sequenced vectors were mapped to the C57BL/6J mouse genome assembly in Ensembl. 5' *hprt* (MHPN) vectors sequenced at both ends are colored black or red; 3' h*prt* (MHPP) vectors sequenced at both ends are colored blue or green. The orientation of the *lox*P site in these vectors is indicated by the direction of the arrow and by the color-coding. End-read sequences are shown in grey. (b) MICER vectors target by insertion. A', a', B' and b' correspond to genomic DNA from the vector and locus and illustrate the structure of the targeted allele. Exons 1−2 and exons 3−9 correspond to the split *hprt* minigene elements in the 5' and 3' *hprt* vectors, respectively. After expression of Cre, these elements recombine, resulting in resistance to hypoxanthine/aminopterin/thymidine. Minigenes for the coat-color markers agouti (*A*) and tyrosinase (*Tyr*) are shown. The location and direction of promoter elements is indicated by an arrow. For the exon 3−9 cassette, which is promoterless, the direction of transcription is indicated (Adapted from Adams et al., 2004).

The following two targeting constructs were procured from the Sanger Institute, Cambridge, UK.

### 4.1.2. Targeting the 5' end of keratin type II cluster

A 5' *hprt* vector construct, named MHPN117k13, was used for targeting the 5' end of the type II keratin cluster. This contained an insert of 6.0 Kb spanning 101202450 -101208417 bp on chromosome

15. A gap of 1.5 Kb was generated using unique restriction sites, *NheI* and *Bsp119I,* to yield 2.0 and 2.4 Kb arms of homology (Fig.4.2a). *NotI* linkers were introduced at the cut sites in order to obtain a *NotI* restriction site. Hence, the plasmid was linearized using *NotI* before gene targeting. The linearized and purified plasmid was transfected into AB2.2 cells and G418 selection was initiated after 24 hours following targeting, at a concentration of 350 μg/ml.

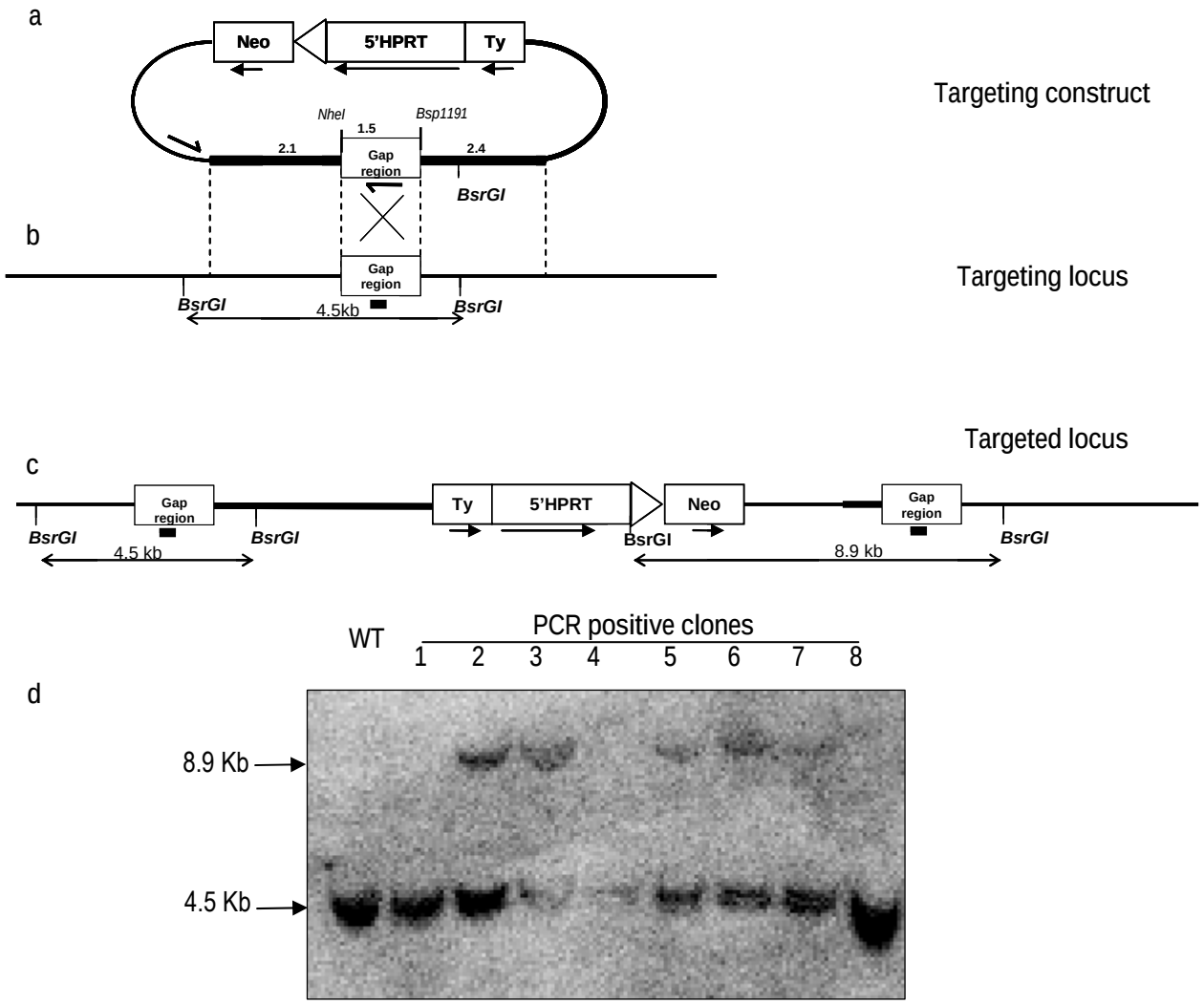


Fig.4.2. Targeting of 5' end of the keratin type II cluster by gap repair insertional targeting. (a) The 5' targeting vector (MHPN117k13) consists of a neomycin resistance gene for gene targeting, a *loxP* site, a 5'-half-*hprt* (hypoxanthine phosphoribosyl transferase) minigene (non-functional *hprt* fragment) for chromosome engineering and a 4.5 kb genomic DNA fragment homologous to the 5' end of the type II keratin cluster. A gap of 1.5 Kb was generated by using *NheI* and *Bsp119I* enzymes. (b) Locus at 5' end of keratin type II cluster. (c) During targeted recombination, the gap is repaired from the chromosomal DNA template which leads to a duplication of the entire region of homology including the repaired gap sequence, which will flank the inserted vector sequence. PCR primers for initial confirmation of homologous recombinants spanned the gap sequence and the proximal vector sequence. (d) Southern blot analysis of ES clones targeted at the 5' end using the sequence from the 'gap' region as a probe which distinguishes *Bsp119I* fragments of 4.5 Kb in the WT and 8.9 Kb in targeted allele.

After about 7 days following selection, individual ES colonies visible to the naked eye were formed. 96 colonies were picked and screened using the primers listed in section 3.1.10 according to the conditions listed in section 3.2.4.1. The plasmid without the gap was used as a positive control. Eight PCR positive clones for the homologous recombination event were expanded and frozen until confirmed by Southern analysis. Southern analysis was carried out as outlined in section 3.2.5.2. The probe was a 397 bp genomic DNA fragment that was designed in the gap region using the primers listed in section 3.1.10. The probes distinguish between 4.5 Kb wild type and 8.9 Kb targeted *Bsp14071 (BsrGI)* digested fragments in homologously recombined clones (Fig.4.2c-d). Five out of the eight PCR positive clones were positive for the homologous recombination at the 5' end of the keratin type II cluster using Southern analysis. Clone # 2 was used to target the 3' end of the keratin type II cluster.

### 4.1.3. Targeting the 3' end of keratin type II cluster

A 5' *hprt* vector construct named MHPN322c09 was requested from Sanger Institute. The insert was excised from this vector at the *AscI* sites, which were present at either ends of the insert, and was cloned into an empty 3' *hprt* vector and was named MHPP322c09. This contained an insert of 6.9 Kb spanning 101876016 – 101882964 on chromosome 15. A gap of 1.4 Kb was generated using a double cutter, *SacI,* restriction sites to yield 3.0 and 2.4 Kb arms of homology (Fig.4.3a). *SacI* restriction enzyme was used to linearize the plasmid and targeted into clone # 2 of the previously targeted clone detailed above (section 4.1.2). Targeting in ES cells was performed as mentioned earlier. The cells were subjected to puromycin selection at the concentration of 3μg/ml for 24 hours following electroporation. Eight clones out of 96 picked clones were positive for the homologous recombination event, as determined by PCR using the primers and conditions listed in section 3.1.10. These clones were expanded and frozen until confirmed by Southern analysis.

Southern analysis was carried out as outlined in section 3.2.5.2. The probe was a 487 bp genomic fragment that was designed within the gap region, using the primers listed in section 3.2.5.2. The probes distinguished between 7.0 Kb wild type and 12.9 Kb targeted *HincII* digested fragments in the correctly targeted clones (Fig.4.3c-d).

All the PCR positive clones were positive for the homologous recombination at the 3' end of the keratin type II cluster using Southern analysis. The results for the targeting experiments are outlined in table 4.1.

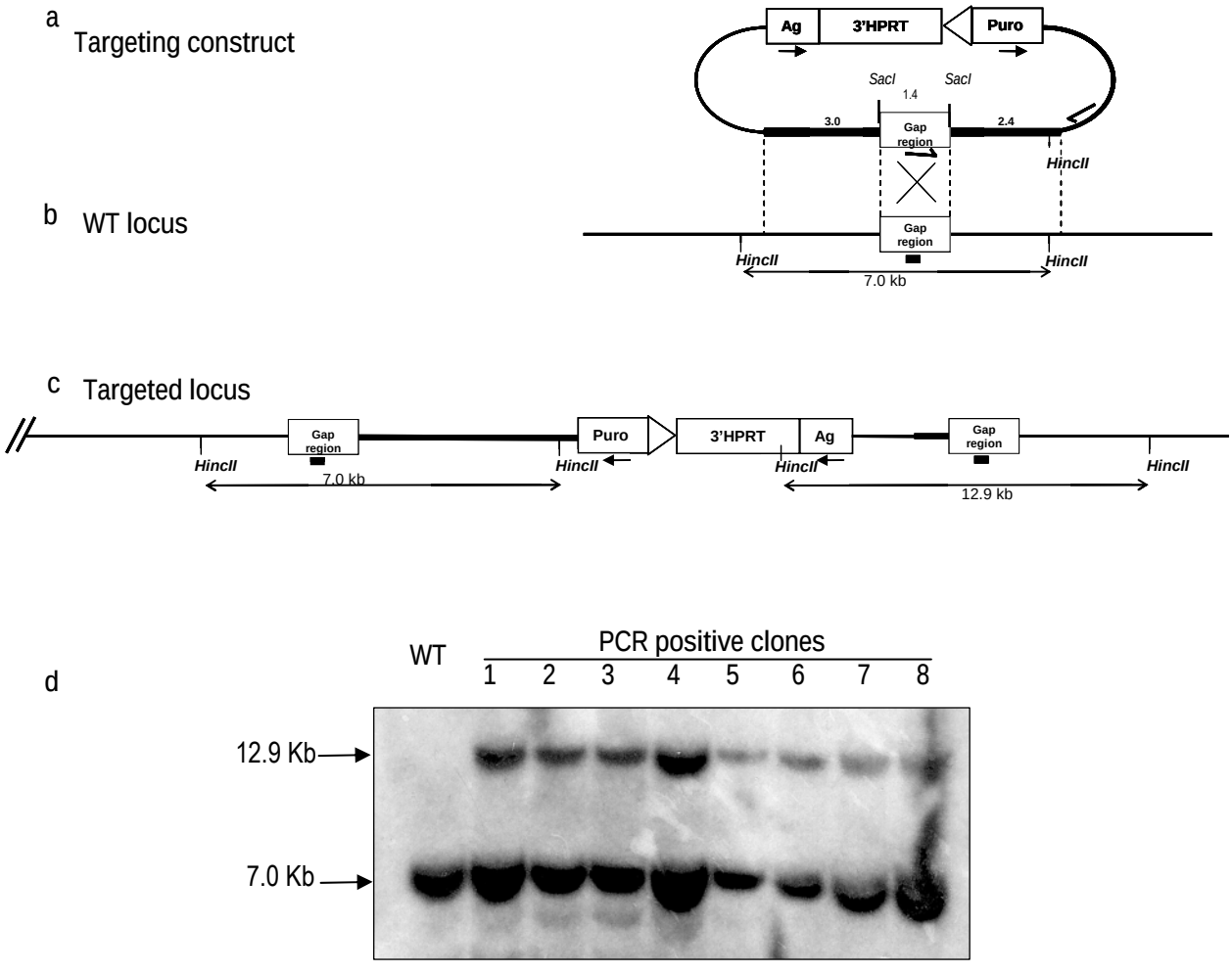


Fig.4.3. Targeting of 3' end of the keratin type II cluster by gap repair insertional targeting. (a)The 3' targeting vector (MHPP322c09) contains a puromycin resistance gene, a *loxP* site, a 3'-half *hprt* minigene (non-functional *hprt* fragment) and a 6.3 kb genomic DNA fragment homologous to the 3' end of the keratin cluster. A gap of 1.4 Kb was generated by using *SacI* restriction enzyme. (b) Locus at 3' end of keratin type II cluster. (c) During targeted recombination, the gap is repaired from the chromosomal DNA template which leads to a duplication of the entire region of homology including the repaired gap sequence, which will flank the inserted vector sequence. PCR primers for initial confirmation of homologous recombinants spanned the gap sequence and the proximal vector sequence. (d) Southern blot analysis of ES clones targeted at the 3' using the sequence from the 'gap' region as a probe which distinguishes *HincII* fragments of 7.0 Kb in the WT and 12.9 Kb in targeted allele.

| Targeting Construct (MICER clone) | Region on chromosome 15 targeted | Insert Size (Kb) | Gap size (Kb) | Size of small arm of homology (Kb) | Size of large arm of homology (Kb) | Targeting frequency |
|---|---|---|---|---|---|---|
| MHPN117k13 (flipped prior to targeting) | 101202450 - 101208417 | 6.0 | 1.5 | 2.1 | 2.4 | 8 % |
| MHPN332c09 (insert released and sub -cloned into 3' HPRT vector) | 101876016 - 101882964 | 6.9 | 1.4 | 2.4 | 2.5 | 8 % |

Table.4.1. Targeting efficiency at the keratin type II locus using insertional vectors. The gap is excluded when calculating the total size of region of homology. An expected targeting efficiency of 8% was obtained with both the targeting constructs.

## 4.2. Identification of *cis* targeted clones

Double targeted ES clones in *trans* will give rise to a deletion and duplication product on Cre expression, while in *cis* will yield only a deletion product (Fig. 2.2 & 2.3). In order to identify if the double targeted ES clones were in *cis* or *trans*, fluorescent *in-situ* hybridization was employed and performed as detailed in section 3.2.5.3. Slide preparation of metaphase chromosome spreads was carried out as suggested by Henegariu et al., 2001. Empty 3' *hprt* and 5' *hprt* vectors were labeled with biotin-dUTP and digoxigenin-dUTP respectively, by nick translation and were used for chromosomal *in-situ* hybridization against spread chromosomes from double targeted ES cell clones (Wrehlke et al., 1999). The 5' *hprt* probe was detected following signal amplification using anti-digoxigenin and Alexa-594 antibodies. The 3' *hprt* probe was amplified and detected using anti-avidin and cy2-labeled streptavidin.

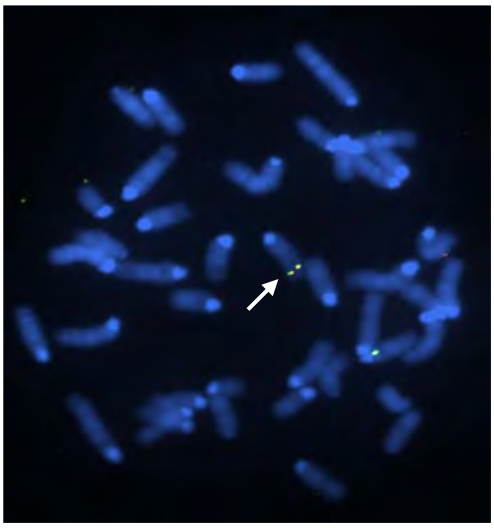

Fig.4.4. Fluorescent *in-situ* hybridization to identify double targeted ES clones in *cis*. Empty 3' *hprt* and 5' *hprt* vectors were biotin and DIG labeled respectively, by nick translation and were used for chromosomal in situ hybridization against spread chromosomes from double targeted ES cells clones. A red and a green signal (or a yellow overlap) on a single chromosome confirms cis targeted clones (arrow).

A red and a green signal (or a yellow overlap) on a single chromosome confirmed double targeting in *cis* (Fig.4.4). One of the three double targeted clones tested by FISH was confirmed to have the targeted constructs in *cis.* This clone was expanded and subjected to Cre expression.

## 4.3. Cre-mediated deletion of the keratin type II cluster

The double targeted clone in *cis* (Fig.4.5a), was expanded and transiently transfected with 200 μg of circular CrePac vector (Taniguchi et al., 1998). This expression vector also expresses the puromycin N-acetyltransferase (pac) gene, which would have hindered the screening procedure if the resistance / sensitivity strategy in order to identify *cis* targeted clones (Fig.2.4) (Ramirez-Solis et al.,

1995; Yu and Bradley, 2001) was adopted. However, since fluorescent *in-situ* hybridization was performed for this purpose, utilizing this vector, which was already available within the University, was efficient. HAT selection was started 24 hours after transfection at a 1x concentration. After about 7 days following selection, individual ES colonies visible to the naked eye were formed. During this time, a Cre-mediated recombination should have occurred, leading to the deletion of the keratin type II cluster along with the puromycin and neomycin selection cassettes as a reciprocal product, thereby uniting the two non-functional halves of the *hprt* cassette, rendering it functional (Fig.4.5b). Such clones were HAT resistant and the transfection efficiency was about 80%. Six HAT resistant colonies were picked and screened using the primers listed in section 3.1.10, according to the condition listed in section 3.2.4.4. The HAT resistant clones were further confirmed by Southern analysis for deletion of the keratin type II cluster (Fig.4.5c). Sequences spanning the 5' *hprt* (616 bp) and the 3' *hprt* (656 bp) cassettes were used as Southern probes in order to distinguish between the double targeted and recombined loci (Fig.4.5c).

All the HAT resistant clones after Cre expression were positive for the Cre-mediated deletion of the keratin type II cluster.

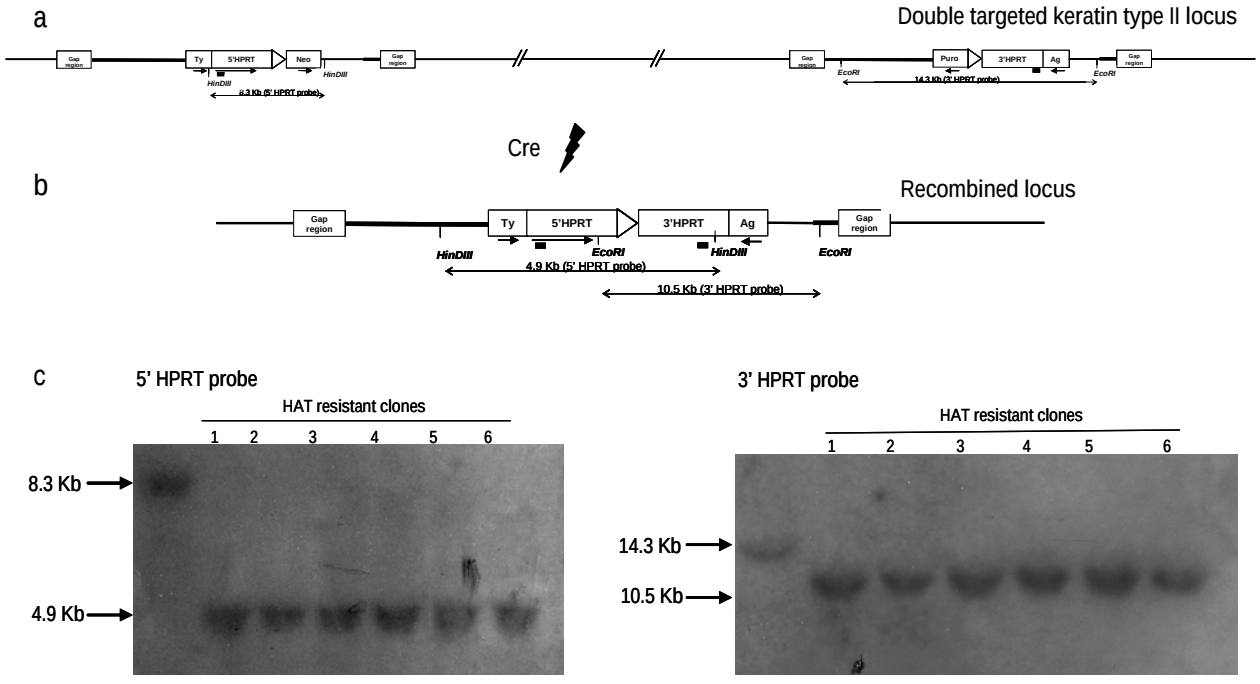


Fig.4.5. Cre-mediated deletion of keratin type II cluster. (a) Double targeted keratin type II locus in *cis*. Both the loxP sites are targeted in the same orientation. (b) Cre-mediated recombination between two *loxP* sites of double targeted clones in *cis* (on the same chromosome). This led to a deletion of the keratin cluster thereby rendering the clones neomycin and puromycin sensitive due to the loss of the *neo*- and *puro*-carrying reciprocal product, but HAT resistant. (c) Southern blot analysis of ES cells following Cre-mediated recombination was carried out using unique 5' and 3' probes spanning the 5' *hprt* and the 3' *hprt*, respectively. The 5' *hprt* probe distinguishes between double targeted 8.3 Kb and a recombined 4.9 Kb *HinDIII* fragments using the 5' *hprt* probe. Similarly, the 3' *hprt* probe distinguishes between double targeted 14.3 Kb and recombined 10.5 Kb *EcoRI* fragments.

## 4.4. Blastocyst injection

Clone # 1 was used for blastocyst injections which were carried out by Mrs. Rodica Maniu, University of Bonn, according to standard protocols. Six male chimeras were generated in total with about 80% contribution from the ES cells as determined by the contribution of ES cells to coat color. The chimeras were bred to C57BL/6 WT females. All the chimeric males produced agouti colored offsprings indicating germline transmission.

## 4.5. Generation of keratin type II null mouse line

The agouti-colored male offsprings from breeding chimeras to WT C57BL/6 mice were genotyped. Consistently, the agouti-colored offsprings carrying the deleted allele had a lighter tail color when compared to the WT, due to the presence of agouti coat color markers present in the targeting construct (Zheng et al., 1999) (Fig. 4.6). Mating heterozygous with wild-type mice, the mutant allele was detected in approximately 50% of progeny (data not shown). They were viable and fertile and exhibited no obvious phenotypic defects. The heterozygous males were backcrossed to WT C57BL/6 females in order to rapidly increase the colony.


**Fig.4.6.Tail color conferred by K14 agouti gene.** Heterozygous mice for the deleted keratin type II cluster consistently had a lighter tail when compared to their wild-type littermates, allowing for rapid visual genotyping.

Heterozygous males and females were in-bred to generate the keratin type II cluster knockout mice.

## 4.6. Analysis of keratin type II null mouse line

The analysis of the mice was carried out at the morphological level by histology, DNA level by PCR for genotyping of mice and embryos, at RNA level by RT-PCR and in-situ hybridization and at protein level by immunoblotting and histochemistry of embryos and extra-embryonic tissues.

### 4.6.1. Genotype analysis of progeny from keratin type II heterozygous intercrosses

Heterozygous offsprings appeared normal and fertile. However no homozygous mutants were recovered at birth (Table 4.2). Based on the observation that the K8 null mice, K18/K19 double deficient mice and K8/K19 (Baribault et al., 1993; Hesse et al., 2000; Tamai et al., 2000) die between E9.5 – E12.5, concepti at various stages during mid-gestation were analysed. Genotypic analysis of embryonic litters revealed that the keratin type II null mutants were recovered at the expected Mendelian ratios until 9.5 days postcoitum (dpc), with most homozygous mutants dying *in-utero* between 9.5 and 10.5 dpc (Table 4.2).

| | Genotype | | |
|---|---|---|---|
| Age | Wild type | Heterozygous | Homozygous mutant |
| 8.5 dpc | 3 | 4 | 2 |
| 9.5 dpc | 477 | 943 | 321 (27/321 inviable) |
| 10.5 dpc | 10 | 20 | 8 (8/8 inviable) |
| 15.5 dpc | 2 | 3 | 0 |
| Postnatal | 6 | 10 | 0 |

Table 4.2. Genotype analysis of progeny from keratin type II heterozygous intercrosses. Genotyped embryos that were in the process of resorbing were scored as inviable. Postnatal mice were scored at P0.

Hence, the fact that these mutants could phenocopy the K18/K19 (Hesse et al., 2000) or the K8/K19 (Tamai et al., 2000) double deficient mutants which died at E9.5 and E10.0, respectively, was not excluded.

### 4.6.2. Transcription of type I keratins is not coupled with that of type II keratins

In order to analyse if the deletion of the type II cluster was complete and to determine if the deletion of the type II cluster had an effect on the type I cluster, the transcription status of the simple

epithelial keratins that are normally expressed during early embryogenesis, was determined by a semi-quantitative RT-PCR analysis from E9.5 embryos.

A complete absence of transcripts for K8 and K7 were seen in the mutants after 35 cycles. A weak signal of K18 transcript was seen in the knockouts. This can be attributed to the presence of processed keratin pseudogenes from residual contaminating genomic DNA (Hesse et al., 2001; Tschentscher et al., 1997). This was further validated by *in-situ* hybridization using K18 specific riboprobes in collaboration with Dr. David Simmons, University of Calgary (Fig.4.8). A complete absence of K18 mRNA on placental sections through trophoblast cells in mutants confirmed that the weak signal of K18 seen using RT-PCR was a result of processed keratin pseudogenes from residual contaminating genomic DNA. Transcripts of keratin 19 were seen at normal levels in both WT and mutants. This indicates that the transcription of the type I keratins is independent from that of the type II keratins and that the regulation of the type II keratin expression does not occur at the transcriptional level.

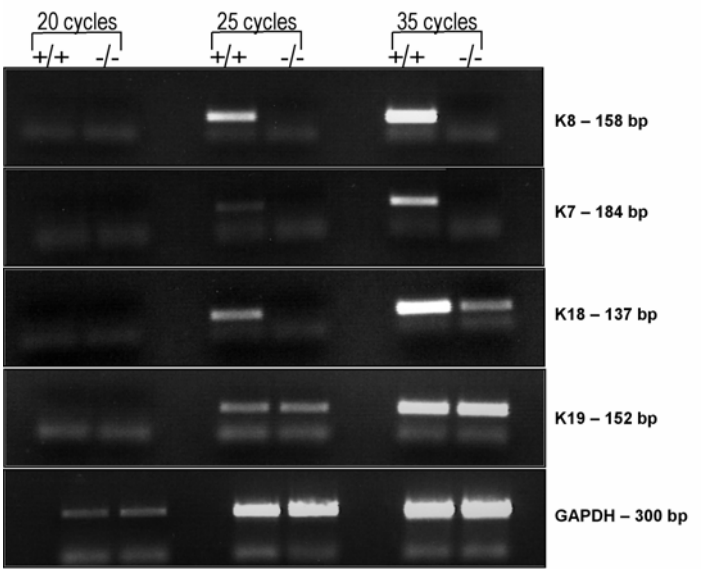


Fig.4.7. Semi-quantitative RT-PCR analyses of simple epithelial keratins in WT and type II keratin null embryos at E9.5. Transcripts of keratins whose genes are encoded in type II keratin cluster were absent in the keratin type II null embryos. A low signal of K18 in the mutants was from unprocessed pseudogenes. Transcripts of K19 were seen at normal levels in mutant embryos when compared to their WT littermates.

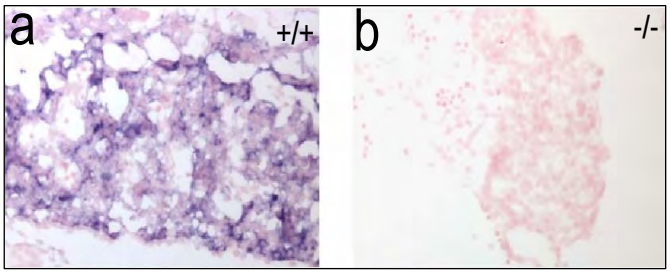


Fig.4.8. RNA *in-situ* hybridization of K18 to WT and mutant placenta. No K18 RNA was detected in the mutant placenta (b) when compared to that of the WT (a), confirming that the faint K18 transcript obtained by RT-PCR was from processed pseudogenes from residual contaminating genomic DNA.

### 4.6.3. Expression of simple epithelial keratins in extra-embryonic tissues

Immunohistochemical analysis of simple epithelial keratins like K8, K18, K7, and K19 which are expressed during early embryogenesis was carried out on acetone fixed cryosections of E9.5 WT and mutant embryos, using a keratin specific antibody.

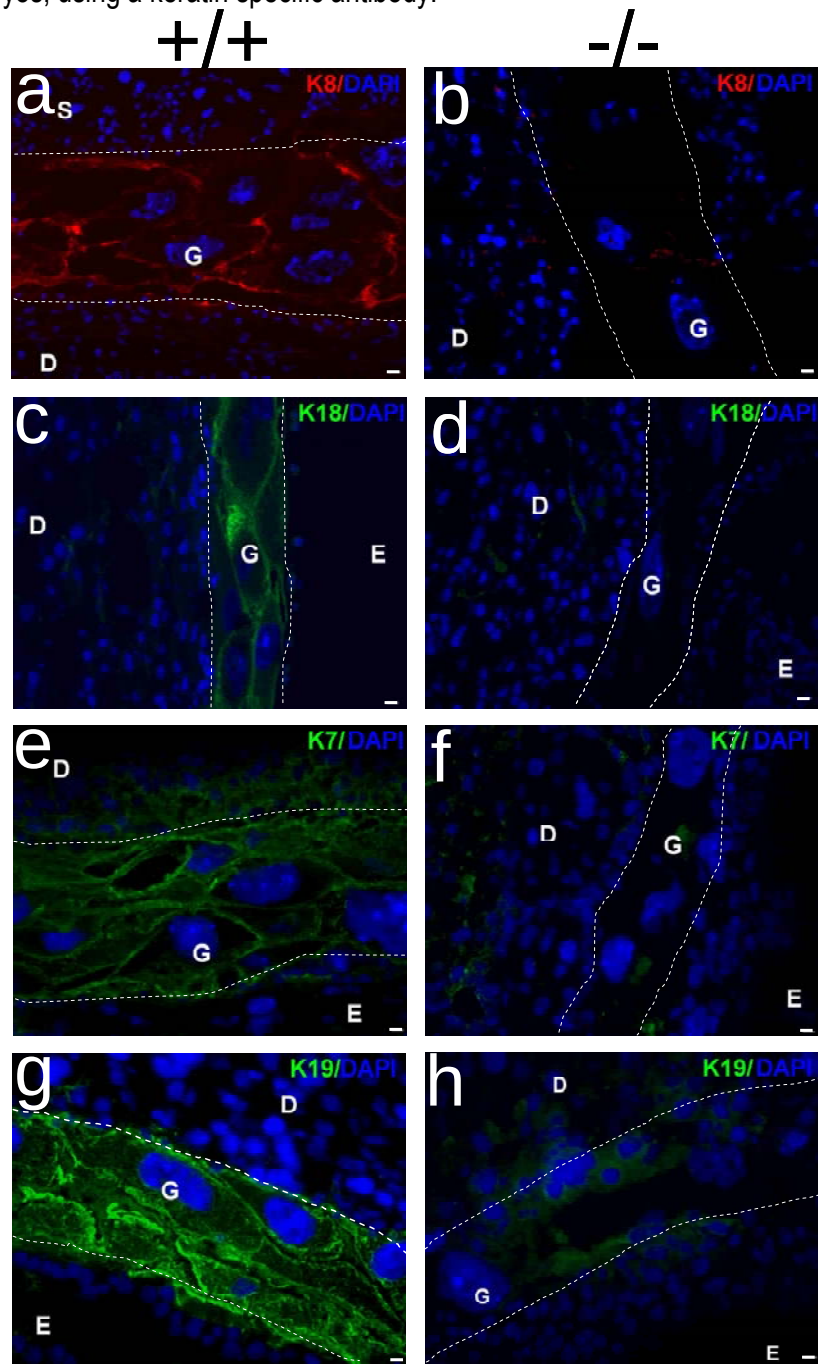


Fig.4.9. Comparison of the placental regions of E9.5 WT *(a, c, e and g)* and mutant embryos (b, d, f and h) for the independent expression of K8, K18, K7 and K19. Absence of any keratin filaments confirmed the complete loss of keratin filaments in the mutants (b, d, f and h). This indicated a complete loss of all type I and type II intermediate filaments during early mouse embryogenesis. Expression of K19 was completely lost in the absence of its type II partner in the mutants although K19 transcripts were detected by RT-PCR. S, spongiotrophoblast; D, decidua; E, embryo; G, trophoblast giant cell. Scale bar, 20 µm.

In the wild type embryo, these keratins are strongly expressed in the trophoblast giant cells, EC, parietal and visceral yolk sac, amnion, surface ectoderm and primitive gut (Lu et al., 2005). The data revealed a complete loss of keratin filaments in the embryo and placenta (Fig.4.9) of the mutants. No traces of the type I keratin K19 was seen in the mutants. In contrast to other keratin null mutants, where an imbalance of keratins led to the aggregation of residual keratins, no aggregates of K19 in the mutants were seen (rev. in Coulombe and Omary, 2002) (Fig.4.9h). It has been reported that type I keratins on forced expression in fibroblasts do not force the expression of its type II keratin partner, but however, the same is true *vice-versa.* These results suggest the possibility that type I keratin expression may be dependent on the accumulation of unpolymerized type II keratin (Giudice and Fuchs, 1987). Type II keratin expression has been shown to precede type I keratins (Lu et al., 2005). Therefore, possibly in the absence of type II keratins, K19 is subjected to proteosome degradation, ensuring the disposal of the relatively insoluble cellular components. Given the data that keratin 8 plays a protective role against TNF-alpha and Fas mediated apoptosis (Caulin et al., 2000; Inada et al., 2001), and the absence of K19 protein left open the question of increased apoptosis in the keratin null mutants. However, the absence of all early simple epithelial keratins provided, for the very first time, a complete keratin null situation during early embryogenesis.

### 4.6.4. Morphological analysis of keratin type II null embryos

Gross morphology of the wild type and keratin type II null mutant littermates at 9.5 dpc showed that these mutants developed normally until 8.5 dpc as seen *in-utero*. By 9.5 dpc, the mutant embryos were smaller than their WT or heterozygous littermates (20-60% smaller) (Fig.4.9). However, all hallmarks for an E9.5 embryo were seen in the mutants confirming that the embryos were not retarded developmentally in the absence of keratins. No viable keratin type II null embryos were recovered after E10.5 (Table 4.1). At 9.5 dpc, mutant embryos appeared to be paler than their WT littermates (Fig. 4.10).

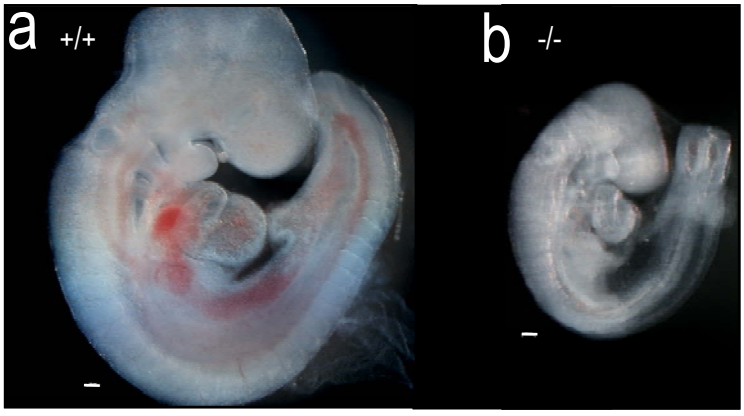


Fig.4.10. Gross morphology of E9.5 WT and mutant littermates. The mutants were smaller (20-60%) and paler than their WT littermates. Scale bar 100 μm.

In collaboration with Prof. Dr. Dieter Hartmann, University of Bonn, it was identified that at E9.5, the intact yolk sacs of the keratin type II null mutants were pale compared with those of their wild-type littermates and vessels were not readily discernible. The yolk sacs of mutant embryos were more translucent and had fewer blood vessels than that of wild type embryos (Fig.4.11a vs. 4.11b). The large vitelline vessel and numerous smaller vessels were clearly seen in WT yolk sacs. In contrast, numerous small pools of blood cells were present in the mutants with no organized vessel formation (Fig.4.11b). Some areas of the yolk sac completely lacked blood vessels in the mutants (arrow). Semi-thin sections through the yolk sac revealed some areas totally devoid of blood vessels in the mutants (Fig.4.11c) when compared to that of the WT (Fig.4.11d),

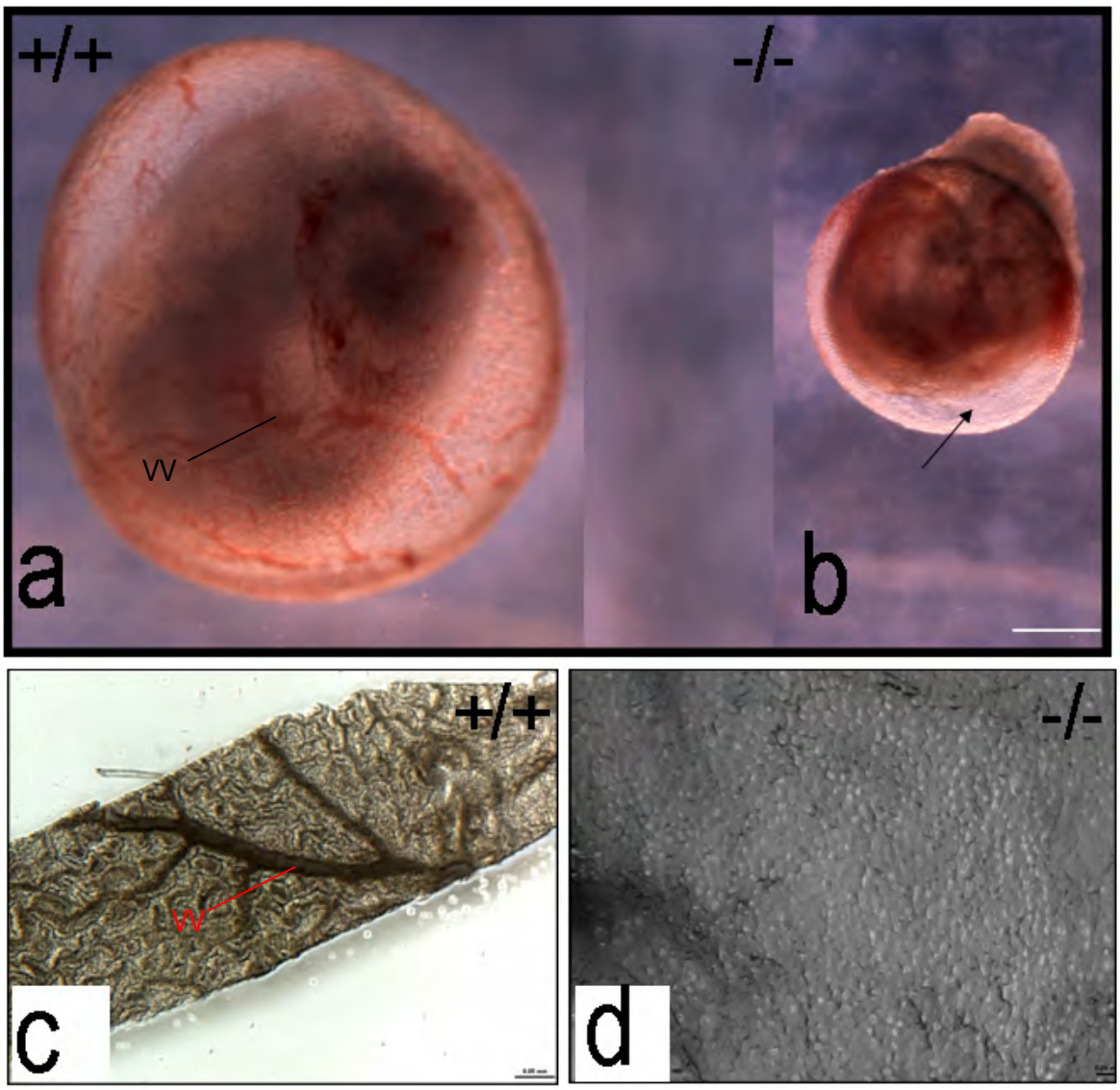


Fig.4.11. Morphology of yolk sac in WT and keratin type II null mutants at E9.5. (a&b) Whole-mount photographs of WT and mutant embryos within its yolk sac at E 9.5, respectively. Reduced vasculature is seen in the mutants when compared to their WT littermates. Some regions within the yolk sac were completely devoid of vasculature [arrow]. The large vitelline vessel [VV] is clearly visible in the WT, whereas in the mutant, a disorganized vessel formation was seen. Scale bar, 100 μm. (c&d) Semi-thin sections through the yolk sac of WT and mutant embryos, respectively. The sections from the WT yolk sac revealed main branches and secondary branches of vasculature. However, the mutants showed discontinuous vasculature and under-developed secondary branches. VV, Vitelline vessel. Scale bar, 100 μm.

Histological analysis of E9.5 yolk sacs revealed a clear difference in morphology between WT and mutant tissue. Individual vessels were clearly visible in WT tissue, with numerous regularly spaced attachments between the visceral endoderm and mesoderm layers (Fig.4.12a & b). However, the visceral endoderm and mesoderm were more widely separated in the keratin type II null tissue, with occasional attachments forming numerous large spaces that were sparsely populated with blood cells (Fig.4.12c & d). These histological findings clearly indicate a defect in either angiogenesis or vasculogenesis or both. In the mouse embryo, primitive erythroid cells begin to develop in yolk sac blood islands between embryonic days 7 and 8 (Haar and Ackerman, 1971; Silver and Palis, 1997). These blood islands are surrounded by a layer of endothelial cells. Low levels of expression of K8, K18 and K19 that are organized in file filaments have been reported to be expressed in the walls of some blood vessels in the umbilical cord of humans (Jahn et al., 1987). Therefore, whether this defect in angiogenesis is a primary or a secondary effect due to the lack of keratins requires further experimentation.

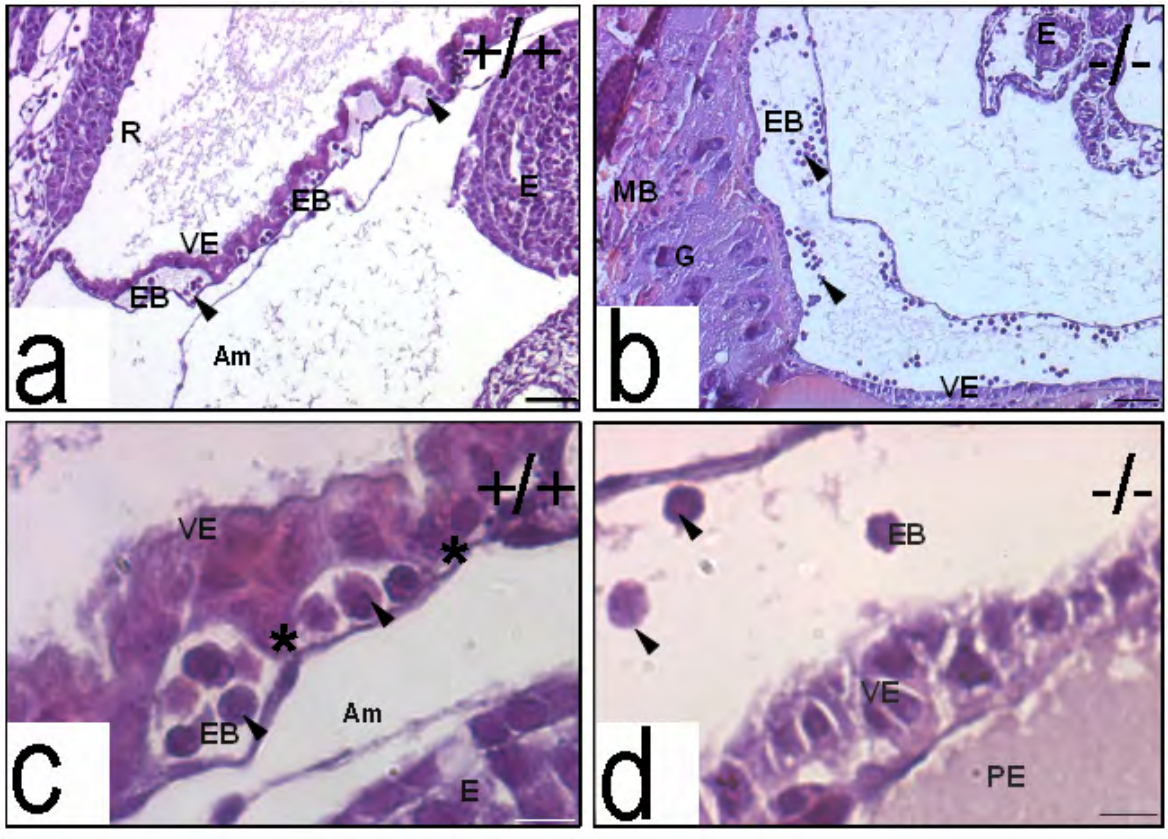


Fig. 4.12. Sections of the visceral yolk sac in WT and mutants. (a & b) Individual vessels are clearly visible in WT tissue (a) by the presence of embryonic blood [EB] and arrow heads, whereas the visceral endoderm [VE] and mesoderm [M] layers are more widely separated in the mutants (b). Scale bar, 10μm. (e&f) Sections of visceral yolk sac from WT and mutants, respectively, at higher magnifications. Regular attachments between visceral endoderm and mesoderm layers are depicted by asterisk in the wild type. Such attachments were rare in the mutants indicating a lack of regular vascular structures carrying lesser amount of fetal blood. Scale bar, 10μm. M, mesoderm; VE,visceral endoderm; EB, embryonic blood; Mb, maternal blood; Am, amniotic membrane; R, Reichert's membrane; PE, parietal endoderm; E ,embryo.

### 4.6.5. The keratin type II null embryos are distinct from other keratin null embryos reported till date

Given the emerging data of the role of keratins in regulating protein synthesis (Kim et al., 2006), cell cycle (Margolis et al., 2006) and protection against apoptosis (Oshima, 2002), the keratin type II null mutants in all these settings were characterized. Embryos *in-utero* seemed to develop normally until E8.5 as judged by eye. By E9.5, they were visibly smaller. To determine the basis for the embryonic lethality of keratin type II null mutants, morphology and histology of extraembryonic tissues at 8.5 -10.5 dpc were examined. The mutant embryos were often developmentally retarded and smaller than their wild-type littermates by 9.5 dpc (Fig.4.10) and the consistent overt defect that might result in embryonic lethality at this stage was attributed to gross abnormalities in primitive hematopoiesis. The placentas of the mutant embryos developed normally until E8.5. Attachment of the allantois to the chorionic plate and formation of a basement membrane between them were normal in mutant conceptuses by light microscopy (Fig.4.13b).

However, there seemed to be a larger number of chorion trophoblast cells in the mutants and the chorionic plate [C] appeared flatter and more compact (Fig.4.13b) when compared to the WT (arrowheads, Fig.4.13a). Morphogenesis of the chorioallantoic interface and intrusion of underlying fetal blood vessels was apparent by E9.5 in wild-type (Fig.4.13c), but the chorionic plate in mutant mice remained flat and failed to interdigitate with the underlying allantoic mesoderm and blood vessels (Fig.4.13c & d). Blood cells in the mutants were sparse (arrowheads, Fig.4.13d) when compared to the WT. This accounted for the paler mutant embryos in comparison with the WT (Fig.4.10). Maternal blood sinuses (asterix) were seen in normal numbers in both WT and mutant deciduas. No mechanical fragility of any cell type was observed in contrast to those seen in the K18/19 (Hesse et al., 2000) and K8/19 (Tamai et al., 2000) double deficient embryos. Moreover, the lack of the labyrinth layer in contrast to the double deficient embryos clearly indicate that the phenotype seen in the keratin type II null embryos is distinct from that reported earlier (Hesse et al., 2000; Tamai et al., 2000).

This is an indication that the phenotype described earlier by the two groups is not a consequence of the loss of keratins; instead, it could be attributed to ‘a gain of toxic function’ due to the presence of keratin aggregates. By E10.5, no live keratin type II null embryos were recovered (Fig.4.13f). These extraembryonic defects together with defective vasculogenesis and angiogeneisis, presumably compromised fetal-maternal circulation and hence efficient exchange of nutrients and oxygen between the embryo and maternal environment, causing the mutant embryos to die around E 9.5.

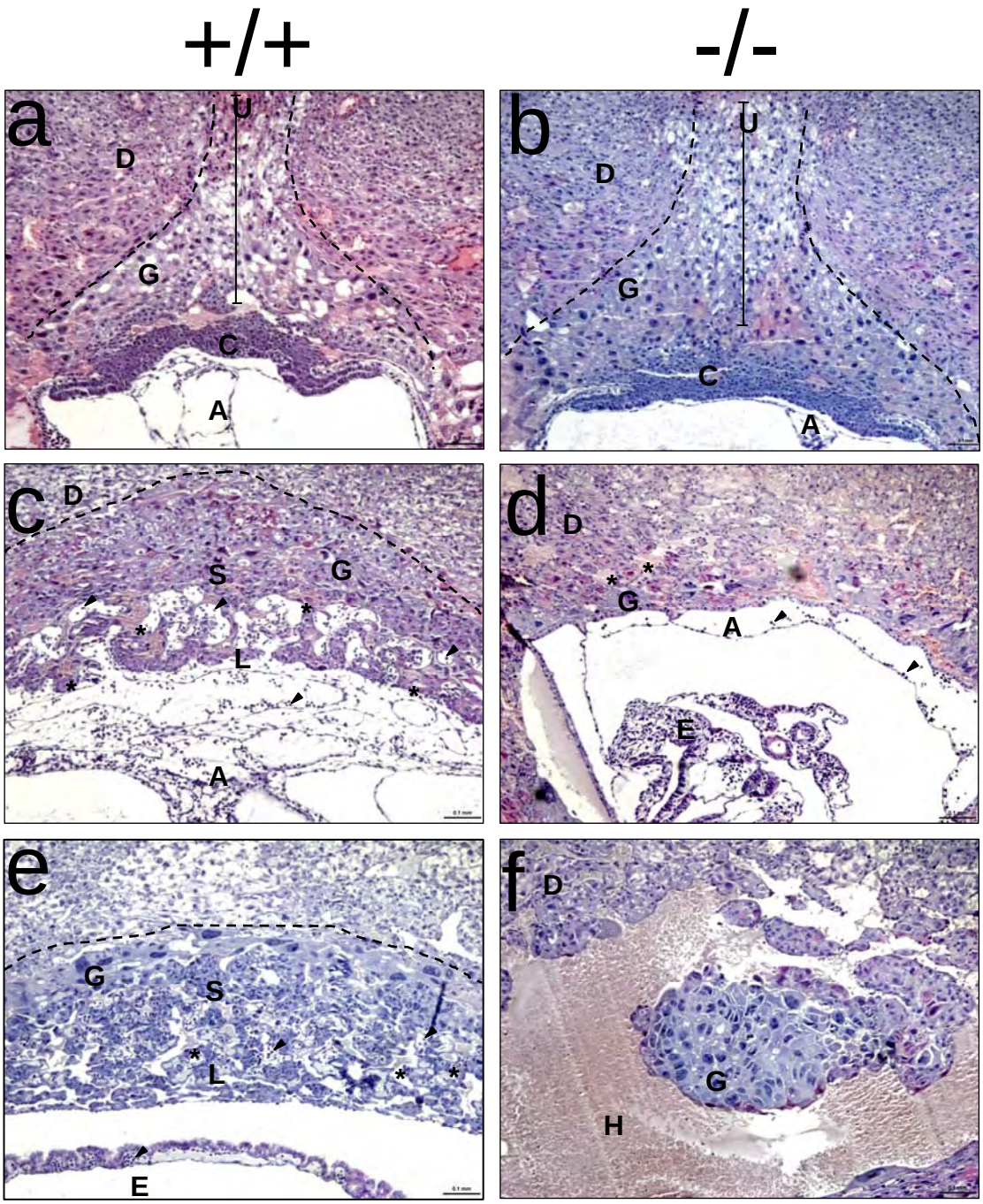


Fig 4.13. Comparison of histological sections through the implantation site of wild-type (*a,c,e*) mutants (b, d, f ). (*a*) In E8.5 WT embryos, the polar extraembryonic ectoderm generates the ectoplacental cone [EC] and the chorionic (ectoplacental) plate [C]. The ectoplacental cone penetrates into the uterine epithelium [U]. It contains embryo-derived diploid and polyploid (giant) trophoblast cells [*G*], as well as maternal blood sinuses [*]. The chorionic plate forms a solid wall of epithelial cells continuous with the ectoplacental cone and is fused to the mesoderm of the allantois [A], which contains extraembryonic blood vessels (arrowheads). (b) The E8.5 mutant embryos, contained larger number of embryo-derived diploid and polyploid (giant) trophoblast cells [*G*], and lesser number of ectoplacental cone precursor cells. (c) At E9.5, the WT placenta was made up of four regions: (*i*) the chorionic plate which is traversed by allantoic capillaries (arrowheads); (*ii*) the labyrinthine zone [L], which is composed of strands of diploid trophoblast cells and of a network of extraembryonic capillaries interspersed with maternal blood sinuses; (*iii*) the spongiotrophoblast zone [S], in which only maternal blood circulates; and (*iv*) the giant cell zone [G]. (d) At E9.5 in the mutants, the placenta contained only two regions. The chorionic mesothelium failed to fold to form the labyrinth layer and the embryo derived spongiotrophoblast layer was also absent. Maternal blood sinuses were still seen [*] although the number of fetal blood cells were drastically reduced [arrowheads] (e) At E10.5, the labyrinthine zone in WT enlarges markedly. (f) At E10.5, the mutant embryos were completely resorped, leaving behind a blood filled cavity [H]. A, allantois; C, chorionic plate; D, diploid trophoblast; E, ectoplacental cone; E, embryo; G, giant cell zone; L, labyrinthine zone; S, spongiotrophoblast zone; U, uterine epithelium; arrowheads and asterix point to allantoic capillaries (containing nucleated erythrocytes) and to maternal blood sinuses, respectively. Scale bar, 100μm.

### 4.6.6. Keratins are not required for cellular proliferation during early embryogenesis

The fact that keratins are not required for the early embryonic development has been reported by a phenotype rescue in K8 null (Kupriyanov and Baribault, 1998) and K18/K19 double deficient embryos by tetraploid aggregation (Hesse et al., 2005). However, emerging data from mouse genetics and human diseases has led to the hypothesis that changes in the expression of certain keratins have a profound impact on cell size, cell proliferation and the response to stress (Gu and Coulombe, 2007; Pallari and Eriksson, 2006). Therefore, in order to analyse whether the mutant embryos are smaller than their wild type littermates due to a proliferation defect besides a nutritional deficiency was attempted. Cell proliferation was measured by immunohistochemistry with anti-phospho-histone H3 (Ser10) antibody on PFA fixed, paraffin embedded transverse sections of E9.5 embryos *in utero* (Fig.4.14a-d). Labeled nuclei per 1000 cells were counted in each of the various cell types like the trophoblast giant cells, embryo, labyrinth, allantois and yolk sac from three independent experiments. Mitotic index was calculated as the percentage of total cells with histone H3 labeled nuclei (Fig.4.14e). No specific staining was observed in the absence of the primary antibody (data not shown). No significant changes in proliferating cells were observed in the mutant embryos in contrast to WT embryos even around the time of death of the mutants, indicating a lack of proliferation defect.

In order to verify if the embryos were smaller due to a reduction in protein translation in the absence of a keratin protein as reported earlier (Kim et al., 2006), the surface area of cells from the extra-embryonic tissue, the trophoblast giant cells (TGC) was measured at random from three independent sections of WT and mutants (Fig.4.14f) using AxioVision LE software. The cell size varied considerably depending on the location of the trophoblast giant cell. However, averaging over 100 cells counted in total, a slight increase of about 8% was observed in the cell size of the mutant TGC's when compared to the WT. However, at this point, it is still uncertain if there is an alteration in protein synthesis which leads to this change, or it is a structural consequence due to the absence of a keratin cytoskeleton. This can be assessed by metabolic labeling using [$^{35}$S] methionine followed by calculating incorporation of radioactivity. An alternative approach has been initiated to analyse changes in protein synthesis by monitoring upstream regulators like Akt and downstream targets like S6 kinase in the mTOR pathway. This will reveal if the changes in cell size of the trophoblast giant cells in the mutants is a consequence of loss of keratins on protein translation.

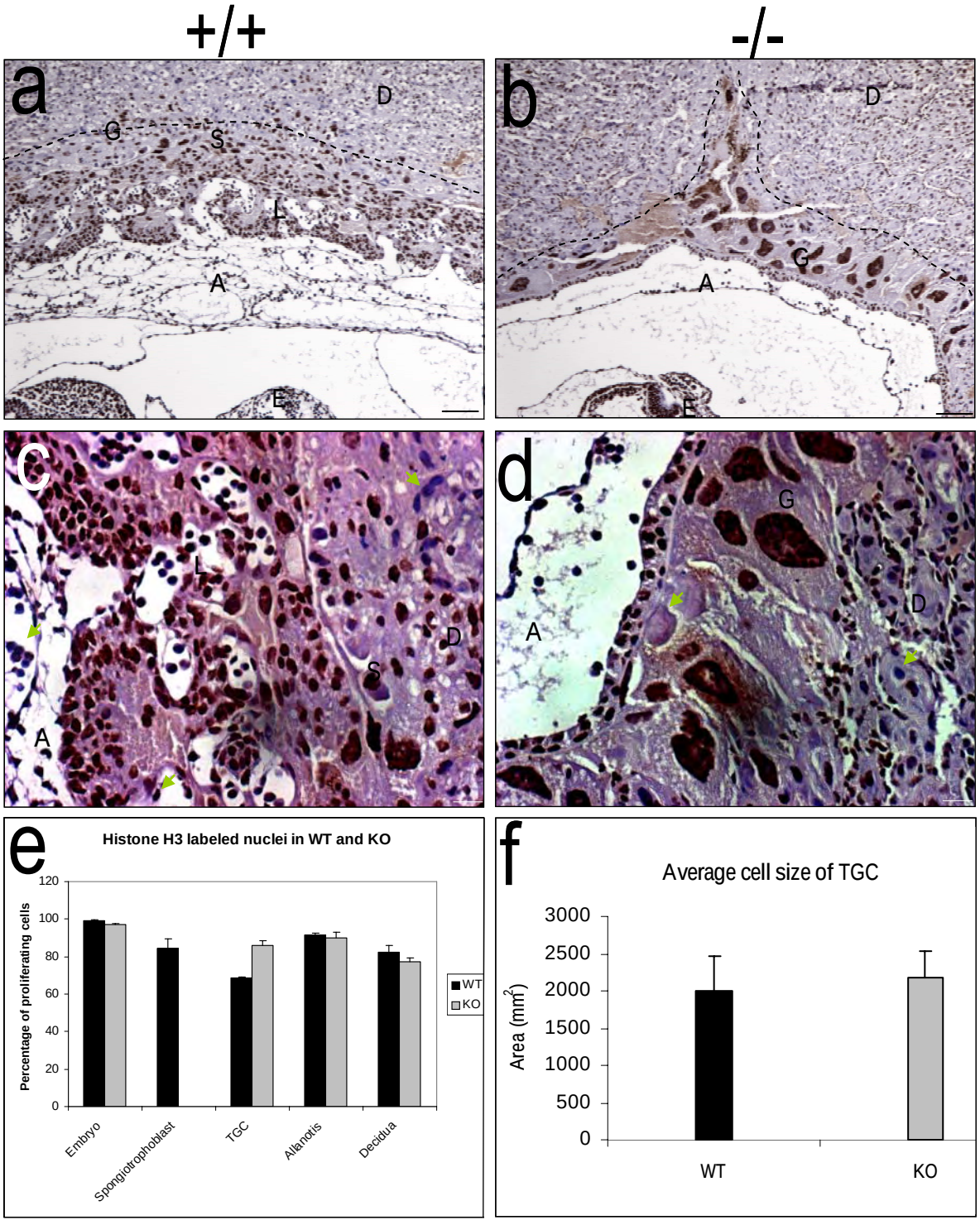


Fig.4.14. Immunohistochemical detection of phopspho-histone H3 in WT and mutant mouse placenta at day E9.5. (a & b) Abundant proliferating cells are seen in all cell types within the developing embryo in WT and in the mutant, respectively. Scale bar, 100 µm. (c & d) Higher magnification images thorough the placenta of WT and mutant indicating labeled and unlabeled nuclei (arrows), respectively. ; Scale bar, 20 µm. (e) Mitotic index was calculated as the percentage of total cells with histone H3 labeled nuclei from three independent experiments. No value for labeled nuclei in the mutant labyrinth was scored due to the absence of this layer in the mutant. (f) Cell surface area measurements performed on trophoblast giant cells of WT and mutants. An increase of 8% in cell surface area was seen in the mutants when compared to the WT. D, decidua; L, labyrinth; S, spongiotrophoblast, G, trophoblast giant cell; E, embryo.

## 4.6.7. Increased rate of apoptosis in mutants is likely a consequence of nutritional deficiency

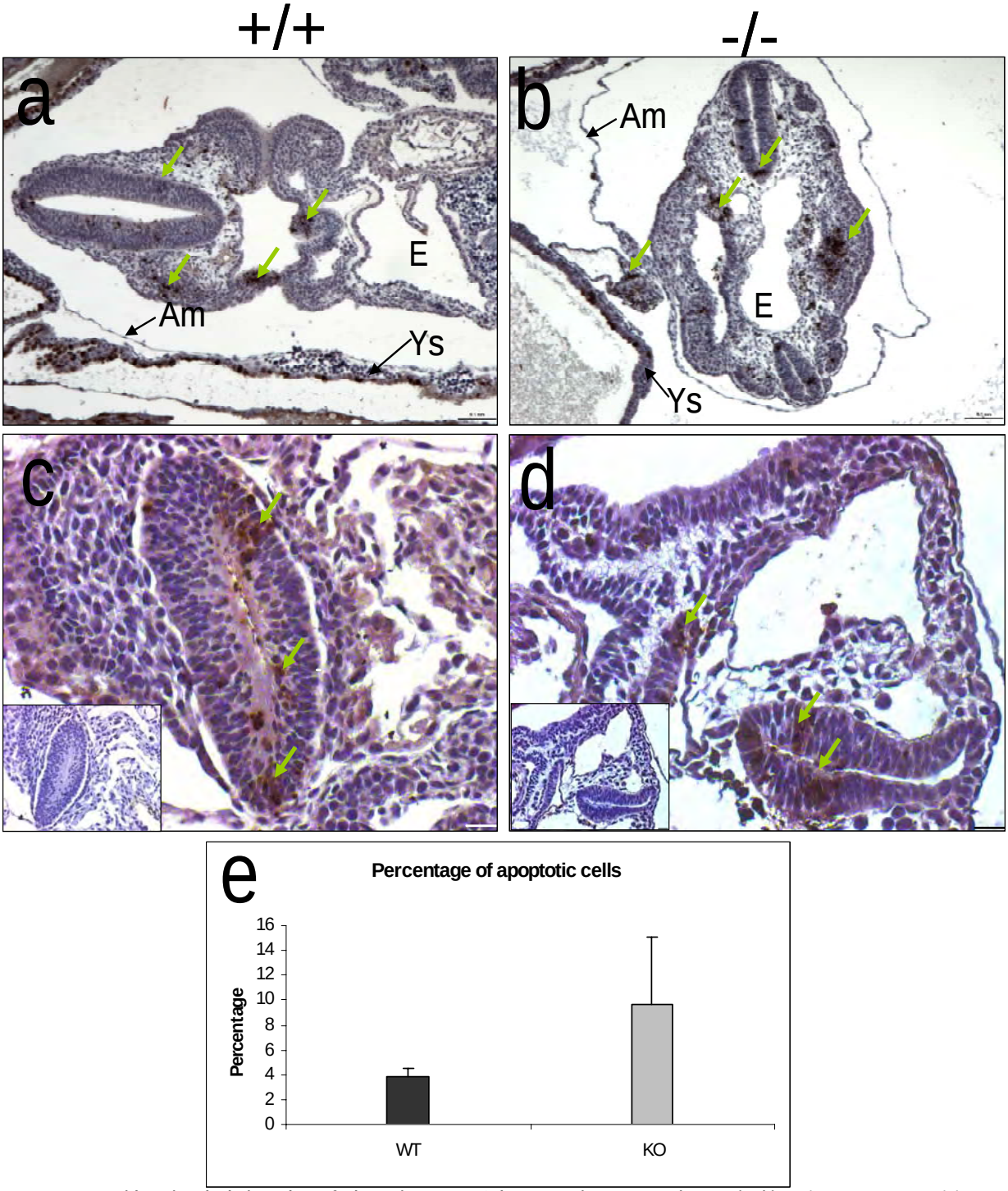


Fig 4.15. Immunohistochemical detection of cleaved caspase-3 in WT and mutant embryos. (a&b) Active caspase-3 staining displayed as a cytoplasmic and/or nuclear pattern in cells undergoing apoptosis in wild type and mutant, respectively. Positive cells for apoptosis had a condensed nucleus, a shrunken cytoplasm, and membranes blebbing consistent with morphological features of apoptosis (arrowheads). E, embryo; ys, yolk sac; am, amniotic membrane. Scale bar, 100μm (c&d) Higher magnification of embryo showing positively stained apoptotic cells in WT and mutant, respectively. Insets in c and d show control slides which did not receive any primary antibody from WT and mutant sections, respectively. Scale bar, 20 μm. (e) The number of apoptotic cells in WT and mutant embryo sections were counted and expressed as a percentage of the total number of cells in the sections.

The type I keratin K18, which was deleted along with all the type II keratins in this work, has been reported to bind TRADD (Caulin et al., 2000). TRADD is an adaptor protein that is recruited to the liganded TNF receptor 1 and essential for downstream signal relay, including the formation of death-inducing signaling complexes. Sequestration of TRADD's interaction with K18 prevents it from being recruited to activated TNFR1, resulting in signal attenuation (Inada et al., 2001). Moreover, enhanced susceptibility to TNF$\alpha$ following abrogation of the keratin–TRADD interaction was reported in K8 null embryos which die at mid-gestation due to a trophectoderm failure (Jaquemar et al., 2003).

Hence, in order to exclude embryonic lethality as a consequence of apoptosis, susceptibility of keratin null embryos to apoptosis was determined by immunohistochemistry with cleaved caspase-3 (*Asp175*) on PFA fixed, paraffin embedded sections of WT and mutant embryos at E9.5. The number of apoptotic cells in a 5$\mu$m sectioned embryo were counted and scored as a percentage from four independent experiments. About 3.8% of cells on an average in the WT were undergoing apoptosis. However, the variability in the percentage of apoptotic cells was very high in the knockouts, ranging from 3.5 % to 13.6%. A positive correlation existed the size of the embryo to the susceptibility to apoptosis. Smaller the embryos, larger were the number of apoptotic cells and *vice-versa*. This could be accounted to the fact that the embryos that were smaller were the ones with more severe vascular and labyrinth defects, hence with greater nutritional deficiency and a higher susceptibility to apoptosis (Fig.4.15). Moreover, the cells undergoing apoptosis were not restricted to epithelial cells, suggesting that apoptosis in these embryos was not a consequence of lack of keratins, but a secondary effect due to the lack of nutrition. Therefore, it can be concluded that this 3-fold increase in apoptosis seen in the mutants is a consequence of nutritional deficiency.

### 4.6.8. Altered cell-signaling in the absence of type II keratins

Given that the keratin type II null mutants die primarily due to nutritional deficiency, accompanied by an increase in apoptosis, it was hypothesized that this would be accompanied by an activation of pro-apoptotic p38 MAP kinase (Davis, 2000). It has been previously shown that p38$\alpha$ mitogen-activated protein kinase (MAPK) is essential for placental, embryonic and yolk sac angiogenesis. P38$\alpha$ mutants die at mid gestation with defects in the placenta, corresponding to a severe reduction in the spongiotrophoblast layer, as well as a near absence of the labyrinth layer due to a failure of vascularization by endothelial cells from the underlying chorionic plate. The authors predict that p38$\alpha$ is required for the vascular remodeling associated with angiogenesis (Mudgett et al., 2000). The defects seen in the keratin type II null mutants have a striking similarity to those of the p38$\alpha$ null mutants.

Protein lysates from a pool of embryo and yolk sac at E9.5 from WT and mutants were subjected to immunoblotting against p38 and activated p38. However, contrary to expectations, a reduction in the activated p38 levels up to 60% was observed from three independent experiments (Fig.4.16).

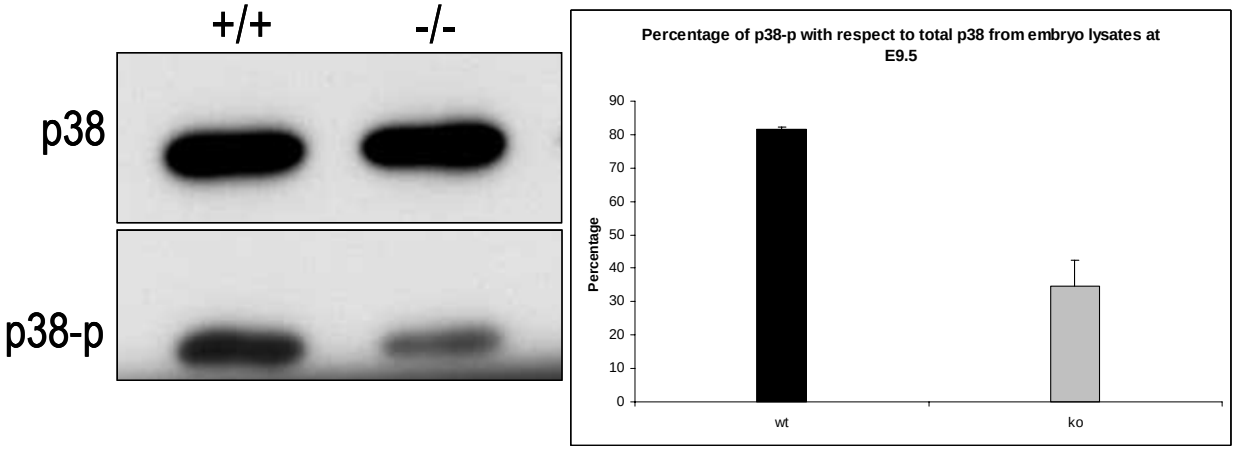


Fig.4.16. Immunoblot analysis of p38 and activated p38 in WT and mutant embryos at E9.5. The relative expression of p-p38/total p38 was assessed by densitometry from three independent experiments. A reduction of activated p38 levels were observed upto 60% in the mutants when compared to that of the controls. The bar graphs illustrate the mean percentage of p38-p.

Moreover, recent data has suggested that K8 when phosphorylated at S73 by p38 MAP kinase, determines keratin organization (Woll et al., 2007). Given this recent finding, it can be speculated that keratins play a role upstream in the p38 MAP kinase pathway in placental angiogenesis. Future work will clarify alterations in upstream and downstream players in this pathway.

### 4.6.9. Analysis of placental differentiation in the absence of keratins

The absence of the labyrinth and the spongiotrophoblast layer, as determined by histological analysis would indicate an alteration in the differentiation of the placental lineage in the absence of keratin filaments. Hence, in order to validate this hypothesis, *in-situ* hybridization on implantation sites of E8.5 and E9.5 embryos was carried out using several lineage markers in collaboration with Dr. David Simmons, University of Calgary, Calgary (Fig.4.17). The most significant change between the WT and mutants was seen in the expression of Syncytin A (*SynA*). *SynA* is a transmembrane protein, involved in the formation of the placenta syncytiotrophoblast layer generated by trophoblast cell fusion at the materno–fetal interface (Dupressoir et al., 2005). *SynA* is expressed in the layer of chorion cells that meet the EPC (chorion trophoblast cells) (Mi et al., 2000). These cells are located opposite to *Gcm1* expressing cells and are predicted to form the second layer of the syncytiotrophoblast cells (D.

Simmons et al., unpublished data). These cells also contribute to labyrinth formation at later stages. *SynA* expression was seen in the mutants at E9.5. However, the S*ynA* expressing cells appeared flat when compared to the WT cells (Fig.4.17g & h) and appeared to have a proliferation defect to elongate and inter-digitate. This was consistent with the histological findings of an almost invisible labyrinth layer (Fig.4.13d).

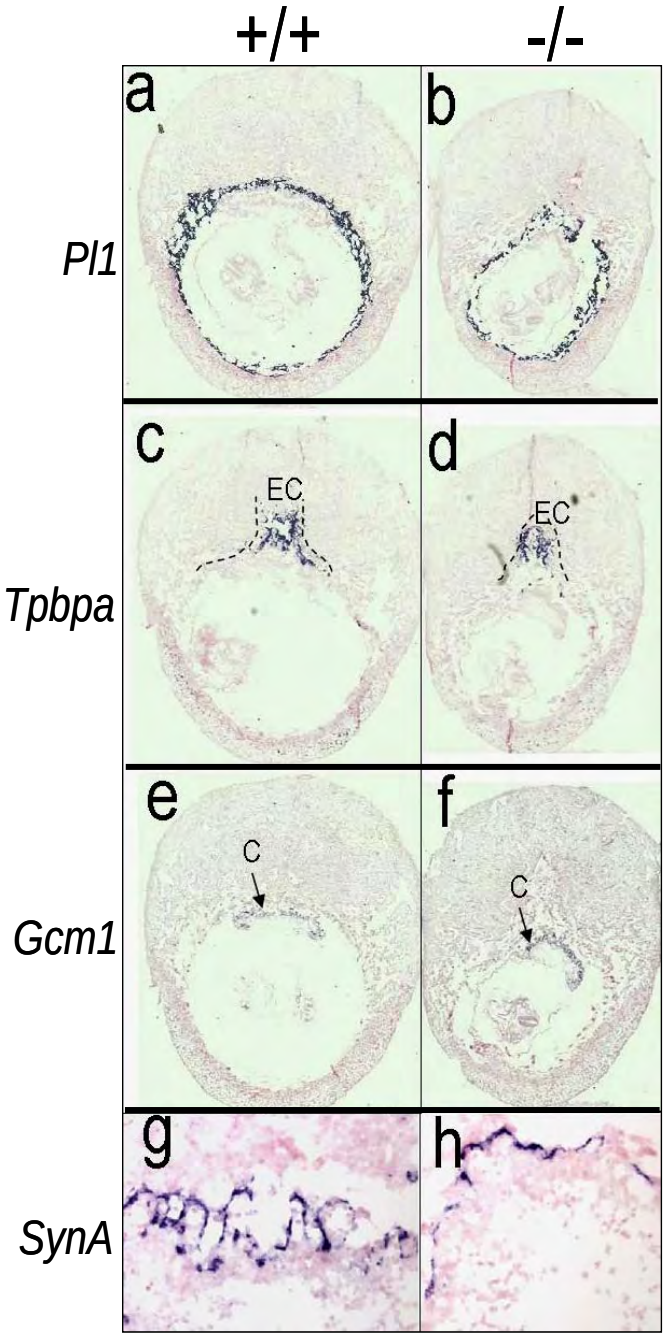


Fig.4.17. *In-situ* hybridization analysis for lineage markers *Pl1*, *Tbpba1*, *Gcm1* and *SynA* mRNA expression in E9.5 placentas. Differentiation of the placenta is appropriate in the mutants (b, d, f and h) as compared to the wild type placenta (a, c, e and g) EC, ectoplacental cone; C, chorion.

Expression of *Gcm1* begins at E8.5 following chorio-allanotic attachment at the leading edge of where the chorion meets the allantois in WT embryos. Sites of *Gcm1* expression become the initial branch points where fetal vessels grow into the chorion and start branching (Anson-Cartwright et al., 2000; Cross et al., 2006). These branching points were established in the mutants indicating that the decreased vascularization seen in the placenta of the mutant cannot be attributed to a failure of the *Gcm1* positive cells to interdigitate to form the labyrinth (Fig.4.17e&f). *In-situ* hybridization with a probe for placental lactogen-1 (*Pl-1*), which is a marker of all TGC's which line the implantation chamber including those that arise from the outer layer of trophectoderm from the blastocyst (called primary TGCs) (Guillemot et al., 1994), detected an expansion of the giant cell layer in mutant placentas. The layer was, however, slightly disorganized (Fig.4.17b vs. 4.16a), but the expression level indicated a normal differentiation pattern of the trophoblast giant cells. The fourth marker, *Tpbpa*, is normally expressed in the ectoplacental cone at E8.5 in precursor cells of the spongiotrophoblast layer and later on in the spongiotrophoblast cells when they begin to form from E9.5 (Lescisin et al., 1988). Normal expression pattern of *Tpbpa* was observed in the ectoplacental cone of mutants as well as the WT at E9.5, indicating that spongiotrophoblast precursor cells are present in cells committed to generate the spongiotrophoblast layer. This would indicate a normal differentiation programme. Expression of the marker for trophoblast stem cells, *Esrrb*, which is normally switched off by E8.5 (Luo et al., 1997), was appropriately switched off in the keratin null mutants (data not shown). This indicated that the failure of the labyrinth formation as seen by H & E stained histological sections, cannot be attributed to a failure of the stem cells to differentiate into the proper precursors for labyrinth formation. Expression of *Prlpa* that is expressed only in the secondary TGCs (Muller et al., 1998), originating from the EPC and the polar trophectoderm was normal in the mutants (data not shown), indicating that the mutants were able to generate additional TGCs following implantation.

In summary, the *in-situ* hybridization data of various placental lineage markers at E9.5 clearly indicate that keratins do not affect cellular differentiation *per se*. The lethality of the mutant embryos at E9.5 cannot be attributed to a differentiation defect, but, to a proliferation defect of the S*ynA* expressing chorionic trophoblast cells. It can therefore be concluded that the keratin type II null mice die due to two structural and functional defects. Firstly, altered angiogenesis and vasculogenesis in the yolk sac which manifests around E7.0 - E8.0 and secondly, due to a reduced feto-maternal interface with a dramatic reduction in the size of the labyrinth.

# 5. DISCUSSION

## 5.1. Functional role of keratin multigene families

Multigene families consist of a group of gene orthologs that have similar structures and distinct functions. The intermediate filament [IF] protein family is one such family (Fuchs and Weber, 1994). Vertebrate IFs are organised into five distinct gene families according to sequence identity and expression patterns (Fuchs and Weber, 1994; Herrmann et al., 2003), among which are the type I and type II keratin gene families. However, unlike many other multigene families such as myosins (S and Saitou, 1999), connexins (Cruciani and Mikalsen, 2006), whose individual members are spread across the genome, gene families like those of keratins (Hesse et al., 2001), Hox (McGinnis et al., 1984) or the MHCs (1999), are clustered. Such gene families have been subjected to evolutionary constraints to maintain this arrangement, thereby representing a functionally significant group (He and Goldwasser, 2005). The evolution of the keratin gene families have been studied for about three decades. Based on 'Phylogeny Analysis Using Parsimony (PAUP)' set of programs, evolutionary trees were derived from the keratin protein sequences. The two keratin families showed extraordinary parallelism in their patterns of gene duplications. In both families, the genes expressed in embryos diverged first. This was followed by immense gene duplications, which eventually created the subfamilies expressed in various differentiated cells, like hair keratin genes, basal cell-specific keratin genes and keratins expressed in hyperproliferative conditions. The parallelism of gene duplications in the two keratin gene families reflects a mechanism in which duplications in one family influence duplication events in the other family (Blumenberg, 1988).

The type I and type II keratins form obligatory heteropolymers by forming stable double-stranded coiled-coil heterodimers, therby forming keratin filaments. The organization of keratin filaments varies with cell types. In most epithelial cells, the keratin filaments spans the entire cytoplasm, from the surface of the nucleus to the cell periphery where it interacts with cell matrix (hemidesmosomes) and cell-cell (desmosomes) adhesion complexes (Gallicano et al., 1998; Guo et al., 1995). However, they form thick bundles in epidermal keratinocytes, they are apically restricted as densely woven mats in enterocytes, and they form subplasmalemmal enrichments in hepatocytes. The regulation of the organization of the keratin filaments within the cells is regulated by differential association of keratin filaments with scaffolding proteins and keratin modifications (Coulombe and Omary, 2002; Coulombe and Wong, 2004) such as the desmosomal plaque proteins desmoplakin/plakophilin/plakoglobin (Hatzfeld and Nachtsheim, 1996; Hofmann et al., 2000; Kowalczyk et al., 1999) and the hemidesmosomal components plectin and bullous pemphigoid antigen1 (Fontao et al., 2003; Steinbock et al., 2000). Plectin, which is a multifunctional cytoskeletal cross-linker may also participate in

attachment to other cytoskeletal elements and the nucleus (Leung et al., 2002; Rezniczek et al., 2004). Moreover, post translational modification like phosphorylation also is suggested to play a vital role in regulating keratin organization since altered phosphorylation is often accompanied by structural changes (discussed below) (Omary et al., 2006).

Until today, the progress made in defining the roles of keratins *in vivo* has originated mostly from studies involving genetically manipulated mice and disease conditions in humans. However, considerable uncertainty has evolved in interpretation of their phenotypes. Gene knockouts and mutational studies of 13 keratins analysed so far in mice have demonstrated phenotypes ranging from major defects causing embryonic lethality or skin fragility to subtle and late onset liver alterations (rev. Magin et al., 2004; rev. Kim and Coulombe, 2007). Several keratin-associated diseases in humans and phenotypes in mice are accompanied by the presence of intracellular aggregates of unpolymerized keratin proteins, that prove toxic to the cell (Omary et al., 2004; Watson et al., 2007; Zatloukal et al., 2004), thereby exhibiting a dominant-negative effect. Moreover, characterizing individual keratin function by loss-of-function studies has been very challenging due to compensatory effects of an alternative keratin (Table 1.1). Significant redundancy among the multiple keratins can be related to a common ancestry (Blumenberg, 1988), clustered organization (Hesse et al., 2001; Hesse et al., 2004) and sequence relatedness of specific keratin genes (Hoffmann et al., 1985).

Recent data have indicated roles for keratin intermediate filaments beyond structural support. The idea of keratins as “signaling platforms” as well as their structural functions may not be completely separable (Coulombe and Wong, 2004; Pallari and Eriksson, 2006; Paramio and Jorcano, 2002). In several epithelia, like in the basal epidermis, the keratin cytoskeleton protects cells against mechanical stress through formation of a three-dimensional cytoskeleton that associates with proteins of hemidesmosomes and desmosomes (Fuchs and Cleveland, 1998; Garrod et al., 2002; Green and Jones, 1996). While these interactions at the cell periphery are well documented and essential for epidermal integrity, associations of keratins with the nuclear envelope is not well understood, but are non-essential for nuclear positioning (Litjens et al., 2006; Magin et al., 1998; Venetianer et al., 1983). Reorganization of keratin IFs in response to extra- or intracellular signals predominantly involves phosphorylation at several Ser residues, leading to generation of granules and an increase of the soluble subunit pool. At the same time, Ser phosphorylation creates binding sites for 14-3-3 family adapter proteins, as demonstrated for K18 (Ku et al., 1998). Most recent findings have indicated a phosphorylation-dependent recruitment of 14-3-3 to K17, thereby regulating protein biosynthesis via mTOR signaling, and also the interaction of 14-3-3 with K8, K18 and K19 being a prerequisite for cell cycle progression (Kim et al., 2006; Margolis et al., 2006). Studies with keratin transgenic mice mimicking the mutations associated with cirrhosis and fibrosis progression, K8-G61C, revealed an

increased susceptibility to stress-induced liver injury and apoptosis. This was attributed to the inhibition of phosphorylation of K8 at S73 by stress-activated protein kinases such as p38, JNK and p42 (Ku and Omary, 2006). Similar susceptibility to stress was also observed in the S73A mutant wherein the site for phosphorylation was destroyed. A "phosphate sponge" hypothesis was formulated suggesting that keratins, during stress, would absorb the stress-activated phosphate kinases, thereby reducing their untoward effects, thereby protecting the cells from injury (Ku and Omary, 2006). Furthermore, in an injury model of lung alveolar epithelial cells, the keratin cytoskeleton disassembles partially in the presence of shear stress coincident with PKCδ-mediated phosphorylation of K8 at S73, indicating alterations in keratin organization in response to mechanical stimuli (Ridge et al., 2005). Therefore, most properties reported for keratins are controlled by highly complex patterns of phosphorylation and molecular associations that have been carried out *in vitro*, which may not be a true representation of the situation *in vivo*.

The work reported here is a novel *in vivo* approach, utilizing the clustering of the keratin gene family since it is well suited for functional studies by subjecting them to a large scale genome deletion.

## 5.2. An *in vitro* chromosome engineering approach to study function of keratin *in vivo*

A very challenging approach to overcome the problem of keratin function redundancy and significance of its evolutionary diversity was undertaken. This thesis utilized the fact that all type II keratin genes are clustered in chromosome 15 in mice without any other known genes within the cluster (Hesse et al., 2001).The evidence that type II keratins are expressed prior to the type I keratins during early embryogenesis (Lu et al., 2005), and the presence of a type II keratin being required for the expression of the type I keratin (Giudice and Fuchs, 1987), offered an opportunity to generate a complete keratin null situation during early embryogenesis by a large scale genome deletion. Hence, it was possible to carry out a true loss-of-function analysis of type II keratins.

Homologous recombination in ES cells using replacement vectors has generated deletion of genomic fragments up to 30 kb (Gu et al., 1993; Zhang et al., 1994). However, inducing large defined chromosomal rearrangements was only achieved in the mid-1990's by taking advantages of the Cre-*loxP* recombinase system (Herault et al., 1998; Ramirez-Solis et al., 1995; Smith et al., 1995; Van Deursen et al., 1995) and defining the chromosomal engineering strategy. This system worked very efficiently in deleting 0.68 Mb of the genomic locus spanning all type II keratins as well as the type I keratin *Krt18* gene. The ES cells heterozygous for the deleted loci grew normally and were not lethal, indicating any consequence of the loss of a single highly dosage-sensitive gene cluster (Zheng et al., 2000). To the best of current knowledge, this is the first time a deletion of such a large gene family has

been carried out in mammals. Over the last 10 years, Duboule and collaborators have used this technique to analyze the molecular mechanisms that modulate expression of Hox genes encoding transcription factors controlling positional information along the trunk and limb axes (Herault et al., 1998; Kmita et al., 2002; Kmita et al., 2000; Kondo and Duboule, 1999; Kondo et al., 1998; Spitz et al., 2001; Zakany and Duboule, 1996). They have deleted up to 13 genes spanning up to 100 Kb of the genomic locus in *Drosophila* and remains the largest gene family reported to be deleted till date. However, the discovery of micro RNA (miRNA) genes within the Hox gene cluster, that regulate the expression of the Hox genes, has added a new dimension to the complexity to the regulation of these Hox genes (Chopra and Mishra, 2006; Tanzer and Stadler, 2004). There are at least three groups of miRNA's residing within the Hox gene cluster. However, no miRNA genes reside within the keratin clusters in mouse and human as per miRBASE sequence database, Release 10.0 August 2007 (http://microrna.sanger.ac.uk/sequences/index.shtml). In summary, it can be stated that the strategy undertaken in this work to create a large scale genome deletion was efficient, and that the interpretation of data is most likely not obscured by affecting miRNA's.

## 5.3. Growth retardation and lethality of keratin type II null embryos is a consequence of defects in the yolk sac followed by placental defects

It has been reported that K8 and K18 form the first IF in embryogenesis in the trophectoderm, complemented by K19 (Brulet et al., 1985; Jackson et al., 1980; Lu et al., 2005). Gene ablations from various IF genes like desmin (Li et al., 1996; Milner et al., 1996), vimentin (Colucci-Guyon et al., 1999), glial fibrillary acidic protein (Gomi et al., 1995; Pekny et al., 1995), neurofilaments (Elder et al., 1998a; Elder et al., 1998b; Rao et al., 1998; Zhu et al., 1998) and lamin A (Sullivan et al., 1999), had suggested that IF proteins may not be required during embryogenesis. Therefore, it was hypothesized that the primary defect in the keratin type II null mutants would manifest in the epithelial cells that normally express keratins like those of the yolk sac and the extra-embryonic tissues like the trophoblast cells. Mice that lack K8 (Jaquemar et al., 2003), both K18 and K19 (Hesse et al., 2000) or both K8 and K19 (Tamai et al., 2000) fail to form keratin filaments in simple epithelial cells, such as trophoblast cells. As a result, mutant embryos die between E9.5 - E10.5 owing to compromised trophoblast cell integrity, which leads to placental site hemorrhages that are particularly associated with trophoblast giant cells. However, despite a compromised keratin cytoskeleton, neither mechanical disruption of the trophoblast cells nor placental hemorrhage was seen in the keratin type II null mutants analysed here.

The keratin type II null mutants died at E9.5 owing to a failure to form a fully functional feto-maternal interface. They lacked a functional labyrinth. However, the defect in the placental labyrinth

alone may not fully explain the growth retardation and lethality of keratin type II null mutants. A number of other mouse mutants with lethality at the same stage and very similar placental defects exhibit only mild or no growth retardation, such as embryos lacking a basic helix-loop-helix transcription factor - *Mash2*, zinc finger transcription factors - *Gata2* & *Gata3,* or Ets family transcription factor - *Ets2* (Guillemot et al., 1994; Ma et al., 1997; Yamamoto et al., 1998). The development of embryos during early organogenesis (E8.5 to E11.5) is critically dependent on the formation of a functional yolk sac circulation. The yolk sac consists of an outer endoderm and inner mesoderm layer, where keratins K8 and K18 are expressed in the former layer (Hesse et al., 2000). At E7.0, blood islands (lined with endothelium) are formed between the endoderm and mesoderm. These fuse to form a primary vascular plexus (vasculogenesis), which then undergoes remodeling (angiogenesis) to produce an extensive vascular network. At ~E8.5, the yolk sac vasculature fuses with the embryonic vasculature, and until the chorioallantoic placenta is established, the yolk sac functions as a primitive placenta. Cessation of blood flow within the yolk sac plexus causing fetal growth retardation have been reported in embryos lacking HNF4 or trombomodulin (Chen et al., 1994; Healy et al., 1995). In addition, a defect in the yolk-sac blood circulation is often associated with the dilation of the pericardium as an indication of osmotic imbalance within the embryo. In accordance, a few keratin type II null embryos at E9.5, exhibited an enlarged pericardium. Embryonic vascular development is initiated from the hemangioblast, a progenitor cell that also gives rise to primitive hematopoietic cells (Choi et al., 1998). It must be first assessed if keratins are expressed in the mesodermal layer of the yolk sac membrane that gives rise to the vasculature in the mouse embryo, given that traces of K8, K18 and K19 have been reported to be expressed in some blood vessels in the umbilical cord of humans (Jahn et al., 1987). Future work will assess whether the loss of type II keratins is associated with defects in primitive erythropoiesis by an indirect immunofluoresence staining using a Ter119 antibody, which identifies erythroid cells within the blood islands. Defects in vascular remodeling can be estimated by characterizing the expression of endothelium specific receptor tyrosine kinase, *tie-2/tek* (Dumont et al., 1994; Sato et al., 1995) and its ligand angiopoietin-1 (Suri et al., 1996), both of which are prerequisites for embryonic angiogenesis. These experiments are underway and have not been reported here due to the shortage of embryos during the time this discussion was written.

Since the vascular defects in the yolk sac manifested before the labyrinth placenta became truly functional, it can be concluded that the vasculogenic and angiogenic defects in the yolk sac are the initial cause for the embryonic death of the keratin type II mutants.

Mutation of genes belonging to the Notch signaling pathway like *Notch1/Notch4* (Krebs et al., 2000), *delta-like4* (Duarte et al., 2004), *Hey1/Hey2* (Fischer et al., 2004) and *Rbpsuh* (Krebs et al., 2004) have been identified to block chorioallantoic branching. These genes are expressed within the

allantoic mesoderm/blood vessels, suggesting that the fetal vasculature may be important for initiation of branching of the chorioallantoic interface. However, in humans, chorionic villi develop before becoming vascularized (Castellucci et al., 2000). Hence, it is possible that the development of the labyrinth layer and vascularization may not be inter-related. It can therefore be concluded that the keratin type II null mice die due to two structural and functional defects. Firstly, altered angiogenesis and vasculogenesis in the yolk sac which manifests around E7.0 - E8.0 and secondly, due to a reduced feto-maternal interface with a dramatic reduction in the size of the labyrinth.

The concept of epithelial-mesenchymal interaction, and the fact that keratins are expressed in epithelia and not in mesenchymal cells, opened a new dimension to analyzing the phenotype of the keratin type II null mice. Could altered mesenchymal-epithelial interactions account for embryonic lethality in keratin type II null mice?

The major components of the mammalian placental membranes are made up of an epithelial surface layer- the trophoblast, and a heavily vascularized mesenchyme - the allantoic mesenchyme. The trophoblast layer makes the most intimate contact with maternal tissues and it displays a wide range of unusual, often invasive, phenotypes. However, one common feature of trophoblast development in all species is a strong correlation between the proliferation and differentiation of this epithelial layer and its physical contact with the developing allantoic mesenchyme. This strongly suggests an epithelial–mesenchymal interaction involving paracrine signals from allantoic mesenchyme acting on adjacent trophoblast (Lacey et al., 2002; Stewart, 1996). One such paracrine signal is the hepatocyte growth factor (HGF), which is a multipotent mitogen, morphogen and motility factor. HGF is secreted as an inactive heparin binding glycoprotein, which remains in this form in the extracellular matrix. The biological actions of HGF are mediated via a transmembrane glycoprotein called *c-met* (Weidner et al., 1993). Activation of *c-met* by hepatocyte growth factor leads to dimerisation of the receptor, followed by autophosphorylation of several intracellular messengers which are thought to mediate its subsequent effects (Somerset et al., 1997). The mitogenic properties of HGF include induction of c-*met* mediated cell division in many epithelial and endothelial cells, including trophoblast and vascular endothelium (Matsumoto and Nakamura, 1996; Zarnegar and Michalopoulos, 1995). During mesenchymal - epithelial cell interaction, HGF and c-*met* localize to the same cell types, induce paracrine signals and initiate proliferation, invasion, and organizing branching tubules (Somerset et al., 1997). Analysis of HGF -/- embryos revealed that the mesenchymal cells of the allantois produce HGF, which acts as a paracrine growth factor on the epithelial derived labyrinthine trophoblast cells, via c-*met*, to aid normal labyrinthine development (Uehara et al., 1995). Several cytokines and growth factors are known to influence trophoblast migration [e.g. EGF (Wright et al., 2006), IGF-2 (McKinnon et al., 2001), HGF (Lala and Chakraborty, 2003)], proliferation [e.g. interleukin (Paiva et al., 2007), leptin (Magarinos

et al., 2007), HGF (Somerset et al., 1998), GM-CSF (Lea and Clark, 1993)] and/or invasion [e.g. LIF (Poehlmann et al., 2005)], each factor utilizing at least one pathway for intracellular signaling in the trophoblast.

In agreement with epithelial-mesenchymal interactions playing a role in placental development, analyses of the keratin type II null embryos was carried out. *In situ* hybridization suggested that differentiation of the epithelial or mesenchymal layers were not affected. The different trophoblast cell layers within the chorion are thought to give rise to the three layers of differentiated trophoblast in the mature labyrinth. Emerging data of gene expression and cell lineage tracing studies supports this model (D. Simmons et al, unpublished data). Detailed ultrastructural studies in the mouse (Hernandez-Verdun, 1974) and hamster (Carpenter, 1972) placenta, as well as cell lineage tracing studies (Anson-Cartwright et al., 2000; Basyuk et al., 1999) during early stages of labyrinth development suggest that the epithelium derived cells, which are committed to express *Gcm1*, give rise to the innermost syncytial layer closest to the fetal capillaries (SynT-II) (Fig. 6.1). By contrast, more apical trophoblast cells, that are committed to express *SynA*, gives rise to both the outer syncytial layer (SynT-I) and the trophoblast giant cells lining the maternal blood sinusoids [sinusoidal trophoblast giant cells (S-TGCs)] (D.Simmons et al., unpublished data). Although these layers have independent cell lineage origins, it is likely that their development is inter-dependent as differentiation of SynT-II begins within a few hours after allantoic attachment (Carpenter, 1972; Hernandez-Verdun, 1974; Hernandez-Verdun and Legrand, 1975), whereas differentiation of SynT-I cells begins ~24 hr later and after morphogenesis has begun (Carpenter, 1972) (Fig. 5.1). Any process that would disturb the balance between proliferation and/or syncytial fusion would alter the integrity and function of the layer as a whole, which in turn may impair gas and/or nutrient transfer to the fetus as well as endocrine activities. In the keratin null mutants, *Gcm1* expression, which begins at E7.5 in the leading edge of the chorion, was normal. However, the chorionic trophoblast derived *SynA* positive cells, although present from E8.5, did not proliferate and elongate to contribute to the formation of the labyrinth. They remained flat and did not take the prismatic shape as that of the wildtype (Fig.4.14g Vs Fig.4.14h). It has already been established that *Syncytin* is a target of *Gcm1* (Yu et al., 2002). It can thus be speculated that the *Gcm1* positive cells might secrete paracrine signals which stimulate the proliferation of the *SynA* positive cells, thereby establishing epithelial-epithelial interaction, which eventually lead to the formation of the syncytiotrophoblast and labyrinth. A combined *in-situ* hybridization-immunohistochemistry of *SynA* and proliferating cell nuclear antigen (PCNA) or histone H3, would validate the proliferation defect of this specific subset of cells. A detailed ultra-structural study would clarify if the formation of the SynTI layer is affected in the keratin type II null mutants, which would be the case if indeed the proliferation of the *SynA* expressing chorion trophoblast cells is altered. It has been reported that the stimulation of PKA signaling leads to an

increase of *Gcm1* transcript levels, which maybe responsible for a concomitant increase of the amount of syncytin transcript (Knerr et al., 2005). Whether this signaling is altered in the keratin type II null mutants would require culture of ectoplacental cone explants from the mutants, stimulation of *Gcm1*, and study the expression of *SynA*. These experiments should be succeeded by migration and proliferation studies, to identify if such a paracrine signal does exist, and to identify altered upstream or downstream targets of the PKA pathway. RNA array analysis would be required to identify transcriptional changes in the keratin type II mutants in contrast to the wild type embryos.

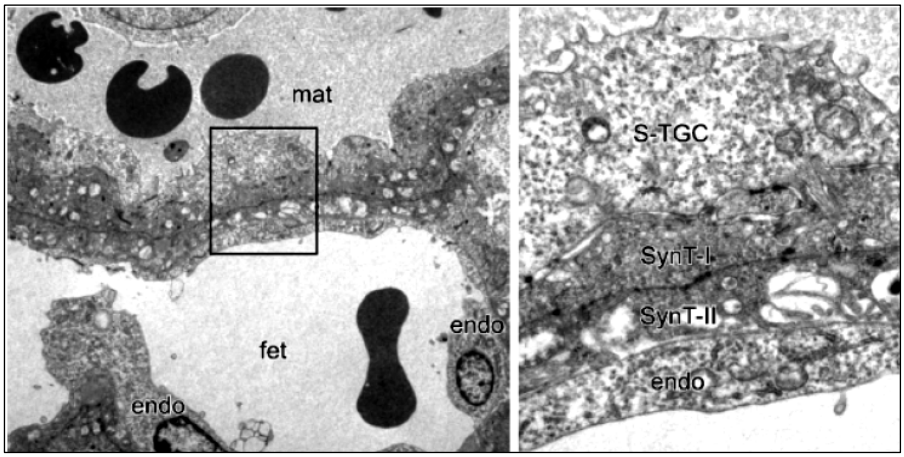


Fig 6.1. Electron micrographs showing the structure of the maternal– fetal interface in the labyrinth layer of the mouse placenta. The fetal blood space (fet) is lined by endothelial cells (endo), whereas maternal blood (mat) lies in direct contact with specialized trophoblast cells called sinusoidal trophoblast giant cells (S-TGC). Two layers of syncytiotrophoblast (SynT) are readily distinguishable ultrastructurally modified from Cross JC et al., 2006.

## 5.4. Altered cell signaling seen in the keratin type II null mutants

The keratin type II null mutants were smaller than their wild type littermates. This however, was not a consequence of proliferation defects. The mutant embryos as well as the extra-embryonic tissues showed comparable levels of proliferating cells with the controls. Moreover, the trophoblast giant cells of the mutants showed a slight increase in cell size when compared to that of the controls (Fig.4.13e) These results argue against the reported role of keratins in cell cycle control (Kim et al., 2006; Margolis et al., 2006). However, it has not been estimated if there is a general reduction in protein translation in the mutants. Metabolic labeling using [$^{35}$S] methionine, followed by incorporation of radioactivity measurements or monitoring the mTOR pathway would strengthen the argument of the role of keratins in cell cycle control.

Although the keratin type II null mutants showed an increased rate of apoptosis of up to three fold (Fig.4.13), this could not be attributed to the primary cause of lethality in the mutants as suggested previously in the K8 null mutants (Oshima et al., 2002). The authors argued that the lack of keratins

rendered the embryo more susceptible to maternal TNF, and this was the primary cause of the lethality in the K8 null mutants at E 12.5. However, a closer look at the keratin type II null mutants revealed that the apoptotic cells were not restricted to the epithelial type and that the rate of apoptosis correlated with the size of the embryo. Smaller the embryo, larger was the number of apoptotic cells, and *vice-versa* (Fig.4.13). This argues against the protective role of keratins against apoptosis as suggested earlier (Oshima et al., 2002), and implies that the increase rate of apoptosis seen in the keratin type II null mutants is a consequence of malnutrition.

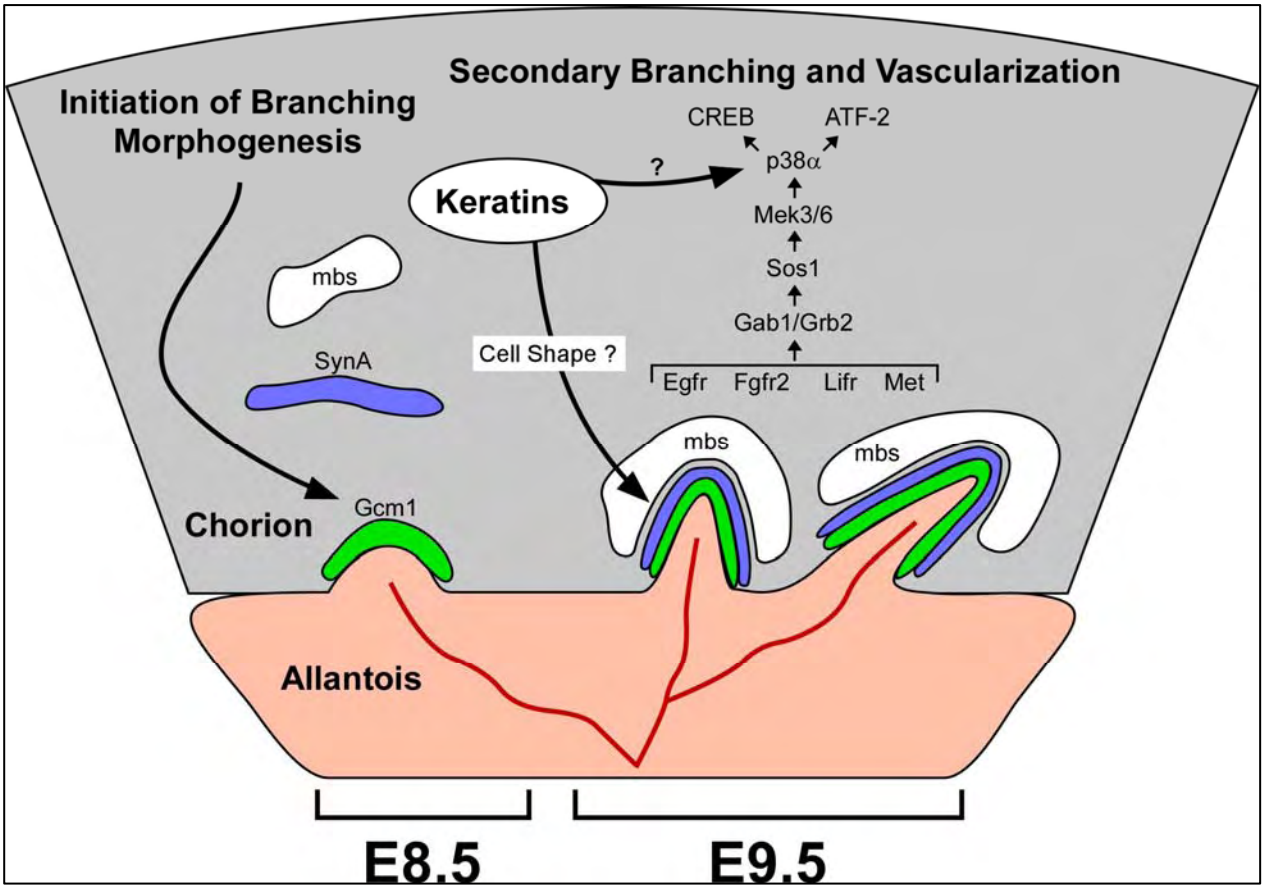


Fig. 6.2. Putative signaling pathways during labyrinth formation. Certain cells within the chorion commit to express *Gcm1* which are the branching checkpoints from E7.5. *Gcm1* likely produces paracrine signals that are picked up by the *SynA* expressing cells within the chorionic trophoblast cells, which then begin to proliferate and elongate by E8.5, following chorioallantoic fusion. These two cell types eventually form the labyrinth where the fetal blood forms intimate contact with the maternal blood sinuses. This stimulation is also mediated by cyclic AMP/protein kinase A (PKA) signaling. It is speculated that keratins also play a role in this paracrine signalling, eventually allowing the *SynA* expressing trophoblast cells to proliferate and elongate. In the absence of keratins, these cells cease proliferation and hence remain flat, thereby failing to form a functional labyrinth. Following branching initiation, various other factors are responsible for branching morphogenesis. *Egfr*, epidermal growth factor receptor; *Fgfr2*, fibroblast growth factor receptor 2; *Gab1*, growth-factor-receptor-bound protein-2-associated protein 1; *Gcm1*, glial cells missing 1; *Grb2*, growth-factor-receptor-bound protein; *Lifr*, leukaemia inhibitory factor receptor; *Mek*, mitogen-activated protein kinase; Met, met proto-oncogene; p38α, p38 mitogen-activated protein-α; *Sos1*, son of sevenless homologue 1 (Courtesy, Dr. Simmons).

Apart from the probable defective paracrine signaling in the keratin type II null mutants, the mutants also showed reduced levels of activated p38, indicating a downregulation of the p38 MAP kinase pathway. Members of the p38 MAPK family, respond to pro-inflammatory cytokines and cellular stresses, and behave as pro-apoptotic signals. They are activated by serial phosphorylation and activation of upstream kinases (the MAPK cascade). The reduced levels of activated p38 seen in the keratin type II null mutants is in strong disagreement of the role of keratins in protection against apoptosis (Oshima et al, 2002), since an upregulation of the activated p38 MAPK would have been expected. This now places keratins in a pathway, independent of the apoptotic pathway.

The phenotype of the keratin type II null mutants is strikingly similar to that observed in p38-$\alpha$ knockouts that die a day later (Adams et al., 2000). These mutants were drastically reduced in size, showed decreased vasculature and a decreased feto-maternal interface. Alterations in upstream targets like MEK3/6 and downstream targets like ATF1 / CREB have to be monitored in the keratin type II null mutants. Mice lacking both MEK3 and MEK6, the two main p38-specific MAPKKs, are not viable, dying at midgestation with defects in the placenta and the embryonic vasculature, very similar to the keratin type II null mutants (Brancho et al., 2003). A combined heterozygous ATF1 and a null CREB situation caused embryonic lethality in mice at E9.5 with a phenotype attributed to indistinguishable extraembryonic mesoderm-derived structures like amnion, allantois, and chorion (Bleckmann et al., 2002). Keratin 8 is reported to have a p38 target site on S73 (Feng et al., 1999). Recent data has demonstrated that in stress situations, K8 becomes phosphorylated at S73 by p38 MAP kinase, and this phosphorylated state determines keratin organization, thereby placing p38-dependent signaling as a major intermediate filament-regulating pathway (Woll et al., 2007). Identifying altered upstream or downstream targets of p38 would be instrumental in identifying the role of keratins in the p38 MAP kinase pathway.

### 5.5. Summarizing the keratin type II null mutants

In summary, the constitutive deletion of keratin type II cluster has revealed a novel role of keratins beyond its well established structural functions. The keratin type II null mutants died at mid-gestation around E9.5. Surprisingly, no cell fragility was observed in either the embryonic or extra-embryonic tissues in the absence of keratin filaments. The lethality of these mutants could be attributed to defective angiogenesis and vasculogenesis in the yolk sac succeeded by defective branching structures that form a feto-maternal interface, leading to nutritional deficiency in the embryos. *In situ* data revealed that type II keratins were not involved in the normal differentiation of various cell lineages during early embryonic development. The mutant embryos were smaller than their wild type littermates;

however, they did not suffer from general defective proliferation. A positive correlation between apoptosis and size of the mutants was observed. Apoptosis was moreover not restricted to epithelial cells, indicating that apoptotic cell death in the mutants could be attributed to a consequence of nutritional deficiency. It is hypothesized that altered paracrine signaling between epithelium in the yolk sac as well as in the placenta contributed to the structural defects of reduced vasculature in yolk sac and absence of labyrinth, eventually leading to death of the mutant embryos. Altered p38 MAP kinase signaling in the keratin type II null mutants has suggested a role for keratins upstream in this pathway. In light of the data presented here, the phenotypes of previous keratin null mutants have to be reconsidered.

### 5.6. Potential of the keratin type II null targeting and future perspectives

The early prenatal lethality observed in the keratin type II null mutants proves the importance of type II keratins during early embryogenesis. However, in order to understand the relative roles of type II keratins in the trophoblast versus embryonic lineages, and to accurately identify the cell lineage that lead to embryonic lethality in the keratin type II mutants, conditional deletion of keratins is required. Moreover, early embryonic lethality has also limited the evaluation of keratin type II gene functions at later stages of embryogenesis, during and after birth. Given the diversity of cell origins that keratins are expressed, a comprehensive study of its function in a particular cell lineage is not possible.

Therefore, in order to circumvent these problems, and in order to identify the specific cell lineage that caused lethality in the keratin type II null mutants, mice were generated from the double targeted ES clones in *cis*, as already reported in the first part of the results. These floxed ES cells were used to generate chimeras and consequently mice homozygous for the floxed keratin type II cluster. With such an invaluable tool, it is now possible to carry out conditional deletion of the keratin type II cluster in a tissue specific and spatially controlled manner. Using an epiblast specific Cre mouse line such as *Sox2*-Cre (Hayashi et al., 2002) or More-Cre (Tallquist and Soriano, 2000), will identify if keratins are required during early embryonic development. The use of lentivirus-mediated pol II-driven Cre recombinase for trophoblast specific gene knockout (Georgiades, et al., 2007) or VE-Cadherin-Cre-recombinase for endothelial specific Cre activity in the yolk sac (Alva, et al., 2006) will further strengthen the hypothesis of this thesis. Moreover, tracing migration of keratin null epithelial cells from a stem cell niche, studying tissue homeostasis, tumor metastasis, wound healing and additional settings offers very exciting areas of research awaiting exploration. These studies will provide important insights into type-specific keratin function and into the general significance for tissue-specific functions of other large gene families.

# SUMMARY AND CONCLUSION

Keratins are major cytoskeletal proteins of epithelia, organized in two large gene families of 28 (type I) and 26 (type II) members spanning 1.2 Mb and 0.68 Mb of genomic loci, respectively. Their expression is tightly regulated in a pairwise and differentiation-related manner in epithelial tissues starting from the 2-cell stage during embryogenesis. Fertilized mammalian eggs and embryonic stem cells are devoid of keratin filaments, raising the question whether they may be involved in stem cell differentiation. Studies from various keratin mutations leading to tissue fragility placed protection against mechanical stress as the primary function of keratins. Recent research has led to the hypothesis that keratins have major regulatory functions in cell proliferation, translation regulation, protection against apoptosis, organelle transport and regulation of signal transduction. The overlapping expression of several type I and II keratins in most epithelia has generated functional redundancy, and therefore has presented a major obstacle towards the analysis of keratin function. This thesis has addressed the function of keratins during development by constitutively and conditionally deleting all type II keratin genes in mice, thereby eliminating all problems related to redundancy. This is the first reported deletion of a large gene family in mammals.

The Cre/*loxP* system was adopted in order to flox the type II keratin gene cluster in mouse ES cells. This floxed allele contained all the type II keratins including the type I keratin *Krt*18, which is one of the first keratins to be expressed during embryonic development. Mice were generated from the floxed ES cells (for conditional deletion) as well as from the Cre expressed ES cells (for constitutive deletion), thereby carrying either the floxed or deleted keratin type II cluster, respectively. This thesis, however, has dealt only with the constitutive deletion of the keratin type II cluster, while the conditional deletion of the cluster in tissues of adult animals is underway.

Mice heterozygous for the deleted keratin type II cluster were inbred to generate keratin type II null mice. However, no keratin type II null pups were recovered at birth. Mutant embryos were smaller than their wild type littermates from ~E9.0, and died at mid gestation (E9.5). Despite the absence of a keratin cytoskeleton, no cell fragility was found in contrary to many other individual keratin knockouts. This shows that the phenotype reported for previous keratin gene knockouts represents gain of toxic functions. No overt proliferation defects were observed in the mutants even around the time of death suggesting that no proliferation defects accounted for lethality. Mutant embryos did exhibit the expected formation of epithelial lineages during embryogenesis, indicating no apparent role of keratins during embryonic differentiation. Mutant embryos suffered from defective vasculogenesis and angiogenesis in the yolk sac, which are the most critical structures required to nourish the embryo, before the placenta can take over from E9.0. Reduced vasculogenesis was accompanied by the loss of endodermal-

mesothelial cell interactions. Moreover, the mutants failed to form an organized labyrinth and the spongiotrophoblast layer at E9.5, although the chorioallantoic attachment at E8.5 was normal. Following chorioallantoic attachment at E8.5, a subset of chorionic epithelial cells expressing Syncytin A, destined to commit to the branching morphogenesis, failed to elongate and inter-digitate to form a functional labyrinth, but rather remained flat. Elevated levels of apoptosis in non-epithelial cells were seen in smaller mutant embryos in comparison to the fairly larger mutants and the wildtype embryos, suggesting a positive correlation between the two. This indicated that apoptosis was not a direct consequence of the absence of keratins but a secondary effect due to nutritional deficiency. Unexpectedly, increased apoptosis did not elevate the pro-apoptotic signal transducer p38 MAP kinase. Infact, a reduced level of activated p38 MAP kinase was observed in the mutants. In agreement, the phenotype of the keratin type II null mutants showed a striking similarity to that observed in p38-α knockouts, although they died a day later than the keratin null mutants.

The observations in this study have revealed major roles of keratins in epithelial-endodermal interactions and cell signaling. Lack of cell fragility in the absence of keratins suggests that mechanical support cannot be considered as their primary function, at least during embryonic development. Therefore, knockouts of individual keratins reported so far, represent dominant-negative, but no loss-of-function, mutations. It further questions previously reported roles of keratins in cell cycle, translational control and apoptosis. Keratins seem to mediate cell signaling, for which their topological organization within a cell is well suited. The data from the keratin type II null mutants suggests that keratins play a role upstream of the p38 MAP kinase pathway. The potential of these mice will be exploited to a great extent in the future by generating cell lines free of keratins for various functional assays as well as conditionally deleting the cluster in a tissue specific and spatially controlled manner. This will for the first time allow to study their role in tumor development and chronic diseases in genetically well-defined settings.

1. Achen, M. G., et al., 1997. Placenta growth factor and vascular endothelial growth factor are co-expressed during early embryonic development. Growth Factors. 15, 69-80.
2. Adams, D. J., et al., 2004. Mutagenic insertion and chromosome engineering resource (MICER). Nat Genet. 36, 867-71.
3. Adams, R. H., et al., 2000. Essential role of p38alpha MAP kinase in placental but not embryonic cardiovascular development. Mol Cell. 6, 109-16.
4. Adamson, S. L., et al., 2002. Interactions between trophoblast cells and the maternal and fetal circulation in the mouse placenta. Dev Biol. 250, 358-73.
5. Alva, J.A., 2006. Ve-Cadherin-Cre-recombinase transgenic mouse: a tool for lineage analysis and gene deletion in endothelial cells. Dev Dyn. 235, 759-67.
6. Ameen, N. A., et al., 2001. Anomalous apical plasma membrane phenotype in CK8-deficient mice indicates a novel role for intermediate filaments in the polarization of simple epithelia. J Cell Sci. 114, 563-75.
7. Anson-Cartwright, L., et al., 2000. The glial cells missing-1 protein is essential for branching morphogenesis in the chorioallantoic placenta. Nat Genet. 25, 311-4.
8. Baribault, H., et al., 1993. Mid-gestational lethality in mice lacking keratin 8. Genes Dev. 7, 1191-202.
9. Baribault, H., et al., 1994. Colorectal hyperplasia and inflammation in keratin 8-deficient FVB/N mice. Genes Dev. 8, 2964-73.
10. Baribault, H., Oshima, R. G., 1991. Polarized and functional epithelia can form after the targeted inactivation of both mouse keratin 8 alleles. J Cell Biol. 115, 1675-84.
11. Baron, M. H., 2003. Embryonic origins of mammalian hematopoiesis. Exp Hematol. 31, 1160-9.
12. Basyuk, E., et al., 1999. Murine Gcm1 gene is expressed in a subset of placental trophoblast cells. Dev Dyn. 214, 303-11.
13. Bi, W., et al., 2005. Inactivation of Rai1 in mice recapitulates phenotypes observed in chromosome engineered mouse models for Smith-Magenis syndrome. Hum Mol Genet. 14, 983-95.
14. Bickenbach, J. R., et al., 1995. Loricrin expression is coordinated with other epidermal proteins and the appearance of lipid lamellar granules in development. J Invest Dermatol. 104, 405-10.
15. Bleckmann, S. C., et al., 2002. Activating transcription factor 1 and CREB are important for cell survival during early mouse development. Mol Cell Biol. 22, 1919-25.
16. Blumenberg, M., 1988. Concerted gene duplications in the two keratin gene families. J Mol Evol. 27, 203-11.
17. Bousquet, O., et al., 2001. The nonhelical tail domain of keratin 14 promotes filament bundling and enhances the mechanical properties of keratin intermediate filaments in vitro. J Cell Biol. 155, 747-54.
18. Bradley, A., et al., 1998. Thirteen years of manipulating the mouse genome: a personal history. Int J Dev Biol. 42, 943-50.
19. Brancho, D., et al., 2003. Mechanism of p38 MAP kinase activation in vivo. Genes Dev. 17, 1969-78.
20. Brulet, P., et al., 1985. Molecular analysis of the first differentiations in the mouse embryo. Cold Spring Harb Symp Quant Biol. 50, 51-7.
21. Bullock, W. E., Wright, S. D., 1987. Role of the adherence-promoting receptors, CR3, LFA-1, and p150,95, in binding of Histoplasma capsulatum by human macrophages. J Exp Med. 165, 195-210.
22. Carpenter, S. J., 1972. Light and electron microscopic observations on the morphogenesis of the chorioallantoic placenta of the golden hamster (Cricetus auratus). Days seven through nine of gestation. Am J Anat. 135, 445-76.

23. Castellucci, M., et al., 2000. Villous sprouting: fundamental mechanisms of human placental development. Hum Reprod Update. 6, 485-94.
24. Caulin, C., et al., 1997. Caspase cleavage of keratin 18 and reorganization of intermediate filaments during epithelial cell apoptosis. J Cell Biol. 138, 1379-94.
25. Caulin, C., et al., 2000. Keratin-dependent, epithelial resistance to tumor necrosis factor-induced apoptosis. J Cell Biol. 149, 17-22.
26. Chen, W. S., et al., 1994. Disruption of the HNF-4 gene, expressed in visceral endoderm, leads to cell death in embryonic ectoderm and impaired gastrulation of mouse embryos. Genes Dev. 8, 2466-77.
27. Chisholm, J. C., Houliston, E., 1987. Cytokeratin filament assembly in the preimplantation mouse embryo. Development. 101, 565-82.
28. Choi, K., et al., 1998. A common precursor for hematopoietic and endothelial cells. Development. 125, 725-32.
29. Chopra, V. S., Mishra, R. K., 2006. "Mir"acles in hox gene regulation. Bioessays. 28, 445-8.
30. Colucci-Guyon, E., et al., 1999. Cerebellar defect and impaired motor coordination in mice lacking vimentin. Glia. 25, 33-43.
31. Copp, A. J., 1979. Interaction between inner cell mass and trophectoderm of the mouse blastocyst. II. The fate of the polar trophectoderm. J Embryol Exp Morphol. 51, 109-20.
32. Coulombe, P. A., Omary, M. B., 2002. 'Hard' and 'soft' principles defining the structure, function and regulation of keratin intermediate filaments. Curr Opin Cell Biol. 14, 110-22.
33. Coulombe, P. A., Wong, P., 2004. Cytoplasmic intermediate filaments revealed as dynamic and multipurpose scaffolds. Nat Cell Biol. 6, 699-706.
34. Cross, J. C., et al., 2002a. Transcription factors underlying the development and endocrine functions of the placenta. Recent Prog Horm Res. 57, 221-34.
35. Cross, J. C., et al., 2002b. Trophoblast functions, angiogenesis and remodeling of the maternal vasculature in the placenta. Mol Cell Endocrinol. 187, 207-12.
36. Cross, J. C., et al., 2003. Chorioallantoic morphogenesis and formation of the placental villous tree. Ann N Y Acad Sci. 995, 84-93.
37. Cross, J. C., et al., 2006. Branching morphogenesis during development of placental villi. Differentiation. 74, 393-401.
38. Cruciani, V., Mikalsen, S. O., 2006. The vertebrate connexin family. Cell Mol Life Sci. 63, 1125-40.
39. Davis, R. J., 2000. Signal transduction by the JNK group of MAP kinases. Cell. 103, 239-52.
40. Doughty, I. M., et al., 1996. Mechanisms of maternofetal chloride transfer across the human placenta perfused in vitro. Am J Physiol. 271, R1701-6.
41. Duarte, A., et al., 2004. Dosage-sensitive requirement for mouse Dll4 in artery development. Genes Dev. 18, 2474-8.
42. Dumont, D. J., et al., 1994. Dominant-negative and targeted null mutations in the endothelial receptor tyrosine kinase, tek, reveal a critical role in vasculogenesis of the embryo. Genes Dev. 8, 1897-909.
43. Dupressoir, A., et al., 2005. Syncytin-A and syncytin-B, two fusogenic placenta-specific murine envelope genes of retroviral origin conserved in Muridae. Proc Natl Acad Sci U S A. 102, 725-30.
44. Dzierzak, E., 2003. Ontogenic emergence of definitive hematopoietic stem cells. Curr Opin Hematol. 10, 229-34.
45. Elder, G. A., et al., 1998a. Absence of the mid-sized neurofilament subunit decreases axonal calibers, levels of light neurofilament (NF-L), and neurofilament content. J Cell Biol. 141, 727-39.

46. Elder, G. A., et al., 1998b. Requirement of heavy neurofilament subunit in the development of axons with large calibers. J Cell Biol. 143, 195-205.
47. Feng, L., et al., 1999. Pervanadate-mediated tyrosine phosphorylation of keratins 8 and 19 via a p38 mitogen-activated protein kinase-dependent pathway. J Cell Sci. 112 ( Pt 13), 2081-90.
48. Fischer, A., et al., 2004. The Notch target genes Hey1 and Hey2 are required for embryonic vascular development. Genes Dev. 18, 901-11.
49. Fontao, L., et al., 2003. Interaction of the bullous pemphigoid antigen 1 (BP230) and desmoplakin with intermediate filaments is mediated by distinct sequences within their COOH terminus. Mol Biol Cell. 14, 1978-92.
50. Franke, W. W., et al., 1983. Protein complexes of intermediate-sized filaments: melting of cytokeratin complexes in urea reveals different polypeptide separation characteristics. Proc Natl Acad Sci U S A. 80, 7113-7.
51. Fuchs, E., Cleveland, D. W., 1998. A structural scaffolding of intermediate filaments in health and disease. Science. 279, 514-9.
52. Fuchs, E., et al., 1994. Cracks in the foundation: keratin filaments and genetic disease. Trends Cell Biol. 4, 321-6.
53. Fuchs, E., Weber, K., 1994. Intermediate filaments: structure, dynamics, function, and disease. Annu Rev Biochem. 63, 345-82.
54. Fujii, T., et al., 1988. Antitumor effect of K18 on metastatic models. In Vivo. 2, 389-92.
55. Gallicano, G. I., et al., 1998. Desmoplakin is required early in development for assembly of desmosomes and cytoskeletal linkage. J Cell Biol. 143, 2009-22.
56. Garrod, D. R., et al., 2002. Desmosomal adhesion: structural basis, molecular mechanism and regulation (Review). Mol Membr Biol. 19, 81-94.
57. Gekas, C., et al., 2005. The placenta is a niche for hematopoietic stem cells. Dev Cell. 8, 365-75.
58. Georgiades, P., et al., 2007. Trophoblast specific gene manipulation using lentivirus-based vectors. Biotechniques. 42, 317-8
59. Gilbert, S., et al., 2004. Keratins modulate c-Flip/extracellular signal-regulated kinase 1 and 2 antiapoptotic signaling in simple epithelial cells. Mol Cell Biol. 24, 7072-81.
60. Giudice, G. J., Fuchs, E., 1987. The transfection of epidermal keratin genes into fibroblasts and simple epithelial cells: evidence for inducing a type I keratin by a type II gene. Cell. 48, 453-63.
61. Gomi, H., et al., 1995. Mice devoid of the glial fibrillary acidic protein develop normally and are susceptible to scrapie prions. Neuron. 14, 29-41.
62. Green, K. J., Jones, J. C., 1996. Desmosomes and hemidesmosomes: structure and function of molecular components. Faseb J. 10, 871-81.
63. Groskopf, J. C., et al., 1997. Proliferin induces endothelial cell chemotaxis through a G protein-coupled, mitogen-activated protein kinase-dependent pathway. Endocrinology. 138, 2835-40.
64. Gu, H., et al., 1993. Independent control of immunoglobulin switch recombination at individual switch regions evidenced through Cre-loxP-mediated gene targeting. Cell. 73, 1155-64.
65. Gu, L. H., Coulombe, P. A., 2007. Keratin expression provides novel insight into the morphogenesis and function of the companion layer in hair follicles. J Invest Dermatol. 127, 1061-73.
66. Guillemot, F., et al., 1994. Essential role of Mash-2 in extraembryonic development. Nature. 371, 333-6.
67. Guo, L., et al., 1995. Gene targeting of BPAG1: abnormalities in mechanical strength and cell migration in stratified epithelia and neurologic degeneration. Cell. 81, 233-43.

68. Haar, J. L., Ackerman, G. A., 1971. A phase and electron microscopic study of vasculogenesis and erythropoiesis in the yolk sac of the mouse. Anat Rec. 170, 199-223.
69. Hashido, K., et al., 1991. Gene expression of cytokeratin endo A and endo B during embryogenesis and in adult tissues of mouse. Exp Cell Res. 192, 203-12.
70. Hasty, P., et al., 1994. Efficiency of insertion versus replacement vector targeting varies at different chromosomal loci. Mol Cell Biol. 14, 8385-90.
71. Hatsell, S., Cowin, P., 2001. Deconstructing desmoplakin. Nat Cell Biol. 3, E270-2.
72. Hatzfeld, M., Franke, W. W., 1985. Pair formation and promiscuity of cytokeratins: formation in vitro of heterotypic complexes and intermediate-sized filaments by homologous and heterologous recombinations of purified polypeptides. J Cell Biol. 101, 1826-41.
73. Hatzfeld, M., Nachtsheim, C., 1996. Cloning and characterization of a new armadillo family member, p0071, associated with the junctional plaque: evidence for a subfamily of closely related proteins. J Cell Sci. 109 ( Pt 11), 2767-78.
74. Hayashi, S., Lewis, P., Pevny, L., McMahon, A.P., 2002. Efficient gene modulation in mouse epiblast using a Sox2Cre transgenic mouse strain. Mech. Dev. 119, S97-S101.
75. He, T., et al., 2002. The intermediate filament protein keratin 8 is a novel cytoplasmic substrate for c-Jun N-terminal kinase. J Biol Chem. 277, 10767-74.
76. He, X., Goldwasser, M. H., 2005. Identifying conserved gene clusters in the presence of homology families. J Comput Biol. 12, 638-56.
77. Healy, A. M., et al., 1995. Absence of the blood-clotting regulator thrombomodulin causes embryonic lethality in mice before development of a functional cardiovascular system. Proc Natl Acad Sci U S A. 92, 850-4.
78. Henegariu, O., et al., 2001. Improvements in cytogenetic slide preparation: controlled chromosome spreading, chemical aging and gradual denaturing. Cytometry. 43, 101-9.
79. Herault, Y., et al., 1998. Engineering chromosomes in mice through targeted meiotic recombination (TAMERE). Nat Genet. 20, 381-4.
80. Hernandez-Verdun, D., 1974. Morphogenesis of the syncytium in the mouse placenta. Ultrastructural study. Cell Tissue Res. 148, 381-96.
81. Herrmann, H., Aebi, U., 2004. Intermediate filaments: molecular structure, assembly mechanism, and integration into functionally distinct intracellular Scaffolds. Annu Rev Biochem. 73, 749-89.
82. Herrmann, H., et al., 2000. The intermediate filament protein consensus motif of helix 2B: its atomic structure and contribution to assembly. J Mol Biol. 298, 817-32.
83. Herrmann, H., et al., 2003. Functional complexity of intermediate filament cytoskeletons: from structure to assembly to gene ablation. Int Rev Cytol. 223, 83-175.
84. Hesse, M., et al., 2000. Targeted deletion of keratins 18 and 19 leads to trophoblast fragility and early embryonic lethality. Embo J. 19, 5060-70.
85. Hesse, M., et al., 2001. Genes for intermediate filament proteins and the draft sequence of the human genome: novel keratin genes and a surprisingly high number of pseudogenes related to keratin genes 8 and 18. J Cell Sci. 114, 2569-75.
86. Hesse, M., et al., 2004. Comprehensive analysis of keratin gene clusters in humans and rodents. Eur J Cell Biol. 83, 19-26.

87. Hesse, M., et al., 2005. Rescue of keratin 18/19 doubly deficient mice using aggregation with tetraploid embryos. Eur J Cell Biol. 84, 355-61.
88. Hoffmann, W., et al., 1985. Amino acid sequence microheterogeneities of basic (type II) cytokeratins of Xenopus laevis epidermis and evolutionary conservativity of helical and non-helical domains. J Mol Biol. 184, 713-24.
89. Hofmann, I., et al., 2000. Interaction of plakophilins with desmoplakin and intermediate filament proteins: an in vitro analysis. J Cell Sci. 113 ( Pt 13), 2471-83.
90. Hunter, P. J., et al., 1999. Mrj encodes a DnaJ-related co-chaperone that is essential for murine placental development. Development. 126, 1247-58.
91. Hutton, E., et al., 1998. Functional differences between keratins of stratified and simple epithelia. J Cell Biol. 143, 487-99.
92. Inada, H., et al., 2001. Keratin attenuates tumor necrosis factor-induced cytotoxicity through association with TRADD. J Cell Biol. 155, 415-26.
93. Irvine, A. D., McLean, W. H., 1999. Human keratin diseases: the increasing spectrum of disease and subtlety of the phenotype-genotype correlation. Br J Dermatol. 140, 815-28.
94. Jackson, B. W., et al., 1980. Formation of cytoskeletal elements during mouse embryogenesis. Intermediate filaments of the cytokeratin type and desmosomes in preimplantation embryos. Differentiation. 17, 161-79.
95. Jahn, L., et al., 1987. Cytokeratins in certain endothelial and smooth muscle cells of two taxonomically distant vertebrate species, Xenopus laevis and man. Differentiation. 36, 234-54.
96. Jaquemar, D., et al., 2003. Keratin 8 protection of placental barrier function. J Cell Biol. 161, 749-56.
97. Jefferson, J. J., et al., 2004. Plakins: goliaths that link cell junctions and the cytoskeleton. Nat Rev Mol Cell Biol. 5, 542-53.
98. Jollie, W. P., 1990. Development, morphology, and function of the yolk-sac placenta of laboratory rodents. Teratology. 41, 361-81.
99. Kim, S., Coulombe, P. A., 2007. Intermediate filament scaffolds fulfill mechanical, organizational, and signaling functions in the cytoplasm. Genes Dev. 21, 1581-97.
100. Kim, S., et al., 2006. A keratin cytoskeletal protein regulates protein synthesis and epithelial cell growth. Nature. 441, 362-5.
101. King, B. F., 1982. A freeze-fracture study of the guinea pig yolk sac epithelium. Anat Rec. 202, 221-30.
102. Klysik, J., et al., 2004. Two new mouse chromosome 11 balancers. Genomics. 83, 303-10.
103. Kmita, M., et al., 2000. Targeted inversion of a polar silencer within the HoxD complex re-allocates domains of enhancer sharing. Nat Genet. 26, 451-4.
104. Kmita, M., et al., 2002. Serial deletions and duplications suggest a mechanism for the collinearity of Hoxd genes in limbs. Nature. 420, 145-50.
105. Knerr, I., et al., 2005. Stimulation of GCMa and syncytin via cAMP mediated PKA signaling in human trophoblastic cells under normoxic and hypoxic conditions. FEBS Lett. 579, 3991-8.
106. Kondo, T., Duboule, D., 1999. Breaking colinearity in the mouse HoxD complex. Cell. 97, 407-17.
107. Kondo, T., et al., 1998. Control of colinearity in AbdB genes of the mouse HoxD complex. Mol Cell. 1, 289-300.
108. Kowalczyk, A. P., et al., 1999. The head domain of plakophilin-1 binds to desmoplakin and enhances its recruitment to desmosomes. Implications for cutaneous disease. J Biol Chem. 274, 18145-8.

109. Krebs, L. T., et al., 2000. Notch signaling is essential for vascular morphogenesis in mice. Genes Dev. 14, 1343-52.

110. Krebs, L. T., et al., 2004. Haploinsufficient lethality and formation of arteriovenous malformations in Notch pathway mutants. Genes Dev. 18, 2469-73.

111. Kruger, O., et al., 2000. Defective vascular development in connexin 45-deficient mice. Development. 127, 4179-93.

112. Ku, N. O., et al., 1998. Phosphorylation of human keratin 18 serine 33 regulates binding to 14-3-3 proteins. Embo J. 17, 1892-906.

113. Ku, N. O., et al., 2003. Keratin mutation in transgenic mice predisposes to Fas but not TNF-induced apoptosis and massive liver injury. Hepatology. 37, 1006-14.

114. Ku, N. O., Omary, M. B., 2006. A disease- and phosphorylation-related nonmechanical function for keratin 8. J Cell Biol. 174, 115-25.

115. Kucera, G. T., et al., 1996. Overexpression of an Agouti cDNA in the skin of transgenic mice recapitulates dominant coat color phenotypes of spontaneous mutants. Dev Biol. 173, 162-73.

116. Kupriyanov, S., Baribault, H., 1998. Genetic control of extraembryonic cell lineages studied with tetraploid<-->diploid chimeric concepti. Biochem Cell Biol. 76, 1017-27.

117. Kwee, L., et al., 1995. Defective development of the embryonic and extraembryonic circulatory systems in vascular cell adhesion molecule (VCAM-1) deficient mice. Development. 121, 489-503.

118. Lacey, H., et al., 2002. Mesenchymally-derived insulin-like growth factor 1 provides a paracrine stimulus for trophoblast migration. BMC Dev Biol. 2, 5.

119. Lala, P. K., Chakraborty, C., 2003. Factors regulating trophoblast migration and invasiveness: possible derangements contributing to pre-eclampsia and fetal injury. Placenta. 24, 575-87.

120. Langbein, L., et al., 1999. The catalog of human hair keratins. I. Expression of the nine type I members in the hair follicle. J Biol Chem. 274, 19874-84.

121. Langbein, L., et al., 2001. The catalog of human hair keratins. II. Expression of the six type II members in the hair follicle and the combined catalog of human type I and II keratins. J Biol Chem. 276, 35123-32.

122. Lea, R. G., Clark, D. A., 1993. Effects of decidual cell supernatants and lymphokines on murine trophoblast growth in vitro. Biol Reprod. 48, 930-5.

123. Lescisin, K. R., et al., 1988. Isolation and characterization of a novel trophoblast-specific cDNA in the mouse. Genes Dev. 2, 1639-46.

124. Leung, C. L., et al., 2002. Plakins: a family of versatile cytolinker proteins. Trends Cell Biol. 12, 37-45.

125. Li, Z., et al., 1996. Cardiovascular lesions and skeletal myopathy in mice lacking desmin. Dev Biol. 175, 362-6.

126. Lindsay, E. A., et al., 2001. Tbx1 haploinsufficieny in the DiGeorge syndrome region causes aortic arch defects in mice. Nature. 410, 97-101.

127. Litjens, S. H., et al., 2006. Current insights into the formation and breakdown of hemidesmosomes. Trends Cell Biol. 16, 376-83.

128. Lloyd, C., et al., 1995. The basal keratin network of stratified squamous epithelia: defining K15 function in the absence of K14. J Cell Biol. 129, 1329-44.

129. Long, H. A., et al., 2006. Periplakin-dependent re-organisation of keratin cytoskeleton and loss of collective migration in keratin-8-downregulated epithelial sheets. J Cell Sci. 119, 5147-59.
130. Loranger, A., et al., 2006. Keratin 8 modulation of desmoplakin deposition at desmosomes in hepatocytes. Exp Cell Res. 312, 4108-19.
131. Lu, H., et al., 2005. Type II keratins precede type I keratins during early embryonic development. Eur J Cell Biol. 84, 709-18.
132. Lu, H., et al., 2006. Keratin 5 knockout mice reveal plasticity of keratin expression in the corneal epithelium. Eur J Cell Biol. 85, 803-11.
133. Luo, J., et al., 1997. Placental abnormalities in mouse embryos lacking the orphan nuclear receptor ERR-beta. Nature. 388, 778-82.
134. Ma, G. T., et al., 1997. GATA-2 and GATA-3 regulate trophoblast-specific gene expression in vivo. Development. 124, 907-14.
135. Magarinos, M. P., et al., 2007. Leptin promotes cell proliferation and survival of trophoblastic cells. Biol Reprod. 76, 203-10.
136. Magin, T. M., et al., 1992. A new mouse embryonic stem cell line with good germ line contribution and gene targeting frequency. Nucleic Acids Res. 20, 3795-6.
137. Magin, T. M., et al., 1998. Lessons from keratin 18 knockout mice: formation of novel keratin filaments, secondary loss of keratin 7 and accumulation of liver-specific keratin 8-positive aggregates. J Cell Biol. 140, 1441-51.
138. Magin, T.M., et al., 2004. Emerging functions: disease and animal models reshape our view of the cytoskeleton. Exp Cell Res. 15, 91-102.
139. Margolis, S. S., et al., 2006. Role for the PP2A/B56delta phosphatase in regulating 14-3-3 release from Cdc25 to control mitosis. Cell. 127, 759-73.
140. Matsumoto, K., Nakamura, T., 1996. Emerging multipotent aspects of hepatocyte growth factor. J Biochem (Tokyo). 119, 591-600.
141. McGinnis, W., et al., 1984. A conserved DNA sequence in homoeotic genes of the Drosophila Antennapedia and bithorax complexes. Nature. 308, 428-33.
142. McGrath, K. E., Palis, J., 2005. Hematopoiesis in the yolk sac: more than meets the eye. Exp Hematol. 33, 1021-8.
143. McKinnon, T., et al., 2001. Stimulation of human extravillous trophoblast migration by IGF-II is mediated by IGF type 2 receptor involving inhibitory G protein(s) and phosphorylation of MAPK. J Clin Endocrinol Metab. 86, 3665-74.
144. Mi, S., et al., 2000. Syncytin is a captive retroviral envelope protein involved in human placental morphogenesis. Nature. 403, 785-9.
145. Milner, D. J., et al., 1996. Disruption of muscle architecture and myocardial degeneration in mice lacking desmin. J Cell Biol. 134, 1255-70.
146. Moll, R., et al., 1982. The catalog of human cytokeratins: patterns of expression in normal epithelia, tumors and cultured cells. Cell. 31, 11-24.
147. Mudgett, J. S., et al., 2000. Essential role for p38alpha mitogen-activated protein kinase in placental angiogenesis. Proc Natl Acad Sci U S A. 97, 10454-9.

148. Muller, H., et al., 1998. Homologues for prolactin-like proteins A and B are present in the mouse. Biol Reprod. 58, 45-51.
149. Ness, S. L., et al., 1998. Mouse keratin 4 is necessary for internal epithelial integrity. J Biol Chem. 273, 23904-11.
150. Nishijima, I., et al., 2003. Two new balancer chromosomes on mouse chromosome 4 to facilitate functional annotation of human chromosome 1p. Genesis. 36, 142-8.
151. Omary, M. B., et al., 2004. Intermediate filament proteins and their associated diseases. N Engl J Med. 351, 2087-100.
152. Omary, M. B., et al., 2006. "Heads and tails" of intermediate filament phosphorylation: multiple sites and functional insights. Trends Biochem Sci. 31, 383-94.
153. Oshima, R. G., 1981. Identification and immunoprecipitation of cytoskeletal proteins from murine extra-embryonic endodermal cells. J Biol Chem. 256, 8124-33.
154. Oshima, R. G., 2002. Apoptosis and keratin intermediate filaments. Cell Death Differ. 9, 486-92.
155. Ottersbach, K., Dzierzak, E., 2005. The murine placenta contains hematopoietic stem cells within the vascular labyrinth region. Dev Cell. 8, 377-87.
156. Paiva, P., et al., 2007. Interleukin-11 promotes migration but not proliferation of human trophoblast cells implying a role in placentation. Endocrinology.
157. Pallari, H. M., Eriksson, J. E., 2006. Intermediate filaments as signaling platforms. Sci STKE. 2006, pe53.
158. Paramio, J. M., Jorcano, J. L., 2002. Beyond structure: do intermediate filaments modulate cell signalling? Bioessays. 24, 836-44.
159. Parast, M. M., et al., 2001. Trophoblast giant-cell differentiation involves changes in cytoskeleton and cell motility. Dev Biol. 230, 43-60.
160. Pardi, G., et al., 2002. Placental-fetal interrelationship in IUGR fetuses--a review. Placenta. 23 Suppl A, S136-41.
161. Paulin, D., 1981. Cytoskeleton organization in differentiating mouse teratocarcinoma cells. Biochimie. 63, 347-63.
162. Paulin, D., et al., 1980. Antibodies as probes of cellular differentiation and cytoskeletal organization in the mouse blastocyst. Exp Cell Res. 130, 297-304.
163. Pekny, M., et al., 1995. Mice lacking glial fibrillary acidic protein display astrocytes devoid of intermediate filaments but develop and reproduce normally. Embo J. 14, 1590-8.
164. Poehlmann, T. G., et al., 2005. Trophoblast invasion: tuning through LIF, signalling via Stat3. Placenta. 26 Suppl A, S37-41.
165. Ramirez-Solis, R., et al., 1995. Chromosome engineering in mice. Nature. 378, 720-4.
166. Ramirez-Solis, R., et al., 1995. Chromosome engineering in mice. Nature. 378, 720-4.
167. Rao, M. V., et al., 1998. Neurofilament-dependent radial growth of motor axons and axonal organization of neurofilaments does not require the neurofilament heavy subunit (NF-H) or its phosphorylation. J Cell Biol. 143, 171-81.
168. Reichelt, J., et al., 2001. Formation of a normal epidermis supported by increased stability of keratins 5 and 14 in keratin 10 null mice. Mol Biol Cell. 12, 1557-68.
169. Reichelt, J., et al., 2004. Loss of keratin 10 is accompanied by increased sebocyte proliferation and differentiation. Eur J Cell Biol. 83, 747-59.
170. Rezniczek, G. A., et al., 2004. Plectin. Methods Cell Biol. 78, 721-55.

171. Ridge, K. M., et al., 2005. Keratin 8 phosphorylation by protein kinase C delta regulates shear stress-mediated disassembly of keratin intermediate filaments in alveolar epithelial cells. J Biol Chem. 280, 30400-5.

172. Rossant, J., Cross, J. C., 2001. Placental development: lessons from mouse mutants. Nat Rev Genet. 2, 538-48.

173. S, O. O., Saitou, N., 1999. Phylogenetic relationship of muscle tissues deduced from superimposition of gene trees. Mol Biol Evol. 16, 856-67.

174. Sato, T. N., et al., 1995. Distinct roles of the receptor tyrosine kinases Tie-1 and Tie-2 in blood vessel formation. Nature. 376, 70-4.

175. Schweizer, J., et al., 2006. New consensus nomenclature for mammalian keratins. J Cell Biol. 174, 169-74.

176. Sibley, C. P., et al., 2004. Placental-specific insulin-like growth factor 2 (Igf2) regulates the diffusional exchange characteristics of the mouse placenta. Proc Natl Acad Sci U S A. 101, 8204-8.

177. Silver, L., Palis, J., 1997. Initiation of murine embryonic erythropoiesis: a spatial analysis. Blood. 89, 1154-64.

178. Smith, A. J., et al., 1995. A site-directed chromosomal translocation induced in embryonic stem cells by Cre-loxP recombination. Nat Genet. 9, 376-85.

179. Soares, M. J., et al., 1996. Differentiation of trophoblast endocrine cells. Placenta. 17, 277-89.

180. Somerset, D. A., et al., 1997. Fetal growth restriction and hepatocyte growth factor. Arch Dis Child Fetal Neonatal Ed. 77, F244-8.

181. Somerset, D. A., et al., 1998. Ontogeny of hepatocyte growth factor (HGF) and its receptor (c-met) in human placenta: reduced HGF expression in intrauterine growth restriction. Am J Pathol. 153, 1139-47.

182. Spitz, F., et al., 2001. Large scale transgenic and cluster deletion analysis of the HoxD complex separate an ancestral regulatory module from evolutionary innovations. Genes Dev. 15, 2209-14.

183. Steinbock, F. A., et al., 2000. Dose-dependent linkage, assembly inhibition and disassembly of vimentin and cytokeratin 5/14 filaments through plectin's intermediate filament-binding domain. J Cell Sci. 113 ( Pt 3), 483-91.

184. Stewart, F., 1996. Roles of mesenchymal-epithelial interactions and hepatocyte growth factor-scatter factor (HGF-SF) in placental development. Rev Reprod. 1, 144-8.

185. Su, H., et al., 2000. Nested chromosomal deletions induced with retroviral vectors in mice. Nat Genet. 24, 92-5.

186. Sullivan, T., et al., 1999. Loss of A-type lamin expression compromises nuclear envelope integrity leading to muscular dystrophy. J Cell Biol. 147, 913-20.

187. Suri, C., et al., 1996. Requisite role of angiopoietin-1, a ligand for the TIE2 receptor, during embryonic angiogenesis. Cell. 87, 1171-80.

188. Svitkina, T. M., et al., 1996. Plectin sidearms mediate interaction of intermediate filaments with microtubules and other components of the cytoskeleton. J Cell Biol. 135, 991-1007.

189. Tallquist, M.D and Soriano, P, 2000. Epiblast-restricted Cre expression in MORE mice: a tool to distinguish embryonic vs. extra-embryonic gene functions. Genesis. 26, 113-5.

190. Tamai, Y., et al., 2000. Cytokeratins 8 and 19 in the mouse placental development. J Cell Biol. 151, 563-72.

191. Taniguchi, M., et al., 1998. Efficient production of Cre-mediated site-directed recombinants through the utilization of the puromycin resistance gene, pac: a transient gene-integration marker for ES cells. Nucleic Acids Res. 26, 679-80.

192. Tanzer, A., Stadler, P. F., 2004. Molecular evolution of a microRNA cluster. J Mol Biol. 339, 327-35.

193. Teesalu, T., et al., 1998. Expression and function of the urokinase type plasminogen activator during mouse hemochorial placental development. Dev Dyn. 213, 27-38.

194. Teesalu, T., et al., 1999. Expression of matrix metalloproteinases during murine chorioallantoic placenta maturation. Dev Dyn. 214, 248-58.

195. Toivola, D. M., et al., 2001. Disturbances in hepatic cell-cycle regulation in mice with assembly-deficient keratins 8/18. Hepatology. 34, 1174-83.

196. Toivola, D. M., et al., 2004. Keratins modulate colonocyte electrolyte transport via protein mistargeting. J Cell Biol. 164, 911-21.

197. Tschentscher, P., et al., 1997. Sensitive and specific cytokeratin 18 reverse transcription-polymerase chain reaction that excludes amplification of processed pseudogenes from contaminating genomic DNA. Clin Chem. 43, 2244-50.

198. Uehara, Y., et al., 1995. Placental defect and embryonic lethality in mice lacking hepatocyte growth factor/scatter factor. Nature. 373, 702-5.

199. Van Deursen, J., et al., 1995. Cre-mediated site-specific translocation between nonhomologous mouse chromosomes. Proc Natl Acad Sci U S A. 92, 7376-80.

200. Venetianer, A., et al., 1983. Cessation of cytokeratin expression in a rat hepatoma cell line lacking differentiated functions. Nature. 305, 730-3.

201. Vuorela, P., et al., 1997. Expression of vascular endothelial growth factor and placenta growth factor in human placenta. Biol Reprod. 56, 489-94.

202. Wald, F. A., et al., 2005. Intermediate filaments interact with dormant ezrin in intestinal epithelial cells. Mol Biol Cell. 16, 4096-107.

203. Walz, K., et al., 2003. Modeling del(17)(p11.2p11.2) and dup(17)(p11.2p11.2) contiguous gene syndromes by chromosome engineering in mice: phenotypic consequences of gene dosage imbalance. Mol Cell Biol. 23, 3646-55.

204. Watson, E. D., Cross, J. C., 2005. Development of structures and transport functions in the mouse placenta. Physiology (Bethesda). 20, 180-93.

205. Watson, E. D., et al., 2007. The Mrj co-chaperone mediates keratin turnover and prevents the formation of toxic inclusion bodies in trophoblast cells of the placenta. Development. 134, 1809-17.

206. Weidner, K. M., et al., 1993. The Met receptor tyrosine kinase transduces motility, proliferation, and morphogenic signals of scatter factor/hepatocyte growth factor in epithelial cells. J Cell Biol. 121, 145-54.

207. Wojcik, S. M., et al., 2000. Delayed wound healing in keratin 6a knockout mice. Mol Cell Biol. 20, 5248-55.

208. Wojcik, S. M., et al., 2001. Discovery of a novel murine keratin 6 (K6) isoform explains the absence of hair and nail defects in mice deficient for K6a and K6b. J Cell Biol. 154, 619-30.

209. Woll, S., et al., 2007. p38 MAPK-dependent shaping of the keratin cytoskeleton in cultured cells. J Cell Biol. 177, 795-807.

210. Woll, S., et al., 2007. p38 MAPK-dependent shaping of the keratin cytoskeleton in cultured cells. J Cell Biol. 177, 795-807.

211. Wong, P., et al., 2000. Introducing a null mutation in the mouse K6alpha and K6beta genes reveals their essential structural role in the oral mucosa. J Cell Biol. 150, 921-8.

212. Wong, P., et al., 2005. Overcoming functional redundancy to elicit pachyonychia congenita-like nail lesions in transgenic mice. Mol Cell Biol. 25, 197-205.
213. Wrehlke, C., et al., 1999. Genomic organization of mouse gene zfp162. DNA Cell Biol. 18, 419-28.
214. Wright, J. K., et al., 2006. EGF modulates trophoblast migration through regulation of Connexin 40. Placenta. 27 Suppl A, S114-21.
215. Yamamoto, H., et al., 1998. Defective trophoblast function in mice with a targeted mutation of Ets2. Genes Dev. 12, 1315-26.
216. Yan, J., et al., 2004. Reduced penetrance of craniofacial anomalies as a function of deletion size and genetic background in a chromosome engineered partial mouse model for Smith-Magenis syndrome. Hum Mol Genet. 13, 2613-24.
217. Yokoyama, T., et al., 1990. Conserved cysteine to serine mutation in tyrosinase is responsible for the classical albino mutation in laboratory mice. Nucleic Acids Res. 18, 7293-8.
218. Yu, C., et al., 2002. GCMa regulates the syncytin-mediated trophoblastic fusion. J Biol Chem. 277, 50062-8.
219. Yu, Y., Bradley, A., 2001. Engineering chromosomal rearrangements in mice. Nat Rev Genet. 2, 780-90.
220. Zakany, J., Duboule, D., 1996. Synpolydactyly in mice with a targeted deficiency in the HoxD complex. Nature. 384, 69-71.
221. Zarnegar, R., Michalopoulos, G. K., 1995. The many faces of hepatocyte growth factor: from hepatopoiesis to hematopoiesis. J Cell Biol. 129, 1177-80.
222. Zatloukal, K., et al., 2004. The keratin cytoskeleton in liver diseases. J Pathol. 204, 367-76.
223. Zhang, H., et al., 1994. Targeting frequency for deletion vectors in embryonic stem cells. Mol Cell Biol. 14, 2404-10.
224. Zheng, B., et al., 1999a. A system for rapid generation of coat color-tagged knockouts and defined chromosomal rearrangements in mice. Nucleic Acids Res. 27, 2354-60.
225. Zheng, B., et al., 1999b. Engineering a mouse balancer chromosome. Nat Genet. 22, 375-8.
226. Zheng, B., et al., 2000. Engineering mouse chromosomes with Cre-loxP: range, efficiency, and somatic applications. Mol Cell Biol. 20, 648-55.
227. Zheng, B., et al., 2002. Visual genotyping of a coat color tagged p53 mutant mouse line. Cancer Biol Ther. 1, 433-5.
228. Zhu, Q., et al., 1998. Disruption of the NF-H gene increases axonal microtubule content and velocity of neurofilament transport: relief of axonopathy resulting from the toxin beta,beta'-iminodipropionitrile. J Cell Biol. 143, 183-93.